Methods

By T. Collett, M. Riedel, J. Cochran, R. Boswell, J. Presley, P. Kumar, A. Sathe,
A. Sethi, M. Lall, and the National Gas Hydrate Program Expedition 01 Scientists

Scientific Investigations Report 2012–5054

U.S. Department of the Interior
U.S. Geological Survey

Contents

Figures

Tables

Methods

By T. Collett, M. Riedel, J. Cochran, R. Boswell, J. Presley, P. Kumar, A. Sathe, A. Sethi, M. Lall, and the National Gas Hydrate Program Expedition 01 Scientists

Introduction

This chapter will describe the methods used in the operations, sample collection and handling, shipboard analyses, and preliminary interpretations developed by the Shipboard Science Party during the course of NGHP Expedition 01. This expedition, while not an Integrated Ocean Drilling Program (IODP) activity, was specifically designed to conform to IODP protocols.

Determining Site Locations

NGHP Expedition 01 drilled, cored, or logged at 20 sites in the Indian Ocean: 1 site in the Arabian Sea, 15 sites in the Krishna-Godavari area in the Bay of Bengal, 3 sites in the Mahanadi region in the northern Bay of Bengal, and 1 site in the Andaman Sea. At each of these sites, the *JOIDES Resolution* utilized Global Positioning System (GPS) coordinates to control positioning. Once the vessel was on location, the ship's thrusters were lowered and a reference beacon deployed. The ship was maintained on location (to a tolerance of typically 5 m by continuous monitoring of GPS data by the ship's computer-controlled Dynamic Positioning System (DPS). Final reported site location is the mean of the positions determined from the GPS data over the time the site was occupied.

Drilling and Coring Operations

Holes were produced through the use of a variety of standard coring systems and specialized pressure coring systems; as well as through standard drilling in the case of logging-while-drilling/measurement-while-drilling (LWD/MWD) and dedicated wire-line logging holes. Conventional coring systems used included the IODP's Advanced Piston Corer (APC) and the Extended Core Barrel (XCB). Both systems collect cores approximately 9.6 m in length within 6.7 cm diameter clear plastic core liners. The typical approach to coring was to utilize the APC corer until first refusal (an incomplete core indicating failure to fully penetrate the sediment), then switch to XCB coring to the full log depth. Pressure coring systems were employed at regular intervals or to target specific zones of interest seen on either prior LWD/MWD drilling holes or on seismic data. Pressure coring systems used include the Hyacinth Rotary Corer (HRC), the Pressure Coring System (PCS) and the Fugro Pressure Corer (FPC). Each of these systems collects cores approximately 1 meter in length, and of the following diameter: FPC, 5.7 cm; HRC, 5.1 cm; PCS, 4.3 cm. Dedicated logging holes were typically drilled through the addition of a center bit to the XCB system.

Drilling depth is measured initially in terms of meters below rig floor (mbrf). From these values, depths in meters below sea floor (mbsf) are calculated by subtracting the water depth. For this purpose, water depth is determined by measuring drilling depth in mbrf to the mud line as preserved in a mud-line core (a core that is fired from several meters above the seafloor such that it captures the seafloor surface). This water depth typically differs from more precise water depth calculations from one to several meters. Core top measurements in mbsf are then determined by subtracting the seafloor depth (mbrf) from the core top depth (mbrf). The core top mbsf measurement is the ultimate depth reference for all other depth calculations.

Logging Operations

Throughout NGHP Expedition 01, a variety of data were obtained through LWD/MWD, through wire-line logging in cored holes, and through wire-line logging in dedicated logging holes. To facilitate project schedules and budgets, all LWD/MWD logging was conducted during one leg of the program (Leg 2). These precoring logging operations are critical to the development of the detailed, site-specific coring, core sampling and pressure core deployment plans. Depth in well logs is measured from the sea-floor as identified through the drill pipe in the gamma-ray log. The data collection and interpretation methods are described fully in "Downhole Logging." In addition, *in situ* temperature measurements were taken with a variety of devices, including the Davis-Villinger Temperature Pressure probe (DVTP) when XCB coring and the APCT or APCT-3 when APC coring.

The standard "Triple Combo" log (density, porosity, and resistivity) and FMS-sonic tool strings were deployed at most of the sites. Both *P*-wave and *S*-wave velocity measurements were made using the Dipole Sonic Imager (DSI) tool. Depth-to-seismic ties were accomplished by means of synthetic seismograms constructed from the wire-line density and acoustic logs. High-resolution formation micro-scanner (FMS) electrical images complemented the resistivity-at-bit (RAB) images and aided in the identification of thin beds, veins, and fractures in gas-hydrate-bearing sediments.

Zero-offset vertical seismic profiles (VSPs) were collected for most of the sites. A single three-component VSI geophone was deployed in the borehole, and a Generator Injection

(GI) gun (105 in^3 generator/45 in^3 injector) was suspended by ship's crane 2 m below the water surface. The gun was fired several times (up to 10 shots) to stack the seismic signals and enhance the signal to noise ratio. The geophone was then moved a set distance up the borehole (5, 10, or 20 m spacing) and the shooting sequence was repeated. This sequence was repeated throughout the interval of interest. In keeping with IODP protocols, all VSP operations were conducted during daylight hours and assisted by mammal watchers posted at both the bow and stern of the ship. No mammals were observed during any of the VSP operations.

Core Curation and Sample Depth Calculation

NGHP Expedition 01 sites (areas of closely spaced holes testing a common geological model), holes, cores, and samples are identified using IODP conventions (fig. 1). An example identifier for a sample, NGHP-01-05C-2H-5, 80–85 cm, includes expedition (NGHP-01), site (05), hole (C), core number (2), core type (H), section number (5), and interval as measured from the top of the relevant section. Core type codes used include H (APC), X (XCB), Y (FPC), E (HRC) and P (PCS).

In addition to relative position within a core section, specific intervals and horizons are also described in "curatorial" meters below the sea floor (mbsf). The mbsf of a sample or horizon is calculated by adding the interval depth of the sample and the lengths of all upper sections to the core top datum as measured with the drill string. Often, cores expand upon recovery, leading to more than 100 percent recovery (for example, 9.8 meters of core recovery whereas bit advance may have been only 9.6 meters). Likewise, because the core top is marked at the highest recovered sediment within a core, there is often an unquantifiable coring gap between cores. As a result, discrepancies may exist between the drilling depth and curatorial depth, including instances where the curatorial depth at the bottom of one core may be greater than that for the top of the subsequent (deeper) core.

In cores with less than complete recovery, the uppermost recovered sediment is assumed to mark the top of the core. Furthermore, all other recovered sediment within the core is assumed to mark a continuous section downward. In other words, when sediment is missing from a core, that missing section is curated as occurring at the base of the core. This convention results in a necessary sampling uncertainty that should be taken into consideration when working with depth data (for example, core to log correlation).

Drilling-Induced Core Deformation

Many cores collected show significant signs of disturbance. Bedding deformation, particularly along the outer edge, is a common effect of the coring process, as are sediment mixing (particularly at the tops of cores), fluidization ("biscuit and slurry"), and liquid injection. Core deformation such as creation of partings also occurs commonly as a result of the depressurization associated with core retrieval. Dissociation of gas hydrate and gas expansion also result from core depressurization (and warming), and can further disturb the sediment. "Lithostratigraphy" provides a further discussion on the nature and interpretation of core characteristics, including those that may serve as indicators of the previous presence of gas hydrate.

Core Handling and Analysis

Cores acquired during NGHP Expedition 01 were generally handled according to ODP/IODP procedures. Modifications to these procedures, similar to those made in ODP Leg 204 and IODP Expedition 311 (recent gas-hydrate-focused expeditions), were designed to enable quick identification of gas-hydrate intervals, maintain aseptic conditions for microbiological sampling, and identify and safely manage hydrogen sulfide gas.

Inspection of the cored sediment began immediately upon recovery with infrared (IR) imaging of the core while still in the liner. These scans were used primarily to identify anomalously cool sections of liner that are indicative of recent or ongoing gas-hydrate dissociation within the enclosed sediments (see "Physical properties"). Many observed thermal anomalies were immediately cut from the core and either

- sent to the geochemistry lab for visual inspection and extraction of interstitial waters for geochemical analyses (see "Inorganic geochemistry"),
- sampled and stored for later shore-based microbiological studies, or
- bagged and preserved in liquid nitrogen-filled dewars or methane-charged pressure vessels.

Visible gas-hydrate samples obtained from the core catcher or otherwise extruded from the core liner were also stored in liquid nitrogen. In most cases, a background sample (nonanomalous) was also taken from each core for immediate geochemical analyses. In some cases, holes preidentified for microbiological sampling were cored using drilling fluids containing microbead tracers to aid in the identification of uncontaminated sections. Gas samples were routinely collected from void spaces within the cores and analyzed in the geochemistry lab (see "Organic geochemistry").

The remainder of the core was then measured for sectioning and labeled with a permanent marker with up orientation, core number, core type, and section number. It was then compressed with a plunger to remove all voids, when possible, and cut into sections 1.5 m or less in length. The most appropriate section or sections were then selected for sampling (typically the most coherent, least disturbed, section that appears to be representative of the background condition of the core). The suite of preplanned samples were then cut, capped, labeled, and stored as appropriate for each sample type. The remaining core sections were transferred to the laboratory and allowed to equilibrate to room temperature before further processing.

Once in the laboratory, the remaining whole round core sections were first tested for thermal conductivity, then passed through the multisensor core logger (MSCL) to obtain

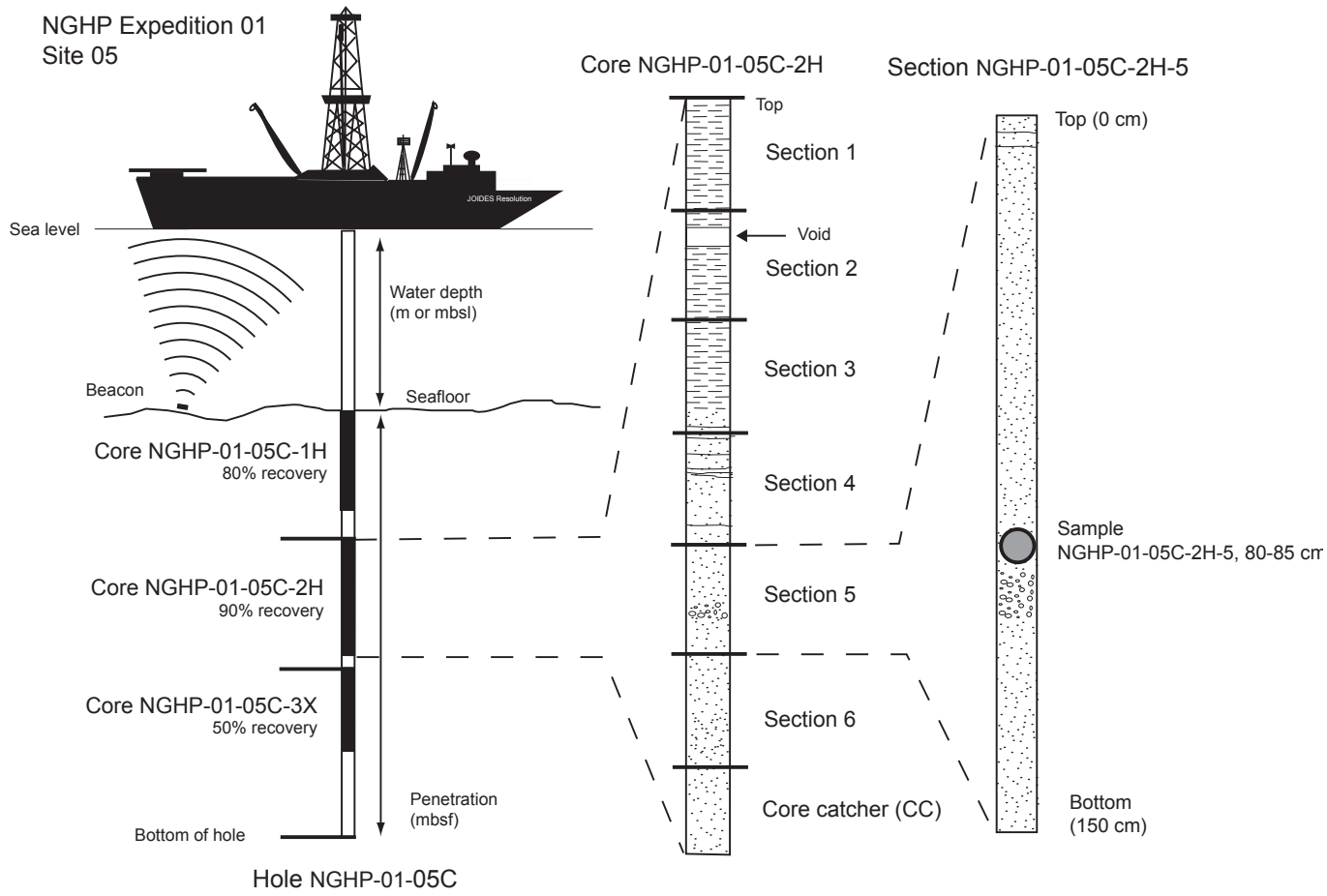

Figure 1. Illustrated conventions for naming sites, holes, cores, and samples. [CC, core catcher; mbsl, meters below sea level; mbsf, meters below seafloor]

measurements of *P*-wave velocity, noncontact resistivity, gamma ray attenuation bulk density, and magnetic susceptibility (see "Physical properties").

The cores were then split, from bottom to top, creating separate archive and working halves. Investigators should note that splitting, using either a pulled wire or a fixed circular saw blade, may further disturb the core and result in the transport of material upward along the surface of each core half.

The working half was then sampled for further physical properties testing (moisture and density, shear strength, split-core acoustic velocity, and contact resistivity (see "Physical properties"). Next, the working half of the core was transferred to the sampling table where it was further subsampled. Subsampling included the regular collection of background material for later sedimentological, X-ray diffraction, carbon dating, and paleomagnetism studies, as well as targeted sampling of notable features such as carbonate nodules, volcanic ash layers, macrofossils, and other features.

The archive half sections were scanned on the digital imaging system (DIS). Visual core descriptions (VCDs, see supplemental data files) of the archive halves were prepared, augmented by microscopic analyses of smear slides. Digital close-up photographs were taken of particular features for illustrations, as requested by scientists (see "Lithostratigraphy"). Both halves of the core were then placed in labeled plastic tubes and transferred to cold storage for the remainder of the expedition.

Two 20-ft refrigerated containers were mounted on the vessel (on the lab stack roof and on top of the core technician shop) during NGHP Expedition 01 for pressure core processing and analyses. The lab stack van (hereafter referred to as the pressure coring system [PCS] van) contained the PCS degassing manifold, and a horizontal multisensor core logger (MSCL). The core technician shop container (hereafter referred to as the HYACINTH van) housed the HYACINTH transfer system and degassing manifold, as well as a pressure multisensor core logger (MSCL–P).

At the end of the expedition, selected cores and samples were offloaded in Chennai in refrigerated containers and transported to the National Gas Hydrate Program Repository in Mumbai, India, or shipped to various researchers in India and elsewhere. The remainder of the cores and samples sailed on to Singapore, where they were shipped to a group of approved postcruise laboratories in the United States, Canada, and Germany or to the USGS facility in Woods Hole, Massachusetts, for further analysis.

Five of the stored pressure cores were stored for further postexpedition analysis in Singapore (see "Singapore Pressure Core Studies" in the Appendix 3 for more information).

Lithostratigraphy

The techniques and procedures used to describe, analyze, and identify the lithologies in cores recovered during NGHP Expedition 01 are described below. They are based on the methodology employed in ODP Leg 204 and IODP Expedition 311 with additions from ODP Legs 172 and 202 and adapted to the specific conditions and equipment available during NGHP Expedition 01. The techniques and procedures described here include visual core descriptions, smear slide and coarse fraction descriptions, and high-resolution digital color core imaging. Any significant deviations from the procedures outlined in this section are discussed in the individual site chapters.

Sediment Classification

The naming conventions adopted during NGHP Expedition 01 follow the ODP sediment-classification scheme of Mazzullo and Graham (1988). Principal names were assigned to sediments based on composition, texture, and degree of lithification as determined primarily from visual description and smear slide analyses. Modifiers to the principal name were determined based on both the abundance and type of the nonprincipal component or components (for example, siliciclastic or biogenic). Major modifiers are listed in order of increasing abundance and tagged with "bearing" or "rich" (see below).

Siliciclastic Sediments

For sediments and rocks composed of >60 percent siliciclastic components, the principal name was determined by the size of the grains (sand, silt, and clay). Textural names were derived from the Udden-Wentworth grain-size scale (Wentworth, 1922) (fig. 2). In this classification scheme, the term clay is independent of mineralogy and refers to all siliciclastic grains <3.9 µm in size, regardless of composition. The relative proportion of different grain sizes was determined by visual percentage estimation using the comparison chart of Terry and Chilingarian (1955) (fig. 3). Once the relative proportions were determined, a modified Shepard (1954) classification scheme was used to assign the principal name (fig. 4). Clay, silt, and sand are the principal names in the Shepard diagram. If any component exceeds 25 percent of the total siliciclastic grains, it becomes a modifier to the principal name. For example, sediment composed of 10 percent clay and 90 percent silt is simply a silt, whereas sediment composed of 30 percent clay and 70 percent silt is a clayey silt.

Millimeters (mm)	Micrometers (µm)	Phi (φ)	Wentworth size class		Rock type
4096		-12.0	Boulder		
256		-8.0	Cobble	Gravel	Conglomerate/ Breccia
64		-6.0	Pebble		
4		-2.0	Granule		
2.00		-1.0	Very coarse sand		
1.00		0.0	Coarse sand		
1/2 0.50	500	1.0	Medium sand	Sand	Sandstone
1/4 0.25	250	2.0	Fine sand		
1/8 0.125	125	3.0	Very fine sand		
1/16 0.0625	63	4.0	Coarse silt		
1/32 0.031	31	5.0	Medium silt		
1/64 0.0156	15.6	6.0	Fine silt	Silt	Siltstone
1/128 0.0078	7.8	7.0	Very fine silt		
1/256 0.0039	3.9	8.0			
0.00006	0.06	14.0	Clay	Mud	Claystone

Figure 2. Grain size divisions for sedimentary rocks (adapted from Wentworth, 1922).

Where diagnostic minerals (for example, glauconite) or unusual components (for example, volcanic glass) compose >5 percent of the sediment, the naming conventions of biogenic and mixed sediments were adopted. Thus, if the mineral component represents 5–10 percent of the sediment, it is hyphenated with the suffix "-bearing" and precedes the major siliciclastic component name. If the component is 11–40 percent of the sediment, it is hyphenated with the suffix "-rich," instead. For example, sediment composed of 15 percent glauconite sand grains, 30 percent silt, and 55 percent clay is called a glauconite-rich silty clay. Where volcanic glass composed >40 percent of the sedimentary components, the name volcanic ash is used.

Biogenic Sediments

Unlike siliciclastic sediments, biogenic sediments, defined as containing >60 percent biogenic components, are not described based on texture. Rather, the principal name for all biogenic sediments is ooze. If the siliciclastic or other biogenic components represents 5 percent–40 percent of a sediment, the naming conventions using "-rich" and "-bearing" described above are followed. Thus, a sediment composed of 30 percent clay and 70 percent radiolarians is called a clay-rich radiolarian ooze; likewise, a sediment composed of 30 percent nannofossils and 70 percent foraminifers is called a nannofossil-rich foraminifer ooze.

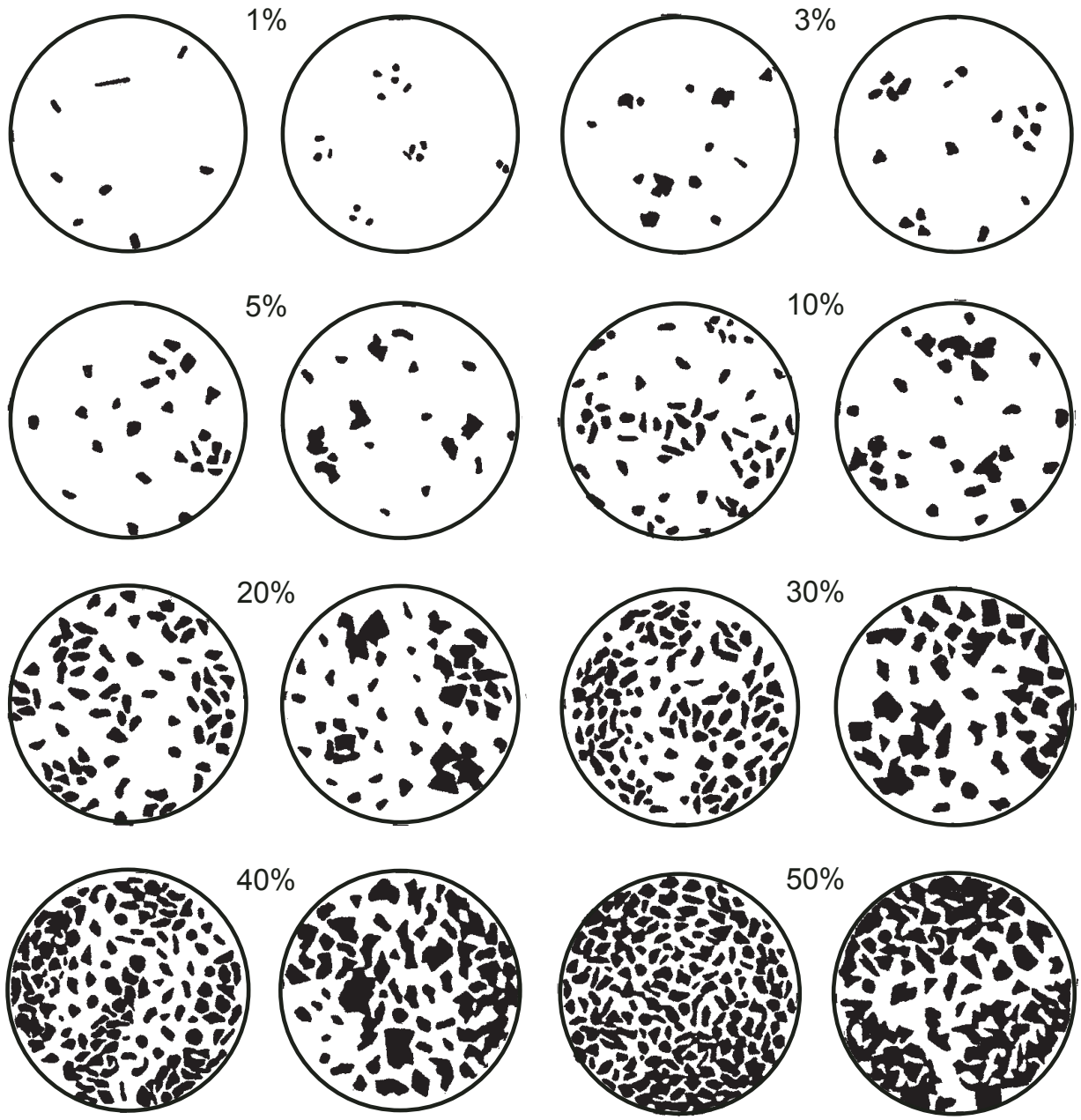

Figure 3. Comparison chart for volume percentage estimation (after Terry and Chilingarian, 1955).

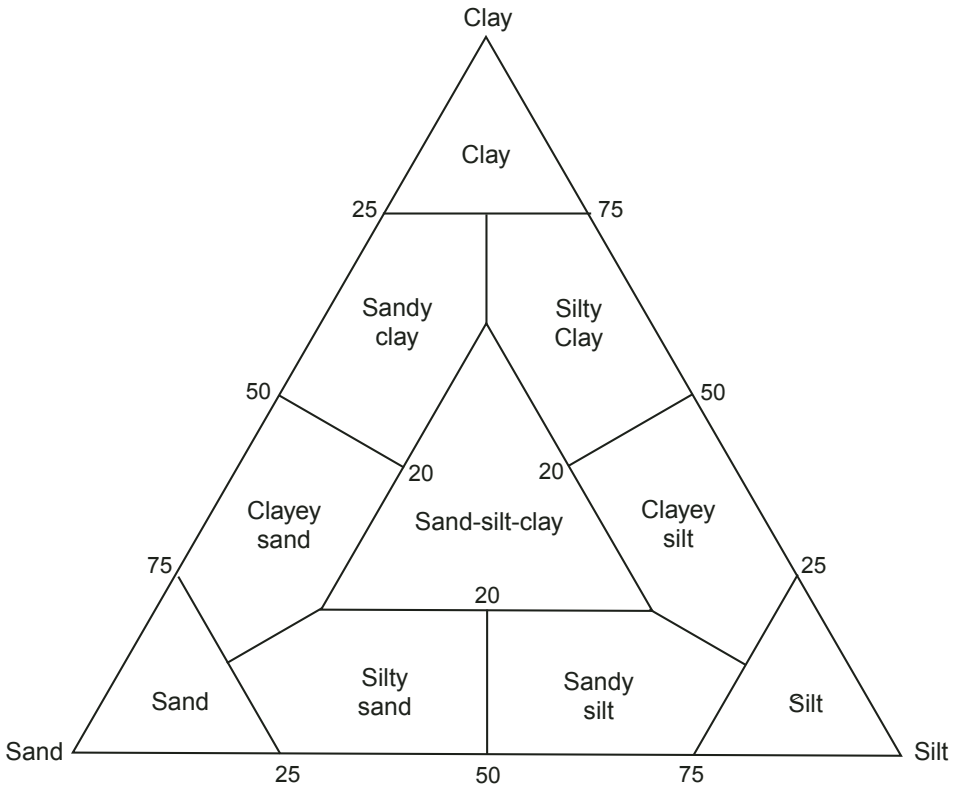

Figure 4. Ternary diagram for siliciclastic textural classification. Numbers indicate percentages.

Mixed Sediments

Subequal mixtures of biogenic and nonbiogenic material, where the biogenic content is 40 percent–60 percent, are termed "mixed sediments" in the ODP classification (Mazzullo and Graham, 1988). The name of a mixed sediment consists of a major modifier(s) consisting of the name(s) of the major fossil group(s), with the least common fossil listed first, followed by the principal name appropriate for the siliciclastic components (for example, foraminifer clay). The same naming conventions for using "-bearing" and "-rich" apply to mixed sediments as described above. An unconsolidated sediment containing 5 percent foraminifers, 40 percent nannofossils, and 55 percent silt is, thus, called a foraminifer-bearing nannofossil silt. Sediment containing 5 percent diatoms, 40 percent clay, and 55 percent nannofossils is called a diatom-bearing nannofossil clay.

Firmness

The definition of Gealy and others (1971) was used to identify the firmness of recovered sediments. Siliceous sediments and rocks are divided into two classes of firmness:

- Soft sediments, which are composed of gravels, sands, silts, and clays (sediment core can be split with a wire cutter); and
- Hard sediments, which are composed of conglomerates, sandstones, siltstones, and claystones (sediment core must be cut by a band or diamond saw).

Calcareous sediments and rocks are divided into three classes of firmness:

- Soft sediments, which readily deform under the pressure of a fingernail or spatula;
- Partly lithified, which are firm but friable sediments that can be scratched with a fingernail or the edge of a spatula;
- Lithified, which are hard, nonfriable cemented rocks that are difficult or impossible to scratch with a fingernail or the edge of a spatula.

Lithified sediments were occasionally recovered during NGHP Expedition 01 as diagenetic precipitates (authigenic carbonates and iron sulfides) or as semilithified to lithified calcareous sediments. Most sediments were soft to hard clays and oozes. For the partly-lithified to lithified carbonate rich sediments we used the following rock names as appropriate:

- *Chalk*—firm, pelagic sediment composed predominantly of calcareous pelagic grains, and
- *Limestone*—hard, pelagic sediment composed predominantly of calcareous pelagic grains.

Visual Core Descriptions

Detailed sedimentologic observations and descriptions were recorded manually for each core section on ODP visual core description (VCD) sheets (see supplemental data files). A wide variety of features that characterize the sediments were recorded, including lithology, sedimentary structures, color, diagenetic precipitates, and core disturbance. Compositional data were obtained from smear slides. The Munsell color designation (hue, value, and chroma) of the sediments was determined by either color spectrophotometry (using a GretagMacbeth ColorEye XTH hand held instrument) or by visual comparison with the Munsell soil color chart (Munsell Color Company, Inc., 1975). This information was synthesized for each core in the Advanced Logic Technology© WellCAD Version 4.0 software package, which generates a one-page graphical description of each core (fig. 5). Symbols used in the WellCAD software are described in each site chapter, usually in figure 1.

Of particular interest during NGHP Expedition 01 were the visual indications of disruption to the sediment caused by the dissociation of gas hydrate in the recovered cores. Massive hydrate was often removed on the catwalk prior to core description (sampled intervals were noted in the barrel sheets), but some less massive forms that were not sampled on the catwalk dissociated within the core and left distinct textural disturbances. The two primary textures identified as resulting from the dissociation of gas hydrate are soupy and mousse-like. Soupy sediments are watery, homogeneous, and fluidized. These sediments are often associated with void spaces in the core because they are able to flow from their original position during core recovery and therefore retain no original sedimentary structures. Sediments containing mousse-like textures can be divided into two descriptive types based on water content. Wet, watery mousse-like sediment texture is soft and deforms plastically under slight pressure from one finger. Mousse-like texture can also occur in drier sediments that are stiffer and tend to form brittle flakes, which break off under the pressure of one finger. These drier, stiffer sediments often appear foliated when split by the core cutter wire. Both types of mousse-like texture contain gas vesicles and obscure primary sedimentary structures.

Mousse-like and soupy textures related to the dissociation of gas hydrate not sampled prior to description were observed at several sites and noted on the digital core description sheets recorded in WellCAD. Remarks made on the digital core-description sheet for each core describe any additional potential indications of gas hydrate near the sampled intervals, including the presence of dry, flaky sediment that may have been dewatered by the formation of gas hydrate nearby. Soupy disturbances at the top of each core (top of first section), however, are not necessarily related to gas-hydrate presence but rather drilling-related disturbance.

Lithology and Grain Size

The lithology and grain size of the described sediments are represented graphically in the WELLCAD-generated descriptions. Intervals that are a few centimeters or greater in thickness can be portrayed accurately in the lithology column. Percentages are rounded to the nearest 10 percent, and lithologies that constitute <10 percent of the core are generally not shown but are listed in the "Description" column.

Bioturbation

Visible bioturbation was classified into four intensity levels based on the degree of disturbance of the physical sedimentary structures:

1. *Rare*—isolated trace fossils; up to 10 percent of physical sedimentary structures are disrupted.
2. *Moderate*— ~10–40 percent disrupted physical sedimentary structures; burrows are generally isolated but may overlap locally.
3. *Common*— ~40–60 percent disrupted by burrows, sedimentary structures are disrupted
4. *Abundant*— >60 percent bedding completely disturbed; burrows are still intact in places.

These categories are based on the ichnofossil indices of Droser and Bottjer (1986) and are illustrated with graphic symbols in the "Bioturbation" column on the WellCAD core description sheets. Visual recognition of bioturbation was often limited in homogeneous sediments, particularly in hemipelagic clay zones without iron sulfide precipitates.

Sedimentary Structures

Each type of sedimentary structure and its exact location are displayed in the "Structure" column on the WellCAD core description sheets. Symbols are used to note the wide variety of sedimentary structures encountered throughout NGHP Expedition 01, and these are listed in the legends for the WellCAD core description sheets included within each site chapter.

Fossils

The presence of macroscopic fossils (for example, shell fragments, preserved whole shells, bivalves, gastropods) is displayed in a separate column on the barrel sheets.

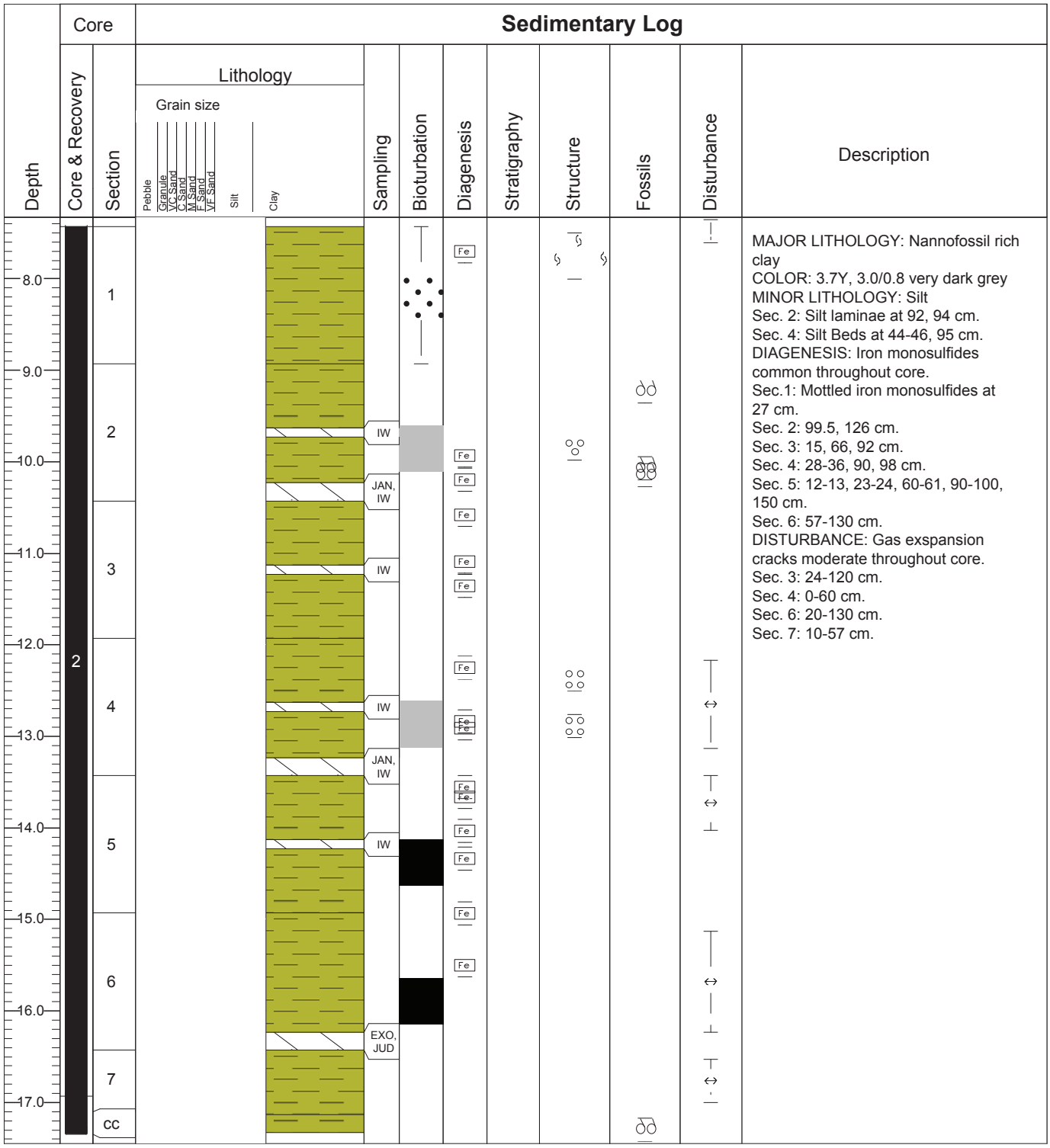

Figure 5. WellCAD core description log example. [cm, centimeters]

Sediment Disturbance

Drilling-related sediment disturbance that persists over intervals of ~10 cm or more is recorded in the "Disturbance" column. Separate terms are used to describe the degree of drilling disturbance in soft and firm sediments:

1. *Slightly disturbed*—bedding contacts are slightly deformed;
2. *Moderately disturbed*—bedding contacts have undergone extreme bowing; and
3. *Very disturbed*—bedding is completely deformed as flow-in, coring/drilling slough, and other soft sediment stretching and(or) compressional shearing structures attributed to coring/drilling (for example, gas expansion).

Soupy intervals are water saturated and have lost all primary sedimentary structures. When the soupy texture is related to gas-hydrate dissociation, it is noted in the description on the WellCAD core sheet.

The degree of fracturing in indurated or semilithified to lithified sediments is described using the following categories:

1. *Slightly fractured*—core pieces in place and broken;
2. *Moderately fractured*—core pieces are in place or partly displaced, but original orientation is preserved or recognizable;
3. *Highly fractured*—core pieces are probably in correct stratigraphic sequence (although they may not represent the entire sequence), but original orientations are lost;
4. *Drilling breccia*—core pieces (small and angular pieces) have lost their original orientation and stratigraphic position and may be mixed with drilling slurry; and
5. Drilling biscuits and drilling slurry surrounding an intact or slightly fractured drilling biscuit.

Cores recovered from gas and gas-hydrate-bearing sediments are often disturbed by gas expansion that causes fracturing. In cases where it is possible to distinguish between disturbance of the core resulting from drilling and disturbance resulting from gas expansion, notes were made in the description section of the WellCAD sheets listing the depths at which gas fracturing or gas expansion cracks were observed.

Samples

The position of whole-round samples removed from the core on the catwalk are indicated in the "Sample" column on the WellCAD core description sheets. The abbreviations used can be found in the core samples database.

Diagenesis

The relative positions of features that are related to diagenesis are displayed in the "Diagenesis" column on the WellCAD core description sheets. These are mineral precipitates (for example, pyrite and authigenic carbonates).

Analysis of Smear Slides

Smear slides were prepared from the archive halves of the cores. With a toothpick, a small amount of sediment was taken and put on a 1 × 3 in glass slide, homogenized, and dispersed over the slide with a drop of deionized water. The sample was then dried on a hot plate at the lowest effective temperature. A drop of Norland optical adhesive #61 and a 2.2 × 3.0 cm in glass cover were added. The cover slip was fixed to the slide in an ultraviolet light box. With a transmitted light polarizing petrographic microscope, both the grain size and abundance of dominant components in a sample were determined. Abundance was estimated with the help of a comparison chart for visual percentage estimation (after Terry and Chilingarian, 1955). Note that smear slide analyses tend to underestimate the amount of sand-sized and larger grains because these grains are difficult to incorporate into the slide. The smear slide tables include information about the location of samples, their grain-size distribution, and whether the sample represents the dominant (D) or the minor (M) lithology in the core. Additionally, they provide estimates of the major mineralogical and biological components from the examination of each smear slide. The presence of authigenic minerals or other noticeable components such as woody debris or unique trace minerals was noted in the "Comments" column.

Coarse Fraction Descriptions

To aid in sediment description at most of the sites, we also sieved, using a 63 μ mesh, ~5 cc of sediment at the location of some smear slides and described the coarse fraction. In combination with the smear slide results, which are slightly biased toward finer grained components, we used the coarse fractions to identify the relative abundances of the larger species and components (for example, foraminifera, diatoms, radiolarians, silicoflagellates, pyrite, quartz, mica, or feldspar). Together these data give us the most complete description of the presence and distribution of sedimentary components throughout the core.

Color Reflectance Spectrophotometry

At some of the earlier sites (mostly on Leg 3A), a hand-held Gretag-Macbeth ColorEye® XTH with a spectral range between 360 and 750 nm and a resolution of 10 nm was used

in the Munsell mode to obtain Munsell color readings for major color zones in cores. Names for these color readings were selected from a Munsell color chart. Freshly split cores were covered with clear plastic wrap (Glad Cling® brand). Additional detailed information about the measurement and interpretation of spectral data can be found in Balsam and others (1997; 1998), Balsam and Damuth (2000), and Giosan and others (2002). For the sites cored on Leg 3B and 4 the standard Munsell soil color chart was used to determine core color.

Digital Color Imaging

All core sections were imaged using the Geotek X-Y digital imaging system (DIS) immediately after being split and scraped. We found it particularly useful to scrape the cores immediately prior to imaging in order to capture the ephemeral nature of some sedimentary features, particularly sulfide precipitates, which become oxidized within minutes of core splitting. All images were acquired at a crosscore and downcore resolution of 100 pixels/cm. In order to retain the relative variability in core color within each hole, we found it more expedient to fix the aperture of the camera at a value that would image most cores without the need for further adjustment. Care was taken to ensure that the system was correctly calibrated using the "white tile" procedure and that the camera position was correctly set up (Shipboard Scientific Party, 2003). A digital ruler was added to the images. Output from the DIS includes an uncompressed TIFF file for each scanned section with a digital ruler on the left side of the image. Red-green-blue (RGB) profiles for all images were also automatically saved.

Inorganic Geochemistry

The majority of shipboard interstitial water (IW) samples were obtained on 5- to 30-cm-long whole-round cores. The sampled intervals are described for each hole in the respective site chapters. After extrusion from the core liner, the surface of each whole-round core sample was carefully scraped clean of contaminated sediment with a clean spatula to remove potential contamination from seawater and sediment smearing in the borehole. In APC cores, 1 cm from the outer diameter, top, and bottom faces was removed; whereas in the XCB cores, where borehole contamination is higher, as much as 90 percent of the sediment was removed from each whole round. In rare cases the whole-round sample had to be discarded. The remaining sediment (~50–300 cm^3) was placed into a titanium squeezer, modified after the stainless-steel squeezer of Manheim and Sayles (1974). Gauge forces often up to 20,000 pounds were applied using a laboratory hydraulic press to extract interstitial water. In a few low water content cores recovered from greater depths, gauge force up to a maximum of 30,000 pounds was applied. Interstitial water was passed through a prewashed dry Whatman No. 1 filter fitted above a titanium screen, filtered through a 0.45 µm Nalgene disposable filter, and subsequently extruded into a new plastic syringe attached to the bottom of the squeezer assembly. In most cases, 25–40 cm^3 of pore water was collected from each sample, which required squeezing the sediment for 5–90 minutes, depending on lithology.

Collection of Subsamples for Shore-Based Analyses

Subsamples for both alkalinity and sulfate determinations were taken and analyzed as soon after interstitial water collection as possible. In addition, a subsample for ammonium analysis (1.00 mL) was pipetted as soon after squeezing as practical into a glass ampoule, acidified with 0.010 mL ultrapure HCl, and flame-sealed. The remaining interstitial water was placed into a new polypropylene (PP) centrifuge tube and split for shipboard and shore-based analyses. Total dissolved inorganic carbon (DIC) samples (1 mL) were preserved with 0.100 mL 5 percent $HgCl_2$ in 2 mL glass vials with septum caps. Samples for dissolved organic carbon (DOC) and volatile fatty acids (0–3 mL) were stored in amber glass septum vials and frozen. Samples for oxygen and hydrogen isotopes (1–3 mL) and major ions (2–8 mL) were flame-sealed in glass ampoules. Minor element samples were pipetted into 5 mL cryovials that had been precharged with 0.040 mL ultrapure HNO_3. DIC isotope samples were syringed into 5 mL vacutainers that were preloaded with 0.100 mL 5 percent $HgCl_2$. In addition, 2 mL samples for shore-based sulfate analyses were immediately pipetted into agilent vials and preserved with 100 mL $Cd(NO_3)_2$ to precipitate sulfide out of solution. The remaining water was used for shipboard chloride, bromide, and sulfate measurements.

Shipboard Interstitial Water Analyses

Routine shipboard measurements were conducted according to standard procedures (Gieskes and others, 1991). Salinity was measured using a Goldberg optical hand-held refractometer. The pH was determined by ion-selective electrode.

Alkalinity was determined by Gran titration with a Metrohm autotitrator. Accuracy and precision were monitored by repeated analyses of International Association of the Physical Sciences of the Ocean (IAPSO) standard seawater, as well as 10 mM sodium bicarbonate and 20 mM sodium carbonate standards. The ion-selective electrode was calibrated and standards were analyzed every ten samples. The average external accuracy and precision were based on the multiple analyses of the standards <2 percent and ~1 percent, respectively.

Sulfate (SO_4^{2-}) concentration was determined by manual dilution and manual injection into a Metrohm 761 ion chromatograph on Legs 3A and 3B and into a Metrohm 861 ion chromatograph on Leg 4, with eluent suppression, on aliquots to which $Cd(NO_3)_2$ had been added as soon as possible after interstitial water collection. Sulfate to chloride and bromide to chloride ratios were determined by comparison of peak heights to those measured for International Association of the Physical Sciences of the Ocean (IAPSO) standard seawater. Sulfate and bromide concentrations were determined by multiplying

the respective ratios by the chloride concentration determined by titration. Based on replicate analyses of IAPSO the standard deviation of the sulfate/chloride ratio determination was 0.25 percent. Combined with the uncertainty of the chloride concentration, the resulting confidence limit for sulfate concentration is 0.3 percent at seawater concentrations based on repeated analysis of IAPSO. Aliquots for shore-based analyses were processed following the sampling plan given in table 1.

High-precision chloride concentrations were determined by Mohr titration using silver nitrate ($AgNO_3$) for most samples. Quantification was based on comparison with IAPSO standard seawater. Most chloride concentrations were determined in duplicate. The reproducibility of the chloride titrations, expressed as 1 σ relative standard deviations, was evaluated by replicate analyses of IAPSO standard seawater and was <0.2 percent.

When the reagent needed for Cl^- titration was exhausted, Cl^- was analyzed by IC, with a precision of 0.7 percent. These samples have been reanalyzed by titration in shore-based studies.

Bromide was as well analyzed by manual injection into a Metrohm 761 ion chromatograph on Legs 3A and 3B and into Metrohm 861 ion chromatograph on Leg 4, with eluent suppressor used for sulfate concentration. The precision based on duplicate analyses of IAPSO standard seawater, expressed as 1 σ relative standard deviations was 1–2 percent.

All figures for Sites NGHP-01-03 through NGHP-01-16 are plotted based on concentration data that were not corrected for drillwater contamination, whereas the figures for Sites NGHP-01-17 through NGHP-01-21 are plotted based on corrected data for drillwater contamination.

Onboard High-Purity Water

Water used for all onboard dilutions, solution preparations, and final washing of equipment (stir bars, spatulae, core squeezer parts) was produced by passing the ship's potable water through an Ever-Pure RT-3 water filter cartridge followed by a Barnstead NANOpure® DiamondTM Analytical (Model D11901) deionization system. The conductivity of the output of the NANOpure system was monitored and had a conductivity of 18.2 Mohm-cm.

Organic Geochemistry

The shipboard organic geochemistry program for NGHP Expedition 01 included three routine sets of analyses:

- Analysis for volatile hydrocarbons, CO_2, N_2+Ar, H_2S, and O_2, in sediment by the headspace method;
- Measurement of free gas or gas voids (FG) (CO_2, N_2+Ar, H_2S, and O_2); and
- Analysis of gas (CO_2, N_2+Ar, H_2S, and O_2) collected from PCS core degassing experiments.

Procedures used during NGHP Expedition 01 are adapted from IODP standard methods that are described by Pimmel and Claypool (2001). Brief comments on routine sampling and deviations from standard practice are noted below.

Gas Sampling

Samples for headspace (HS) analysis were collected on the opposite core end facing the interstitial water sample to integrate the interstitial water and gas datasets. The sampling frequency was increased near the first visible evidence of gas bubbles in sediment to achieve a high depth resolution at the sulfate-methane interface (SMI).

Upon core retrieval, a 5-cm^3 sediment sample was collected with a 5-mL cut-off plastic syringe from a freshly exposed end of a core section and was extruded into an organically-clean 20-mL glass serum vial. For this purpose, the plunger was held at the sediment surface while inserting the barrel to avoid trapping air bubbles. Sediment volume was determined by weight, recorded to nearest 0.1 gm and known density as determined by physical properties. The samples were immediately sealed with a 20-mm thick septum and metal crimp cap and heated at 60 °C for 20 minutes. Air blanks incubated with septum fragments inside confirmed that no hydrocarbons (C_1–C_3) were released by the septum or glassware. The concentrations reported represent minimum proxy measurements of the actual concentrations due to limitations of the gas headspace method due to degassing during core recovery (Kvenvolden and Lorenson, 2000).

Gas samples from voids caused by gas expansion in the core were collected by piercing the core liner and allowing gas to expand into a 60-mL syringe connected to the penetration tool. Excess gas was stored in preevacuated 30-mL serum vials capped with butyl-rubber stoppers and overpressured by injecting about 60-mL of sample gas into them. For long-term storage the vial septa were coated with silicon glue to prevent gas leakage.

Gas samples from the PCS were collected from an inverted 1000-mL graduated cylinder attached to the PCS via an air-purged line regulated by a series of valves. Gas was released from the PCS in increments and the volume of gas recorded at 5 °C. Excess gas was stored in the same manner as described for the void gas.

Gas Analysis

The HS samples were removed from the 60 °C oven before analysis and allowed to cool to room temperature, about 25 °C, prior to sample injection. 10-mL of gas was extracted from the vial using a standard 60-mL syringe and injected onto a gas chromatograph. The vials were then frozen to preserve the sample for TOC and Rock Eval analyses postcruise.

Gas analyses were performed on an Agilent 3000A-micro gas chromatograph equipped with two independent columns. Column 1 was a 8-m × .32 mm PLOT U column that separates

Table 1. Sample division plan for interstitial waters.

[ml, milliliters; µl, microliters]

PORE FLUID DIVISION SCHEME													
NGHP Expedition 01													
Code	Alkalinity	SO_4/H_2S	DIC concentrations	Acetate	NH_4	DIC Isotopes	DOC/VFA	O/H	Majors/Cl	Minors SIO	Minors OSU (Leg 4)	Shipboard	Total
	IWPA	IWPSO	IWGTC	IWGTLA	IWGN	IWGIC	IWGOC	IWGI	IWGSM	IWPSM	IWPOM	IWPS	
Subsample container	Plastic test tube with cap	1.5 ml centrifuge tube	2 ml agilent vial	2 ml agilent vial	1 ml ampoule	5 ml vacutainer or 2 ml agilent vial	4 ml amber autosampler vial	2 or 5 ml ampoule	2, 5, 10, or 20 ml ampoule	5 ml plastic cryotube	Torres Nalgene bottle	1.5 ml centrifuge tube	
Treatment		100 µl $Cd(NO_3)_2$	100 µl $HgCl_2$		10 µl Optima HCl	100 µl $HgCl_2$	Freeze			40 µl Optima HNO_3	40 µl Optima HNO_3		
>35 ml	3	1	1	0.5	1	3	3	3	7	5	8	1.5	37.0
30 ml	3	1	1	0.5	1	2	2	2	6	5	5	1.5	30.0
25 ml	3	1	1	0.5	1	2	2	2	4	3	4	1.5	25.0
20 ml	3	1	1	0.5	1	2	1	1	3	2	4	1	20.5
15 ml	0	1	1	0.5	1	2	0	2	2	2	3	1	15.5
10 ml	0	1	1	0	0	1	0	1	1	2	2	1	10.0
5 ml	0	1	0	0	0	0	0	0	1	1	1	1	5.0

C_1–C_4 hydrocarbons, air gases (O_2 + N_2+ Ar – one peak), H_2S, and CO_2. Column 2 was a 10-m × .32 mm MolSieve 5A PLOT column that separates O_2, N_2+Ar, CO_2, and CO. Detection limits vary but at best are about 15 parts per million by volume (ppmv) for methane and increase for higher molecular weight gases such that the detection limit for butane is about 100 ppmv. Precision of the measurements varies from 0.5 to 2 percent. The GC is controlled by EzChrom software run on a PC laptop computer.

For the HS, void gas, and PCS gas analyses, the gas composition is expressed as component parts per million by volume (ppmv) relative to the analyzed gas. To the extent that sampling procedures are uniform, the differences in the HS results reflect differences in the amount of gas remaining in the cores. The volumetric units were converted to concentration units (mM) to facilitate comparisons with dissolved interstitial water constituents using the following equation:

$$CH_4 = \chi_M \times P_{atm} \times V_H \bullet R^{-1} \times T^{-1} \times \phi^{-1} \times V_S^{-1},$$

where

V_H = volume of the sample vial headspace,

V_S = volume of the whole sediment sample,

χ_M = molar fraction of methane in the headspace gas (obtained from GC analysis),

P_{atm} = pressure in the vial headspace (assumed to be 1 bar),

R = the universal gas constant,

T = temperature of the vial headspace in degrees Kelvin, and

ϕ = sediment porosity (determined either from moisture and density measurements on adjacent samples or from porosity estimates derived from gamma ray attenuation (GRA) data that were representative of the sampled interval as described in "Physical properties").

The minimal concentration of dissolved methane that remains in the aqueous phase (for example, Duan and others, 1992; Xu, 2002, 2004) is not accounted for. The internal volumes of 15 representative headspace vials were carefully measured beforehand and were determined to average 21 cm^3. This volume was taken as constant in calculations of gas concentrations.

Sediment

Approximately 200 gm of wet sediment were collected for every core (approximately every 9 m) in organically-clean 60 mL jars and frozen to preserve sediment for shore-based studies of solvent extractable organics.

Microbiology

Cell Enumeration

Sediment in 1 cm^3 plugs was taken for shore-based direct microscopic determination of bacterial numbers. These plugs were taken from the end of selected core sections immediately after the sections were cut on the catwalk. On average, one sample per core was collected. Potentially contaminated sediment was removed with a sterile scalpel, and a sterile 3 cm^3 plastic syringe with the luer end removed was used to take a 1 cm^3 plug. The 1 cm^3 plug was extruded into a sterile plastic centrifuge tube containing 9 mL of filter-sterilized (0.2 µm) 2 percent formaldehyde in 3.5 percent NaCl. The tube was shaken vigorously to disperse the sediment particles and subsequently stored at 4 °C.

Relationship of Microbial Characteristics to Hydrate

In order to determine whether fine-scale microbial characteristics in the sediments (for example, microbial community dynamics, numbers of methanogens) are dictated by the presence of gas hydrate in the sediments or some other factor(s) a series of whole round cores (WRC) were collected (for shore-based analysis) from core sections that showed evidence of gas hydrate and from adjacent sections that apparently lack gas hydrate.

WRCs removed from the single gas-hydrate/nongas-hydrate-bearing core units were wrapped in Saran wrap, double-bagged in Whirlpak bags, labeled, flushed with N_2, and then sealed in cryo-storage bags. Subsequently, WRC samples were refrigerated (4 °C) or frozen (–80 °C) as soon as possible.

Hydrogenase Activity

Five-cm-long WRCs were collected for shore-based hydrogenase activity determinations (Soffientiono and others, 2006). Whole rounds were cut on the catwalk, capped, bagged with oxygen scrubbers (Anaerocult® A mini, EM SCIENCE) and stored at –80 °C.

Contamination Assays

To confirm the suitability of the core material for microbiological research, contamination assays were conducted to quantify the intrusion of drill water using a particulate tracer technique described in ODP Technical Note 28 (Smith and others, 2000), except that the extraction of the particulate tracer, fluorescent microspheres, has been modified to increase the sensitivity of the assay by suspending the sediment sample in a solution of saturated NaCl. The solution is centrifuged and the supernatant containing the microspheres is filtered through polycarbonate filters (0.2-µm pore size). The microspheres are

counted, and data are reported as number of microspheres per gram of sediment. The isolation and counting of the microspheres has taken place on shore.

Physical Properties

The determination of physical properties of cored sediments compliments sedimentologic studies, petrophysical analyses, and the interpretation of well logs. They are important to relate gas-hydrate occurrences to geologic controls and the physical nature of the host material. These data are also used to provide modeling parameters, to predict engineering behavior, and to provide baseline information on sediment attributes. Porous media effects have been found to play an important role in the concentration of gas hydrate and physical characteristics of the subsurface influence the nature of fluid and gas migration (see, for example, Expedition 311 Scientists, 2005).

Soon after cores arrived on the catwalk, they were wiped with cloth rags to remove excess water or sediment and were scanned using a track-mounted infrared camera system with an integrated video logging system (fig. 6). These scans recorded the temperature (T) of the outer surface of the butyrate liner. After cutting into 1.5-m-long sections, IR images were obtained of selected core cross sections. Cold spots in the IR images, interpreted to represent dissociating or dissociated gas hydrate, were used to select interstitial water, headspace gas, gas hydrate, and other samples on the catwalk. The IR images were also processed to provide downcore temperature images and plots. The core sections were then moved into the laboratory to equilibrate to room temperature, which typically required 2–4 hours according to core-end-temperature probes. Gamma density, *P*-wave velocity, noncontact electrical resistivity, and magnetic susceptibility were measured using a Multisensor Core Logger-Standard (MSCL-S) provided by Geotek, Ltd. After MSCL logging and thermal conductivity measurements were finished on whole-round core, the core sections were split. Numerous other stand-alone measurements were conducted including:

- Electrical resistivity using a four-pin Wenner array,
- *P*-wave velocity, and
- Shear strengths by mini-vane (fig. 6B), Torvane, and Pocket Penetrometer.

Moisture content and grain density were determined on subsamples after drying and bulk density, porosity, and unit weights were determined from phase relations described in Winters and others (2004).

Selected cores were taken directly from the catwalk for special gas hydrate dissociation experiments and imaging. Methods used to determine *in situ* temperature and to monitor the temperature of cores during acquisition and recovery are also described in this section.

Core Temperature Measurement and Infrared Thermal Imaging

The temperature history of a core sample from *in situ* to shipboard conditions is needed to understand the impact on recovered microbiology, gas hydrate, and other samples. During the coring process, frictional heat is generated, warming the cores by a poorly known and variable amount. Frictional heat is also generated by rotary drilling, even though the bit is being cooled by seawater that is pumped downhole at near-bottom-water temperatures (4–5 °C). During core recovery, the sediments are first exposed to cooler temperatures, with the minimum occurring at the seafloor. Significant warming starts as the cores pass through the ocean's thermocline on the way to the surface, and continued warming occurs once a core arrives on deck. During NGHP Expedition 01, surface seawater and ambient air temperatures were 30 °C and 29 ±3 °C, respectively. Because of these and other complications discussed below, temperatures of marine cores are not commonly measured. However, since the process of core retrieval is fairly uniform, the temperatures at which neighboring cores arrive on the catwalk should be relatively consistent unless there are additional heat sources or sinks. Dissociation of gas hydrate, which is an endothermic process, represents one such heat sink, resulting in anomalous cold spots in the core. Other processes that can lead to cold spots in cores include gas exsolution from pore water and adiabatic expansion of gas.

The primary benefits of using IR cameras include:

- Rapid identification of gas-hydrate-induced temperature anomalies on the surface of the core liner used to guide sampling,
- Quantification of the relative proportions of different gas-hydrate textures,
- Assessment of the thermal structure of entire cores and the differences in thermal structure between APC and XCB cores,
- Estimation of the cross-sectional temperature gradient in cores prior to sampling for microbiology and to support postexpedition thermal modeling of hydrate abundance and dissociation kinetics, and
- Estimation of gas-hydrate concentrations from processed images.

The IR camera is also quicker and simpler to use and has a much higher spatial resolution than an array of thermocouples. The spatial distribution of thermal anomalies observed indicates that the camera can detect small volumes of gas hydrate if they are adjacent to the core liner. Determining quantitative estimates of gas hydrate in cores from the IR data requires substantial postcruise analysis. For NGHP Expedition 01 many of the analyses of the IR data were completed shipboard and concatenated images of each core were made available as prime data for the expedition.

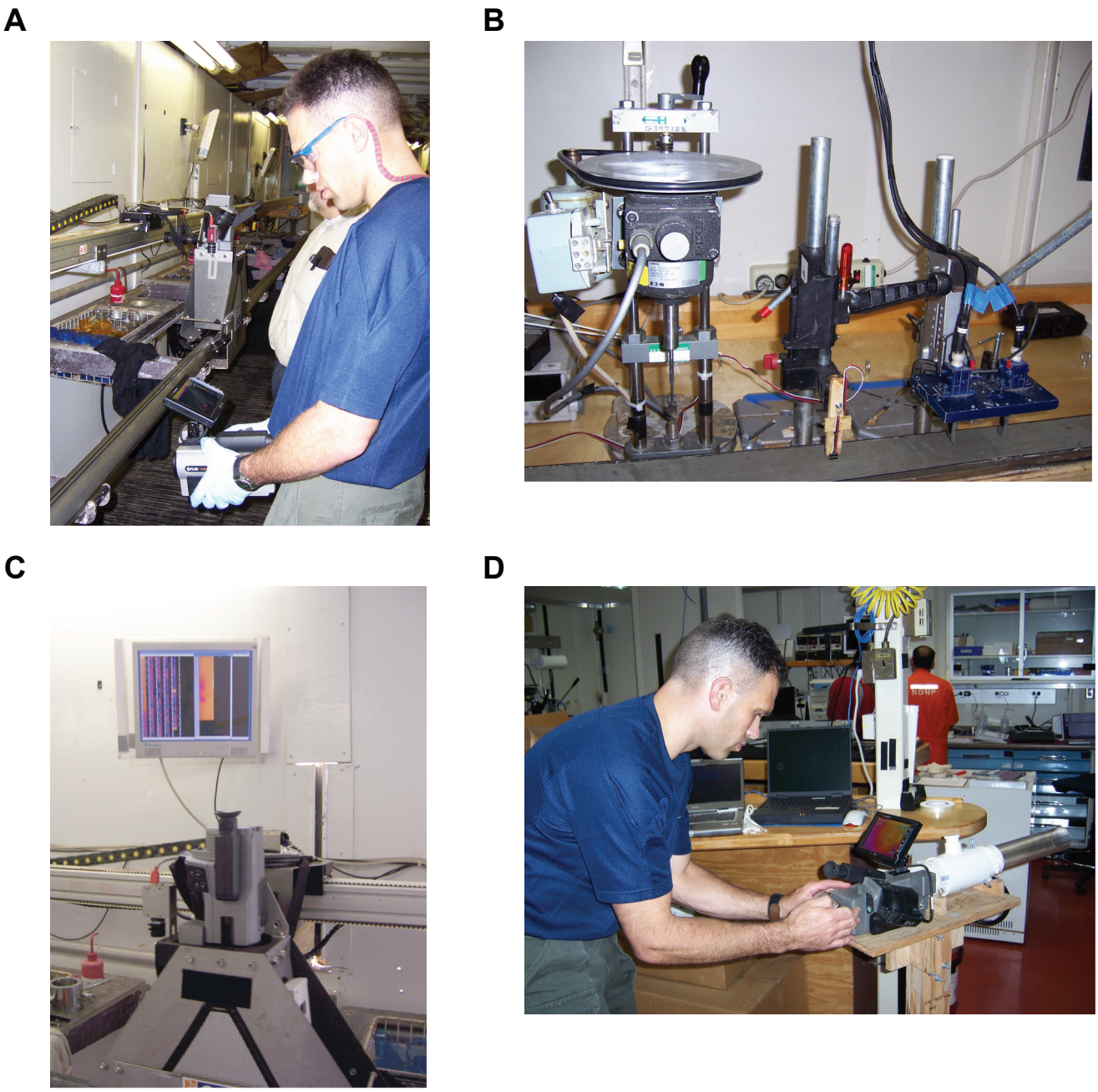

Figure 6. (A) The IR (infrared) track system and hand-held IR camera used during NGHP Expedition 01. The camera on the track is recording the surface temperature of the core liner and is displaying the image in real time on the screens mounted on the wall above the track. The hand-held camera is used to image discrete sections of the core liner. (B) Mini-vane-shear machine (left), electrical resistivity apparatus (center), and *P*-wave velocimeter (right) used to measure properties on split cores. Typically electrical resistivity, velocity, and shear strength are determined in that order. (C) IR camera (foreground) and real-time display showing incremental temperature sections of the core-liner. Darker colors indicate lower temperatures and presumably are the result of the dissociation of larger amounts of gas hydrate or gas hydrate that was closer to the perimeter of the core. Gas exsolution and adiabatic pressure release can also create low temperature anomalies. (D) Hand-held IR camera attached to a device for imaging the cut ends of core sections.

Methodology

During NGHP Expedition 01, a ThermaCam SC 2000 camera (FLIR Systems) was used to map temperature variations along cores. The FLIR System camera provides temperature-calibrated images over a temperature range from –40 °C to 1,500 °C. For shipboard measurements, the camera was set to record a more limited range of temperatures from –40 °C to 120 °C (Range 1). To perform the critical task of rapid identification of gas hydrate within the core on the catwalk, the FLIR System IR camera was mounted on a track above the catwalk and driven automatically by a stepper motor controlled by custom software (fig. 6A). The track and software were provided by Geotek, Ltd. The camera was mounted with the lens 33 cm above the core liner, providing a 15.5-cm field of view along the core. To minimize the effect of external IR radiation reflecting off the core-liner surface, the camera was enclosed in a skate. The entire port side of the catwalk, normally open to the atmosphere, was enclosed with 17-mm thick plywood. Images and data for each core were acquired as the camera was moved along the track in 13-cm increments. During the scan, images were saved in FLIR System proprietary format as bit maps and as temperature arrays. Bit map images and temperature arrays were automatically concatenated and output as single files for analysis. A physical properties scientist, a co-chief scientist, and other personnel on the catwalk observed the scan results by looking at one of four monitors connected to the computer controlling the scan (fig. 6C). The locations of thermal anomalies were identified from the concatenated images on the catwalk monitors and whole-round samples (for example, gas hydrate, pore water, and microbiology samples) were collected as defined by the core-sampling plan for the hole.

The track/core liner-mounted IR imaging camera was supplemented on most cores by discrete imaging using a second SC 2000 camera in a handheld mode to obtain section-end IR images as quickly as possible after the section cuts. These images were collected using a device to mate the camera lens and the core liner, providing a fixed focal length while minimizing stray IR radiation from the catwalk environment (fig. 6D). Images from a section near the middle of the core were commonly collected for each core, and systematically recorded and uploaded to a shipboard data server.

Monitoring the Catwalk Environment

A total of seven temperature measurement devices were deployed on the catwalk. These included five HOBO pendant devices deployed in fixed locations on the catwalk to characterize the ambient thermal, light, and humidity conditions during IR imaging of cores. These data enable corrections to be made to the temperature scaling of the IR images should that prove necessary. These data also provide the ability to adjust core IR temperatures for the presence of potential thermal gradients along the catwalk, although this has not proven to be necessary.

HOBO pendants were deployed at five locations along the core rack, and provide a record of temperature and light intensity as a function of time and position on the catwalk. In addition, a single point mid-way on the catwalk was monitored for both temperature and humidity. Details of the devices and their deployment locations follow. HOBO pendants (T accuracy: ± 0.47 °C; resolution: 0.1 °C; light intensity: 0–320,000 lux with an equivalent response >40 percent of the human eye from 400 to 1130-nm wavelength, Onset Computer Company) were positioned at –0.3, 2.35, 3.9, 6.2, and 7.7 m along the catwalk relative to the top of the core and at ~5 cm below the lower edge of the core liner. In addition, one device that measured and logged both temperature and humidity was attached to the plywood sun shield, 5 m horizontally from the top of the core and ~75 cm above the core (HOBO Pro RH/Temp H08-32-08, T accuracy: ±~0.2 °C, resolution: ±~0.05 °C; relative humidity range, 0–100 percent; drift <3 percent/yr except for when humidity >70 percent, in which case drift can be >3 percent). A similar device was attached to the IR camera skate itself. Prior to processing the first cores and again near the end of NGHP Expedition 01, an ice bath calibration check was performed on most temperature loggers used on the catwalk or for core temperature measurement. All tested devices returned values that were within or significantly better than the manufacturer's specifications.

Monitoring Core Equilibration by Direct Contact Measurement of Core Temperature

Direct measurement of core temperature was made on a routine basis using HOBO weatherproof temperature loggers (HOBO Outdoor/industrial 4-channel External Temperature Logger, H08-008-4, Onset Computer Corporation) and stainless steel sheathed thermocouples (TMC6-HC, ±0.5 °C, accuracy, ±0.41 °C precision, 3 min response time in air, 15 sec response time in stirred water, Onset Computer Corporation) for Legs 3A and 3B. The probes were inserted ~6 cm into the center of the bottom of three to four sections per core. Temperature measurement was started after sections were brought into the core lab for thermal equilibration. Thermocouples were checked for accuracy in water-ice baths prior to the beginning of coring. Full thermal equilibration of cores typically took 2–4 hours and temperature probes were left in the cores until the temperature was > ~18.5 °C. Direct contact temperature probes were typically inserted 8 cm into the bottom of cores on the catwalk immediately after the first IR scan. These probes were left in place as long as possible, usually about ten minutes, while the core was being sampled and cut into sections. The typical temperature probe arrangement was three probes in a straight horizontal line from the perimeter to the center of the core and a fourth probe at the top of the core.

Infrared Image Processing and Extraction of Thermal Anomaly Data

Following initial image concatenation and creation of temperature arrays, temperature images for each core were combined to make montages of downhole temperature anomalies. Temperature arrays for each core were processed in a spreadsheet by averaging cross-core temperatures at a given pixel depth. The outer edges and the central portion of the array are removed to eliminate thermal artifacts along the sides of the core and a central reflection from the IR camera. The resulting averaged temperature at each depth was then concatenated into a downcore array and plotted. Thermal anomalies were identified from downcore temperature profiles. An analysis of shipboard thermal data showed that changes in temperature values indicative of gas hydrate were relatively insensitive to ambient catwalk temperature and illumination conditions. The T values provide an approximate measure of gas-hydrate abundance, albeit influenced by the proximity of gas hydrate to the core liner. Gas hydrate undergoing dissociation and directly in contact with the core liner produces a larger T than gas hydrate insulated from the liner by sediment. It is important to note that depth measurements from the IR scans are relative to uncut core liners, prior to sectioning and removal of voids. Depth assignments of IR temperature anomalies have to be adjusted to precisely match the curated depths of core sections during postcruise analysis.

Correlation of Infrared Thermal Anomalies with Interstitial Water Chlorinity Anomalies and Headspace Gas Composition

Selection of catwalk samples for interstitial water (IW) chemistry was, in part, based on IR anomalies. For selected IW samples, IR images and visible digital images were taken in the Chemistry Lab to identify internal parts of the sample that were still cold. Subsampling was then more selective for parts of the sample formerly containing gas hydrate. For most of the samples, gas hydrate had already dissociated, but the thermal signal was almost always obvious. Each core sampled for IWs was also sketched to show which sections were background and which ones were hydrate samples based on the IR images.

Multisensor Core Logger (MSCL)

The MSCL–S (Standard) had four physical property sensors mounted on an automated track (fig.) that sequentially measured bulk density using gamma ray attenuation (GRA), *P*-wave velocity (V_p), non-contact electrical resistivity (NCR), and magnetic susceptibility (MS) (fig. 8). MSCL measurements are nondestructive to sediment fabric and are used to compare sediment from adjacent or distant holes. Data quality is a function of both core quality and sensor precision. Optimal MSCL measurements require a completely filled core liner with minimal drilling disturbance. Precision is a function of measurement time for MS, non-contact electrical resistivity, and GRA density but not for V_p. Technical notes on the Multisensor Core Logger and sensors are available from Geotek, LTD. (2007).

Core sections logged on the MSCL were measured at an interval of 2 cm for gamma ray attenuation (GRA), density, and *P*-wave velocity. A spatial resolution of 4 cm was used for the noncontact resistivity and magnetic susceptibility. For each measurement, magnetic susceptibility and NCR data were collected for 10 seconds while GRA density data was collected for 6 seconds.

Calibrations for each sensor were completed prior to logging each site. Three standards (deionized (DI) water, Bartington Magnetic Susceptibility check piece, and water with a salinity of 17.5 ppt; fig. 9) were run at the beginning of each core to confirm measurement accuracy and check for sensor drift.

Gamma Ray Attenuation Density

Gamma density was measured through the center of the core using a 10mCi ^{137}Cs source and a NaI scintillation detector. The detection energy window is set to measure only primary (unscattered) gamma photons (0.662 MeV), providing raw gamma attenuation data in counts per second. Gamma density is derived from gamma attenuation and is reported as g/cm^3. The gamma beam is collimated through a 5-mm hole providing a downcore spatial resolution of about 1 cm. The precision is a direct function of total counts and hence is dependent upon the count time used (1 s) and the core thickness and density.

Although the empirical calibration procedure for GRA is based on bulk density measurements (that is, of a known graduated aluminum and water standard), the measurements will vary from true gravimetric bulk density because of variations in mineralogy. Gamma attenuation coefficients for different materials vary as a function of atomic number. Fortuitously, most earth-forming minerals have similar low atomic numbers (like those of aluminum). Consequently, the correlation of GRA density and bulk density is usually very good.

GRA data are of highest quality when measured on nongassy APC cores because the liner is typically filled with sediment. GRA measurements on XCB cores may exhibit more variability because of disturbance caused by rotary coring which tends to form alternating hard “biscuits” and softer ground-up “infilling” material.

Compressional-wave Velocity

Compressional-wave velocity (V_p) was measured on the MSCL track with the *P*-wave logger (PWL). The PWL transmits a 500-kHz *P*-wave pulse through the core at a specified repetition rate. Ultrasonic velocity is measured using a pair of Geotek Acoustic Rolling Contact Transducers. The travel

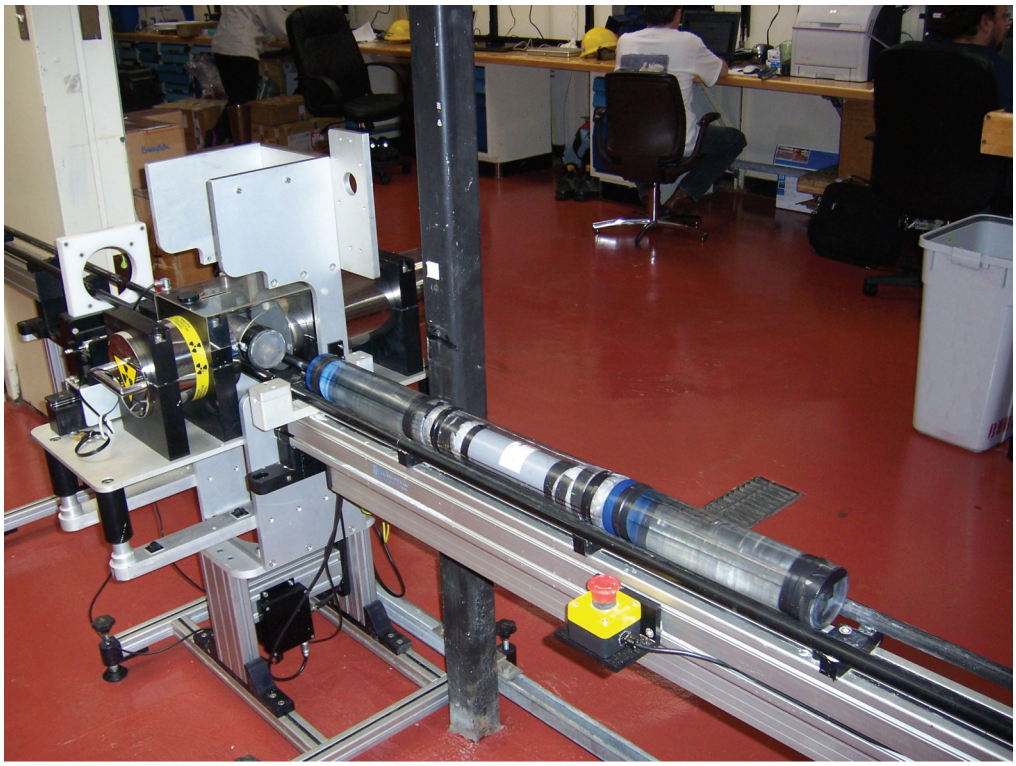

Figure 7. Multisensor Core Logger (MSCL) with calibration standards on the track and measuring sensors on the left.

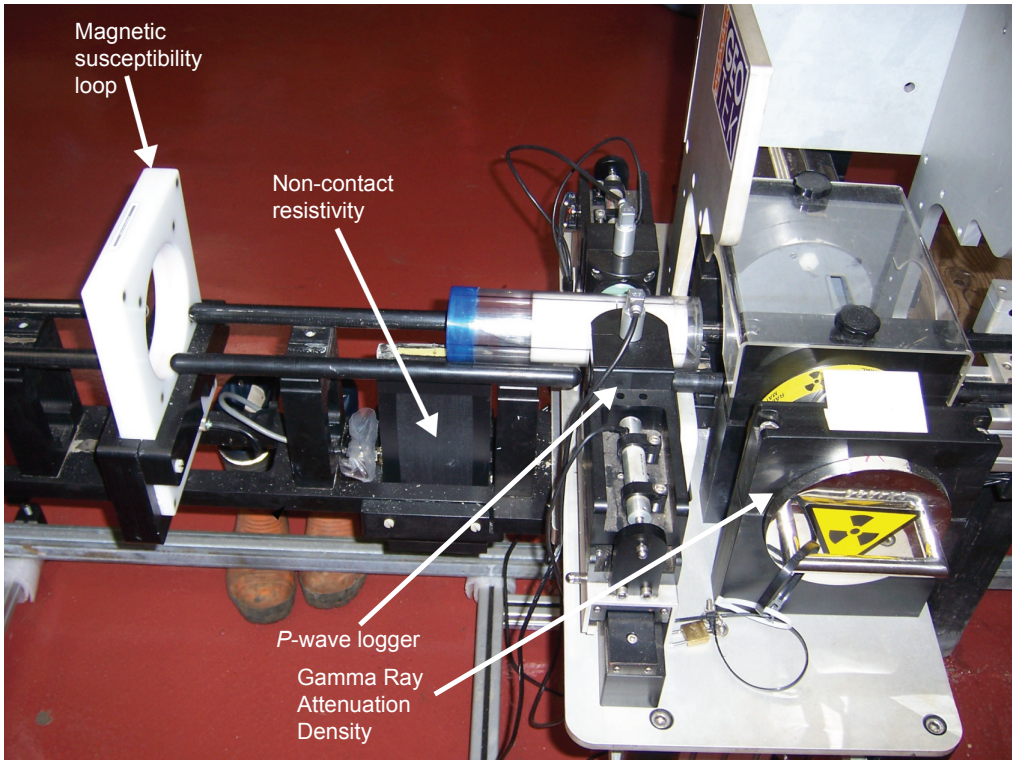

Figure 8. Instruments on the Multisensor Core Logger (MSCL) used during NGHP Expedition 01, include (right to left) gamma ray densitometer (right), *P*-wave velocimeter, non-contact electrical resistivity device (below the core end cap), and magnetic susceptibility loop.

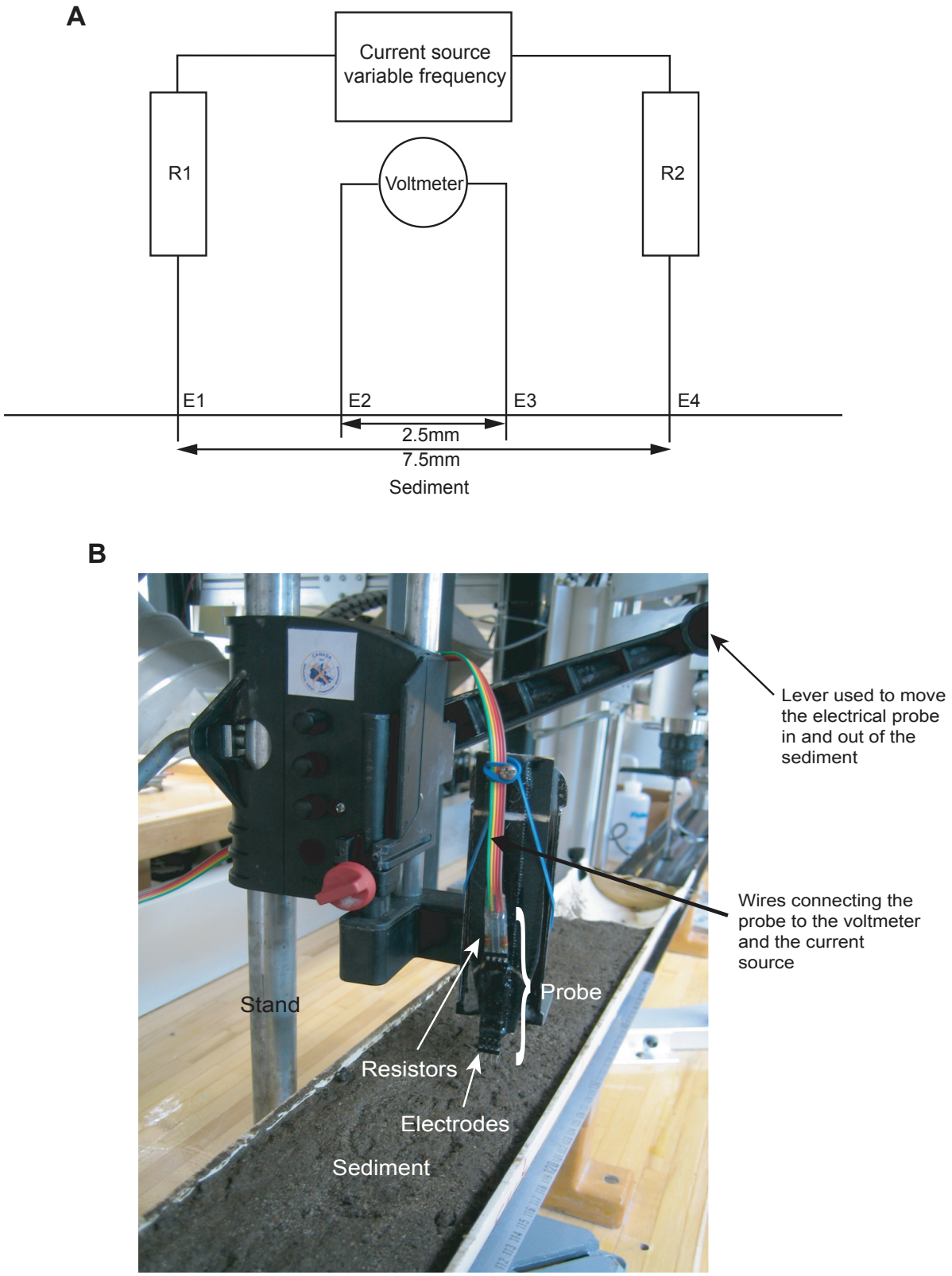

Figure 9. (A) Split-core electrical resistivity measurement system. Current is passed between electrodes E1 and E4 and the potential difference is measured between E2 and E3. R1 and R2 are 5 k ohm resistors. (B) Photo of the electrical resistivity setup. In this photo, the probes are shown perpendicular to the core. During NGHP Expedition 01 the probes were oriented parallel to the axis of the core. [mm, millimeters]

time for wave pulse propagation through the core diameter is measured with a precision of 50 ns. At the same time, the core diameter is measured using a set of displacement transducers (precision 0.02 mm) that are mechanically coupled to the acoustic transducers. This produces an ultrasonic velocity with a precision of ± 1.5 m/s and a likely accuracy of ~ 5 m/s. Core temperatures are obtained with a platinum resistance temperature probe (precision 0.05 °C) and a measured velocity is corrected to a velocity at a reference temperature (20 °C). Ultrasonic velocity is reported in m/s and has a typical downcore resolution of about 2 cm.

Noncontact Resistivity (NCR)

Electrical resistivity is measured with the Geotek, Ltd. NCR sensor, containing inductive coil arrays which make resistivity measurements through whole plastic core liner. The NCR technique operates by inducing a high-frequency magnetic field in the core from a transmitter coil, which in turn induces electrical currents in the core that are inversely proportional to the resistivity. A receiver coil measures very small magnetic fields that are regenerated by the electrical current. To measure these very small magnetic fields accurately, a difference technique has been developed that compares the readings generated from the measuring coils to the readings from an identical set of coils operating in air. As with other parameters, the measurements are sensitive to core temperature and should be obtained in a stable temperature environment for best results. Electrical resistivity is reported in ohm-m with an accuracy of about ±5 percent and integrates over a core length of ~3–4 cm.

Magnetic Susceptibility

Magnetic susceptibility is measured with a 13.0 cm (Legs 1, 3A, and the later part of 4) and an 8.0 cm (Legs 3B and the initial part of 4) diameter Bartington loop sensor. The frequency of the low-intensity, alternating- magnetic field produced by the sensor is sensitive to changes in the magnetic susceptibility of material within about 6.0 cm (for the 13.0 cm diameter loop) or 4 cm (for the 8.0 cm loop) on either side of the loop. Data were masked out to account for this effect at section ends and at locations of significant voids determined by both visual inspection of the cores as well as by anomalously low gamma density values (<1.3 g/cc). Magnetic susceptibility, a dimensionless number, is reported as corrected volume susceptibility in SI units with an accuracy typically ~±4 percent.

Thermal Conductivity

Thermal conductivity measurements on whole-core samples were made using a TK04 (Teka Bolin) system described by Blum (1997). One measurement was made on each core. The measurement system employs a single needle probe (von Herzen and Maxwell, 1959) heated continuously in "full-space configuration." The thermal conductivity needle, containing a heater wire and calibrated thermistor, was calibrated before leaving the manufacturer. It was tested on a material of known thermal conductivity (red rubber) prior to use and produced results within acceptable specifications. Four measurements were taken on each measured section and final thermal conductivity values are the average of the best three out of four measurements.

At the beginning of each measurement, temperatures in the samples were monitored automatically, without applying a heater current, until the background thermal drift was <0.04 °C/min. Once the samples equilibrated, the heating circuit was turned on and the temperature rise in the probe was measured. The temperature of the probe has a linear relationship with the natural logarithm of the time after the initiation of heating:

$$T(t) = (q/4k)\ln(t) + C$$

where

T = temperature,
q = heat input per unit length per unit time,
k = thermal conductivity,
t = time after the start of heating, and
C = constant.

The thermal conductivity (k) was determined by fitting the temperatures measured during the first 150 s of each heating experiment (for details see Kristiansen, 1982; Blum, 1997). Data are reported in W/(m×K), with measurement errors of 5–10 percent in high-quality cores. Measured values are compared to a best-fit equation for thermal conductivity of sediment from the Cascadia accretionary prism and Nankai Trough (Davis and others, 1990):

$$k = 1.07 + (5.86 \times 10^{-4} \times D) - (D^2 \times 3.24 \times 10^{-7})$$

where

k = thermal conductivity, and
D = depth below the seafloor [m].

Contact Electrical Resistivity Measurements

Within the physical properties laboratory, electrical resistivity was the first of the contact measurements made on the working half of split cores. This prompt processing minimized evaporation of porewater. Split cores were sometimes wrapped in cellophane after cutting to further decrease water loss.

The measuring device consisted of a four-pin Wenner array and a digital temperature probe (fig. 9). The pins were gold plated and approximately 3 mm in length, separated from each other by 2.5 mm. The outer two pins were connected to a circuit board with an AC voltage source acting through current limiting resistors. The inner two pins were connected to a Fluke voltmeter. The entire instrument was connected to a PC through an RS–232 output thus allowing all raw data processing and display to be automated.

The probe was pushed into the sediment and a direct current (DC) 90 Hz square wave of 18 volt amplitude with a 10 k-ohm resistance (that is, 1.8 mA current) was sent between the outer two electrodes. The sediment resistivity was derived by measuring the voltage between the two inner electrodes. An alternating current (AC) was used rather than a DC current to prevent charge build-up around the electrodes and unwanted electrochemical effects. The temperature of the sediment was also recorded so that the resistivity of the sediment could be corrected to a temperature of 20 °C

Electrical resistivity, *R*, is defined by the following formula:

$$R = \frac{V}{I * C}$$

where

V = voltage,

I = current, and

C = a cell constant.

The cell constant was determined using standard seawater with a known resistivity, *Rw*, which can be described by the following formula:

$$Rw = (2.8 + 0.1 \times T)^{-1}$$

where

T = temperature in °C.

Measurement of the temperature, voltage, and current allows the cell constant to be determined. The instrument is thus calibrated by adjusting the cell constant until *Rw* equals 0.209 ohm-meters (the resistivity of Standard Mean Ocean Water (SMOW) with a salinity of 34.992 ppt) for a temperature of 20 °C.

Sample resistivity, *Ro*, was derived using the following formula:

$$Ro = R \times (1 + 0.025 \times (T - 20))$$

where

R = the measured sample resistivity, uncorrected for temperature, and

T = the temperature in °C.

Electrical resistivity was measured along split cores every 10–20 cm in the top of cores and less frequently in the presence of expansion cracks and voids deeper in the core. The probe was set up so that it was perpendicular to the bedding (that is, parallel to the core). Measurements were omitted if the sediment was visibly altered during core recovery or if evidence of gas expansion was present.

When results became erratic, the electrodes were replaced. The probe electrodes were also washed in distilled water and dried before calibrating. The system was calibrated daily.

Directional *P*-wave Measurement

P-wave velocity was measured parallel to the longitudinal axis of split cores by measuring the travel time between two fixed-distance, spade-mounted ultrasonic transducers that were inserted into the sediment (fig. 10). A Velocity Test Unit (VTU) provided an impulse-type bi-phase excitation voltage to the transmitting transducer and conditioned the received signal. Resonant frequencies of the transducers are approximately 425 kHz. Acoustic signals and core temperature measured using a Fluke 45 dual-display multimeter were displayed using a Labview program which allowed the first motion to be manually picked. Once-a-day calibrations using distilled water, adjusted for temperature, accounted for system-induced time delays. *P*-wave measurements were made on each split core section until the acoustic signal could not be accurately detected by the receiving transducer. *P*-wave velocities were generally more reliable in shallow core sections. Cores from deeper in the subsurface often contained cracks and voids due to gas expansion, causing the instrument to give unreliable results.

Mini-vane Shear Strength

Miniature-vane shear tests were performed at approximately 1.25-m intervals down core with a Wykeham-Farrance model 23500 vane shear machine and a 12.7-mm diameter by 12.7-mm high four-bladed vane (fig. 11). The vane shear-strength tests were performed proximal to the sites of the electrical resistivity and V_p measurements (fig. 12). The vane was inserted one vane height deep into the sediment and was turned at 90° per minute by applying a constant rotation rate to the top of a Lebow torque sensor. Voltages representative of torque values were recorded in analog form using a Daytronic strain-gage conditioner.

Peak, residual, and remolded vane shear strengths were determined at each test location. Residual strength was determined after 90° of vane rotation and remolded strength was determined after quickly rotating the vane through an additional complete 360° rotation. If cracking, which reduces the strength of the sediment, was observed during shear, the measurement was omitted.

Torvane Strength

A Torvane device was used to measure shear strength near the exposed sediment surface of split cores. This device is operated by inserting adapters 5 mm into the exposed sediment surface. The top of the spring-loaded Torvane is rotated thereby producing a torque that shears the sediment (fig. 13). A pointer records the maximum torque value, which is proportional to the shear strength. One full revolution of the Torvane top produces a shear strength value of approximately 100 kPa.

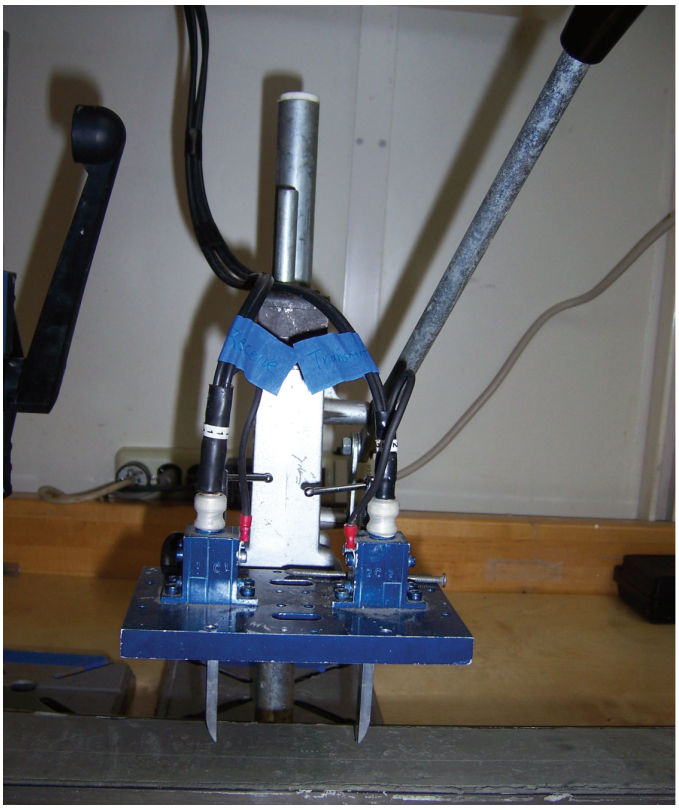

Figure 10. *P*-wave velocimeter with spade probes about to be inserted into a section of split core. The right spade contains a *P*-wave transmitting transducer and the left spade contains a receiving transducer.

The Torvane comes in three diameters, 19, 25, and 48 mm, which measure a maximum shear stress up to 20, 100, and 250 kPa, respectively. Each size records on a continuous scale of 0–10 units, and measurements are multiplied by approximately 2, 10, and 25, respectively to obtain shear strength in units of kPa.

Pocket Penetrometer Strength

In addition to the mini-vane and Torvane tests, a Pocket Penetrometer was also used to determine shear strength (fig. 14). This device consists of a 6.35-mm diameter spring-loaded plunger that is pushed to a depth of 6.35 mm into the exposed sediment surface. A direct reading scale indicates the unconfined compressive strength (UCS) in kg/cm^2. The maximum shear strength that can be determined with this device is 220 kPa.

Pocket penetrometer shear strength (Spp) is determined from:

$$\text{Spp (kPa)} = \text{UCS (kg/cm}^2\text{)} \times 49$$

where

UCS = the unconfined compressive strength reading from the pocket penetrometer strength scale.

If very soft sediment was tested, a 25.4-mm diameter adapter was applied to the end of the plunger. The maximum shear strength that can be determined with the adapter is 13.8 kPa.

If this adapter was used, the shear strength, Spp, is determined from:

$$\text{Spp (kPa)} = \text{UCS (kg/cm}^2\text{)} \times 3.1$$

where

UCS = the unconfined compressive strength reading from the pocket penetrometer strength scale.

Moisture and Density Analysis

Moisture and density analysis (MAD) was used to measure wet mass, dry mass, and dry volume to determine moisture content, grain density, bulk density, porosity and void ratio, as described in Blum (1997). Sample plugs of ~10 cm^3 were placed in 10-mL beakers. Care was taken to sample undisturbed parts of the core and to avoid drilling slurry. One sample per section was taken at or near the location of

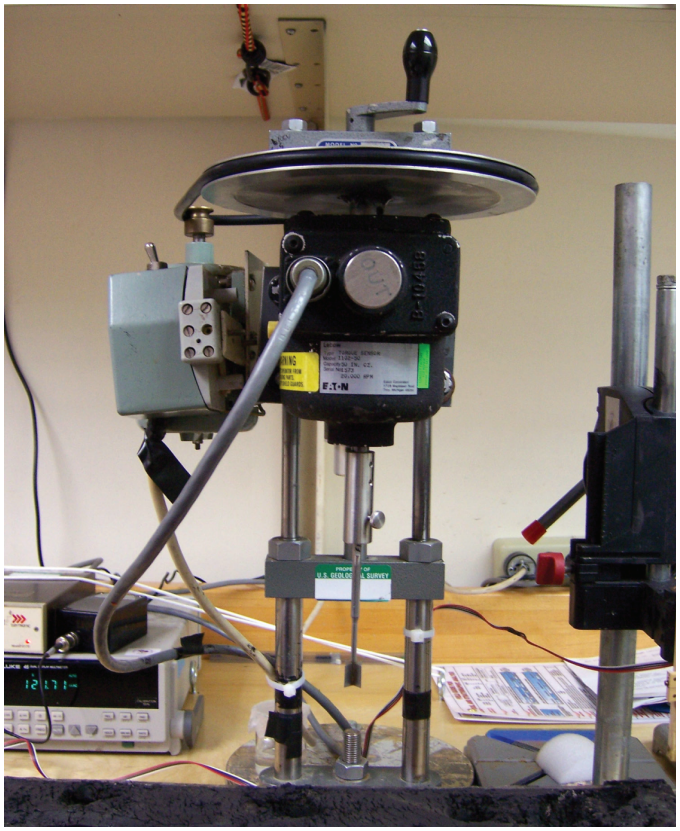

Figure 11. Mini-vane-shear machine with a 12.7-millimeters diameter by 12.7-millimeters high vane attached to a torque sensor. A test is performed by inserting the vane into the sediment and applying a torque to the top of the torque sensor through a drive belt attached to an electric motor. Recorded torque is proportional to the sediment shear strength.

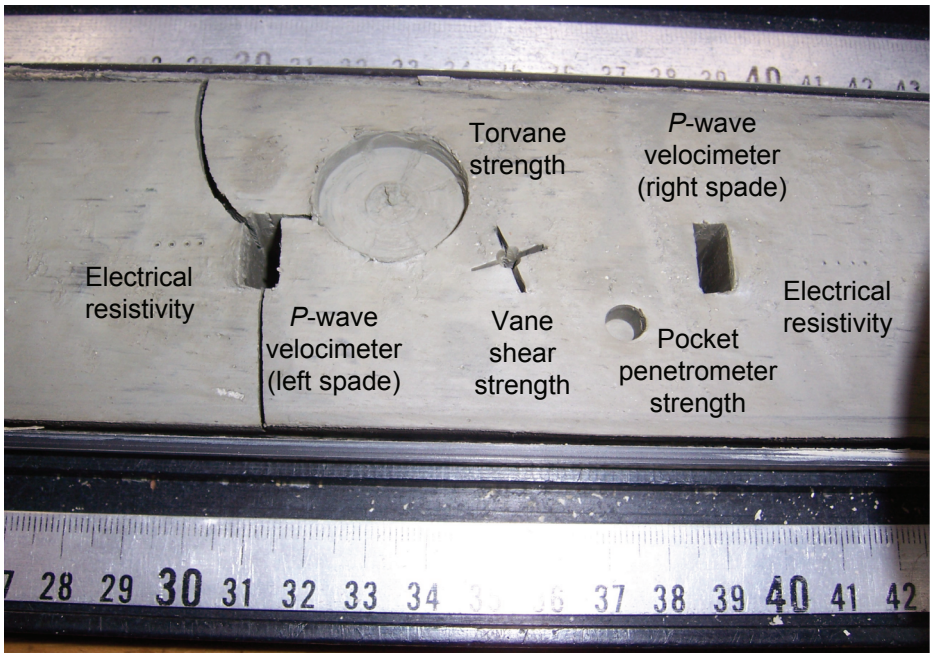

Figure 12. Artifacts of physical property testing in a core section. Test performed (from left to right) are: electrical resistivity using a four-pin Wenner array, *P*-wave velocity (left spade), Torvane (regular adapter), vane-shear strength, Pocket Penetrometer (no adapter), right spade of the *P*-wave velocimeter, and another electrical resistivity using a four-pin Wenner array.

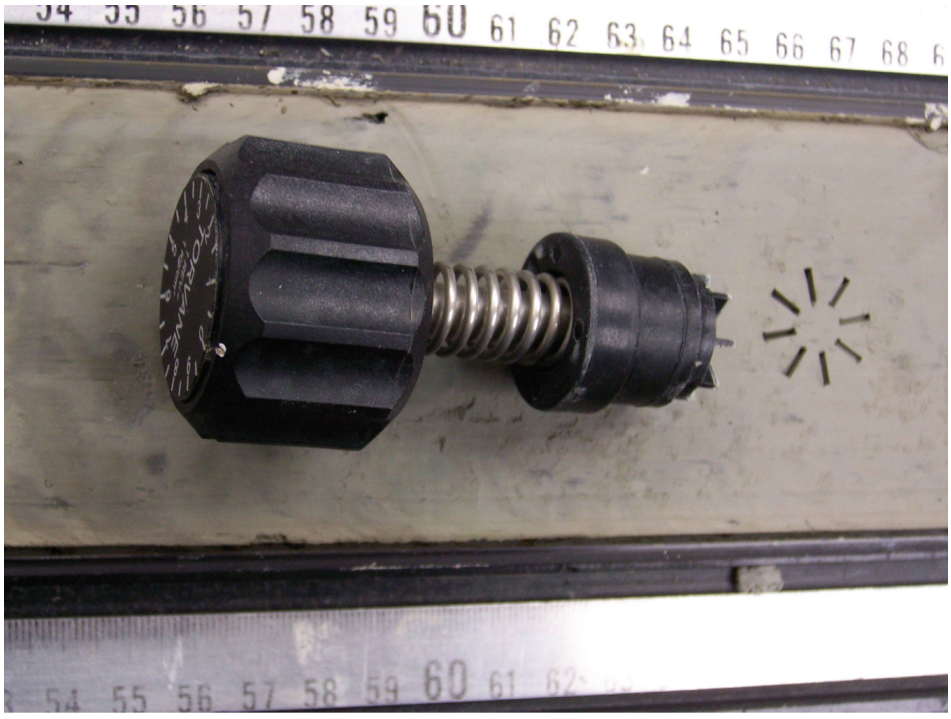

Figure 13. Torvane with regular adapter attached. Notice the blade orientations in the surface of the sediment. This test was not actually performed at this location in the core.

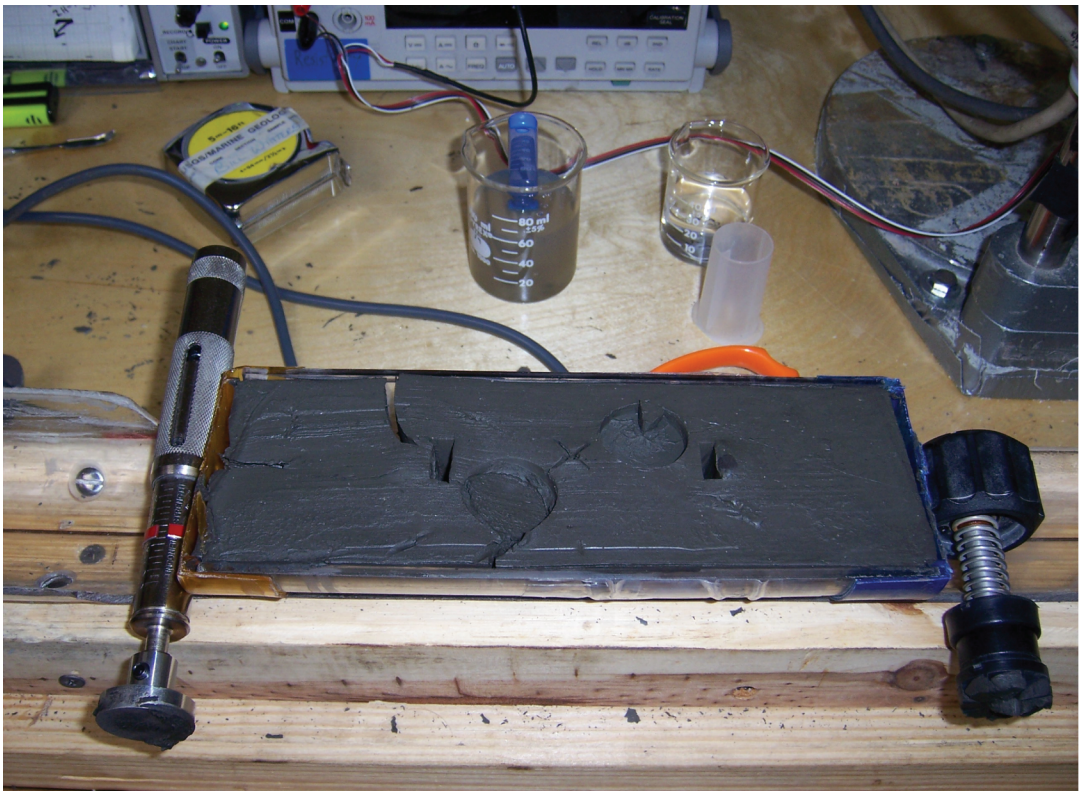

Figure 14. Pocket penetrometer (left) and Torvane (right) strength-measuring devices. The pocket penetrometer is pushed straight down into the sediment thereby depressing a plunger. The amount of force required to penetrate the sediment is related to its strength. The top of the Torvane is rotated and the torque required to shear the sediment in contact with the blades is related to the shear strength.

other physical property measurements. Immediately after the samples were collected, wet sediment mass was measured. Dry mass and volume were measured after samples were heated in an oven at 105 ±5 °C for 24 hours and allowed to cool in a desiccator. Sample mass was determined to a precision of 0.01 g using two Scientech 202 electronic balances and a computer averaging system to compensate for ship motion (fig. 15). The balance system was supplied by Dr. Tim Brewer of the University of Leicester, UK, and a similar backup system was provided by Mr. Brad Julson and Mr. William Mills of IODP.

After drying, the volume of dried solids was determined with two automatic gas pycnometers using helium as the purge and expansion gas (fig. 16) (ASTM, 1997). The grain density of the pycnometer specimen was calculated using the mass of solids that was determined immediately prior to insertion of the sample into the pycnometer. All mass determinations were made quickly to prevent moisture in the air from being absorbed by clay minerals.

The balance system was calibrated while the ship was in port and as stable as possible. Calibrations were performed daily on the two pycnometers and a sample of known density was run periodically to evaluate instrument performance.

All physical property calculations, except those specified, were corrected for the presence of residual salt left on the solid particles after driving off the pore fluid by oven drying. In the natural environment, salt and other particles that are dissolved in the pore fluid behave as part of the aqueous phase. The calculations remove the salt precipitate mass and volume from the solids and add it back to the fluid phase. Average salinity values for each core were used for the corrections. A default 35 ppt value was assumed for cores without salinity measurements. Sediment phase relations were back calculated assuming 100 percent water saturation of the pore voids. Visible drainage from the core sections at sea was rarely observed, primarily because of the fine-grained nature of the sediment.

The following equations were used in calculating the physical property values (from Winters and others, 2004):

$$rd = Ms/Vt$$

where

rd = the dry bulk density,
Ms = the mass of solid sediment grains, and
Vt = the calculated total specimen volume;

$$rw = Mt/Vt$$

where

rw = the wet bulk density,
Mt = the total mass of the specimen, and
Vt = the calculated total specimen volume;

Figure 15. Marine-going balance systems incorporating a dual load-cell design. A reference mass is placed on one cell and a beaker containing a sediment sample of unknown mass is placed on the other.

$$rs = Ms/Vs$$

where

rs = the corrected grain density,
Ms = the mass of solid sediment grains without salt, and
Vs = the volume of the sediment grains without salt measured with a gas pycnometer;

$$n = Vsw/(Vs + Vsw)$$

where

n = the porosity based on calculated specimen volume,
Vsw = the volume of seawater, and
Vs = the volume of solid sediment grains;

$$e = Vv/Vs$$

where

e = the void ratio,
Vv = the volume of voids, and
Vs = the volume of solid sediment grains;

$$WCt = Msw/Mt$$

where

WCt = the corrected water content based on the total specimen mass,
Msw = the mass of sea water in the void space, and
Mt = the total mass of the specimen;

$$WCs = Msw/Ms$$

where

WCs = the corrected water content based on the solid grain mass,
Msw = the mass of sea water in the void space,
Ms = the mass of the solid sediment grains without residual salt.

In situ Temperature

Various downhole temperature tools were used during NGHP Expedition 01. The Advanced Piston Corer Temperature Tool (APCT) fits into the cutting shoe of the APC and measures temperature during regular piston coring. We also used a new generation of this tool (see "Advanced Piston Corer Temperature Tool 3(A)") that was developed by A. Fisher and H. Villinger. In more indurated sediments where piston coring is not possible, we used the Davis-Villinger Temperature Probe (DVTP).

At the beginning of the cruise, an ad hoc calibration of all the tools was performed by submerging the tools in an ice-water bath (see Appendix 4). This test revealed temperature offsets for all tools except for the APCT-3. Offsets from 0 °C are: APCT #10: –0.65 °C; APCT #16: –0.45 °C, APCT-3: 0 °C; DVTP (T1): –0.50 °C; DVTP (T2) +0.92 °C. The uncorrected and corrected *in situ* temperatures are given in the tables found in the site chapters. The uncertainty in the ad hoc calibration correction determined from the ice bath is

Figure 16. Two gas displacement pycnometers used to measure the volume of solid sediment samples. The apparatus on the left can measure one sample at a time, whereas the right machine can measure 5 samples concurrently. Grain density is calculated by dividing the known mass of sediment by the volume of sample determined using a pycnometer.

not included in the estimated uncertainty of the measurements because it may not remain constant during an experiment, as indicated by an apparent change in the correction for DVTP (T2) during the course of the expedition.

Uncertainties in Extrapolated *In situ* Temperatures and Temperature Gradients

Because of the large scatter in the measured thermal conductivity, which is typical in gas-rich sediments, a thermal conductivity of 0.95 W/(m×K), with an uncertainty of 0.1 W/(m×K) was assumed when extrapolating observations to *in situ* conditions. An uncertainty of 0.1 W/(m×K) in thermal conductivity results in an uncertainty of ~0.02 °C in the extrapolated *in situ* temperature in this range of thermal conductivity. Perturbation of multiple free parameters to find the thermal conductivity that minimizes residuals has not yet been done, as was done for Leg 204 (Trehu, 2006).

A description of data quality is given in the site chapter tables. A good-to-excellent quality measurement will show a sharp frictional pulse when the probe was inserted into the sediments and a similar strong frictional pulse when it was extracted. Temperature decay between insertion and extraction should be smooth. Such observations were classified as very good or excellent. Many of the measurements made during this expedition showed one or more secondary frictional pulses between insertion and extraction. These were classified as fair or good, depending on the number and magnitude of secondary frictional events. Data that did not show a good frictional pulse on insertion and subsequent temperature equilibration were classified as poor and were not used for calculating thermal gradients.

The probes measured the temperature of the water just above the seafloor. While these measurements are useful for detecting inconsistencies between different tools, the bottom water temperature on continental margins can change daily by a few tenths of a degree due to tidal currents. The bottom water temperature was therefore not used in calculations of the thermal gradient at each site. Instead, the calculated seafloor intercept can be compared to the observed bottom water temperature as a check on validity of modeling the thermal profile as a linear gradient.

Advanced Piston Corer Temperature Tool (APCT)

The APCT tool (fig. 17) consists of electronic components, including battery packs, a data logger, and a platinum resistance-temperature device calibrated over a temperature range of 0–30 °C. Descriptions of the tool and data analysis principles can be found in Graber and others (2002). The thermal time constant of the cutting shoe assembly where the APCT tool is inserted is ~2–3 min. The only modification to normal APC procedures required to obtain temperature

measurements is to hold the corer in place 5–10 min near the seafloor to record bottom water temperatures and to hold it for ~10 min in the hole after cutting the core. During this time, the APCT tool logs temperature data on a microprocessor contained within the instrument as it approaches equilibrium with the *in situ* temperature of the sediments. The tool can be preprogrammed to record temperatures at a range of sampling rates. A sampling rate of 10 s was used during NGHP Expedition 01 Legs 3A, 3B, and 4. A calibration test was performed prior to the beginning of Leg 3A using an ice chest at 0 °C (see Appendix 4).

Advanced Piston Corer Temperature Tool 3 (APCT-3)

The APCT-3 (fig. 18; Heesemann, and others, 2006) was designed to be a replacement for the APCT, which is no longer supported by the manufacturer. Like the APCT tool, the APCT-3 fits into the cutting shoe of the APC. Data are recorded in solid-state memory. Temperature is measured with a termistor located at the end of a spike at the toe of the cutting shoe. The larger memory capacity compared to the APCT allows for a finer sampling rate (up to 1 Hz).

The APCT-3 was calibrated at 0 °C using an ice chest (see Appendix 4). It was calibrated over the range of 2–10 °C in a controlled water bath prior to IODP Expedtion 311 (Heeseman, and others, 2006).

Davis-Villinger Temperature Probe (DVTP)

The DVTP (fig. 19) is described in detail by Davis and others (1997) and summarized by Graber and others (2002). The probe is conical and has two thermistors. The first is located 1 cm from the tip of the probe and the second is 12 cm above the tip. A third thermistor is in the electronics package. Thermistor sensitivity is 1 mK in an operating range of –5 to 20 °C. In addition to the thermistors, the probe contains an accelerometer sensitive to 0.98 m/s^2. The accelerometer data are used to track disturbances to the instrument package during the equilibration interval. Data were recorded with a sampling rate of 3 s.

Unlike the APCT and APCT-3 tools, the DVTP requires a dedicated tool run, which consists of lowering the tool by wire line to the mudline where there is a 5–10 min pause to collect temperature data within the drill pipe. Subsequently, it is lowered and latched in at the bottom of the drill string with

Figure 17. Advanced Piston Corer Temperature Tool (APCT) consists of electronic components, including battery packs (in the foreground), a data logger, and a platinum resistance-temperature device calibrated over a temperature range of 0° to 30 °C. The only modification to normal APC procedures required to obtain temperature measurements is to hold the corer in place 5–10 min near the seafloor to record bottom water temperatures and to hold it for ~10 min in the hole after cutting the core.

Figure 18. Advanced Piston Corer Temperature Tool 3 (APCT–3) replaces the APCT. Like the APCT tool, the APCT-3 fits into the cutting shoe of the APC. Data are recorded in solid-state memory. The larger memory capacity compared to the APCT allows for a finer sampling rate (up to 1 Hz). Notice the smaller batteries (in the front of the electronics housing) compared to the batteries used in the APCT.

the end of the tool extending 1.1 m below the drill bit. The extended probe is pushed into the sediment below the bottom of the hole and temperature is recorded for 10–20 min. Upon retrieval, a second stop of 5–10 min is made at the mudline.

Advanced Piston Corer Methane Tool (APCM) and Pressure Core Sampler Methane Tool (PCSM)

The APCM (fig. 20) and the PCS methane tool (PCSM) continuously record the temperature, pressure, and electrical conductivity changes in the core headspace from the time the core is cut through its ascent to the rig floor, and are derivatives of MBARI's Temperature-Pressure-Conductivity (TPC) tool. The origin of the tool's name is derived from its initial deployments to study gas hydrates which typically contain methane. However, in reality, the tool does not sense the presence of methane itself. The APCM sensors are mounted in a special piston head on the standard APC piston, and the data acquisition electronics are embedded within the piston. The PCSM is a slimmed-down version of the APCM tool and is mounted on the top of the PCS manifold mandrel. Both tools operate passively and require little shipboard attention. Variations in the relative amounts of *in situ* gas and gas hydrate can be determined from the pressure and temperature behavior during core recovery (Ussler and others, in press).

The tools consist of an instrumented sensor head with the electronics and battery pack housed in a sealed case. The three sensors (temperature, pressure, and conductivity) and a data port are packaged in the face of the 2-in-diameter (5.08 cm) sensor head. The temperature sensor has an accuracy of ±0.05 °C. The pressure sensor is a 0- to 10,000-psi (0–68.95 MPa) "Downhole Series" transducer with a ±0.15 percent full-scale accuracy that is especially designed for temperature stability. The electrical conductivity sensor is a three-pin bulkhead connector with an inconel body and gold-plated 0.040 in (10 mm) diameter Kovar pins.

Thermal Data Reduction

Similar data reduction procedures were used for all temperature tools. Because equilibration to *in situ* temperatures takes much longer than the ten minutes during which the instrument records subseafloor temperature, extrapolation based on the theoretical impulse response of the tools is required. The transient thermal decay curves for sediment thermal probes are a function of the geometry of the probes and the thermal properties of the probe and the sediments (Bullard, 1954; Horai and Von Herzen, 1985). Analysis of data requires fitting the measurements to model decay curves that are based on tool geometry, sampling interval, and tool and sediment thermal properties. For the APCT and APCT-3 tools, decay curves based on the model of Horai and Von Herzen (1985) were used, as implemented in the software program TFIT. A new, more accurate, numerical model for the impulse response of the APCT-3 is currently under development by M. Heesemann. For the DVTP tool, the impulse response of Davis and others (1997), as implemented in the software program CONEFIT, was used.

It is generally not possible to obtain a perfect match between the model temperature decay curves and the data because

- The probe does not reach thermal equilibrium during the penetration period;
- Contrary to ideal theory, the frictional pulse upon insertion is not instantaneous; and
- Temperature data are sampled at discrete intervals, so that the exact time of penetration is uncertain.

Additional uncertainty in the *in situ* temperature occurs because of tradeoffs between sediment thermal conductivity, penetration time, and temperature, and because of poorly understood effects related to the presence of gas hydrate (Trehu, 2006).

Figure 19. Davis-Villinger Temperature Probe (DVTP) that is used to measure temperature in the bottom of the drill hole. The device contains two thermistors: one is 1 cm from the tip of the probe and the second is 12 cm above the tip. Thermistor sensitivity is 1 mK in an operating range of –5 to 20 °C. In addition to the thermistors, the probe contains an accelerometer sensitive to 0.98 m/s^2. The extended probe is pushed into the sediment below the bottom of the hole and temperature is recorded for 10–20 min.

Paleomagnetism

Discrete samples were collected from working halves of split-core sections in round containers marked with arrows pointing upcore. Routine sampling intervals were once in every core section or every 50 cm in high-resolution cores. Areas of deformation were avoided. The samples were stored in sample bags and flushed with N_2 before being sealed and stored at 4 °C. All discrete samples were analyzed postcruise by Randolph Enkin, National Resources Canada.

Figure 20. Advanced Piston Corer Methane Tool (APCM) records temperature, pressure, and electrical conductivity changes in the core headspace from the time the core is cut through its ascent to the rig floor, and was derived from MBARI's Temperature-Pressure-Conductivity (TPC) tool. The origin of the tool's name is derived from its initial deployments to study gas hydrates which typically contain methane. However, in reality, the tool does not sense the presence of methane itself. The APCM sensors are mounted in a special piston head on the standard APC piston, and the data acquisition electronics are embedded within the piston. The Pressure Core Sampler Methane Tool (PCSM) (not shown) is a slimmed-down version of the APCM tool and uses the same electronics package as the APCM.

Pressure Coring

On NGHP Expedition 01, pressure cores retrieved at *in situ* pressures were used to determine methane hydrate distribution and quantity using nondestructive measurement of the physical properties of the cores at *in situ* pressures and destructive methane collection and mass balance measurements. The techniques used were similar to those used on IODP Expedition 311 (Expedition 311 Scientists, 2005).

Pressure cores were collected using the IODP Pressure Core Sampler (PCS), the HYACINTH Fugro Pressure Corer (FPC), and HYACE Rotary Corer (HRC) pressure corers (see "Description and operation of pressure co"). After a pressure core was retrieved, initial nondestructive measurements, including gamma density and *P*-wave velocity, as well as X-ray images, were used to characterize the nature and distribution of gas hydrate within the sediment (see "Nondestructive measurements on pr"). Some cores were then depressurized on board ship (see "Pressure-core depressurization ex") to determine total methane composition and concentration in sediments (see "Calculating the quantity of gas hydrate or fr"), or stored at *in situ* pressure for further analyses on shore (see Appendix 3). All depressurized cores had nondestructive measurements made on them while undergoing depressurization and following depressurization to document gas evolution, gas-hydrate dissociation, and other changes in the core. The released gas volume and nondestructive measurements were used to guide subsampling for interstitial water, physical properties, and other related analyses.

Why Pressure Core?

Pressure coring is crucial for understanding the concentration of gas hydrate and free methane gas in marine sediments, their nature and distribution, and their effect on the intrinsic properties of the sediment. Methane and other components of natural gas in deep sediment may be present in three phases:

- If the concentration of methane in pore water is less than its solubility, the methane is dissolved.
- If the concentration of methane is greater than its solubility and the sediment is within the GHSZ, excess methane beyond saturation is present as solid methane hydrate.
- If the concentration of methane is greater than its solubility and the sediment is outside the GHSZ, excess methane beyond saturation is present as a free gas (methane gas bubbles).

However, reliable data on methane concentration is impossible to obtain from conventional coring techniques because natural gas solubility decreases significantly as pressure decreases during the recovery of cores to the surface. Conventional cores containing methane release large volumes of gas (Wallace and others, 2000; Paull and Ussler, 2000), and any gas volume measurements made on conventional cores are gross underestimates of the *in situ* natural gas concentrations.

The only way to directly determine the *in situ* concentrations of natural gas in the subseafloor is to retrieve cores that are sealed immediately after the coring process and recovered to the surface without any losses of the constituents. To achieve this objective, the core must be sealed in an autoclave that is able to withstand the hydrostatic pressure at the coring depth when brought to the surface. This was the concept behind the original ODP pressure core sampler (PCS) and the PCS has proven to be an essential tool for estimating *in situ* gas concentrations (Dickens and others, 1997, 2000a,b; Milkov and others, 2004; Expedition 311 Scientists, 2005).

Although the PCS is very effective at obtaining samples that are suitable for overall gas concentration analysis, it was not designed to be used for other types of analyses that might reveal the physical structure of gas or gas hydrate in the core. It is also not possible to transfer or sample the PCS core without releasing the pressure. To enable a more comprehensive investigation of gas-hydrate-bearing sediments, the HYACINTH program developed the next generation of pressure coring tools and techniques to nondestructively analyze the cores and to take subsamples for microbiological, chemical, and physical analysis at *in situ* pressures.

Description and Operation of Pressure Coring Systems

Pressure Core Sampler (PCS) Operations and Core Flow

The Pressure Core Sampler (PCS) is a downhole tool designed to recover a one-meter-long sediment core with a diameter of 4.32 cm at *in situ* pressure up to a maximum of 69 MPa (Pettigrew, 1992; Graber and others, 2002). The pressure autoclave consists of an inner core barrel, which ideally collects a 1,465 cm^3 sediment core, and an outer chamber, which holds 2,964 cm^3 of seawater/drilling fluids (fig. 21). The PCS has been successfully used to study *in situ* gases in gas-rich and gas-hydrate-bearing sediments during ODP Legs 164 on the Blake Ridge (Paull and others, 1996; Dickens and others, 1997), 201 on the Peru margin (Dickens and others, 2003), and 204 on Hydrate Ridge (Tréhu and others, 2003; Milkov and others, 2004), as well as on IODP Expedition 311 to the Cascadia Margin (Expedition 311 Scientists, 2005). For IODP Expedition 311, the steel outer and inner barrels of the PCS autoclave were replaced with aluminum with a maximum working pressure of 25 MPa so that it could be used with the Geotek MSCL–P X-ray system (see "Measurements on PCS Cores").

The PCS tool was assembled in and on top of the core tech shop and generally deployed as on ODP Leg 204 and IODP Expedition 311 (Tréhu and others, 2003; Expedition 311 Scientists, 2005). To minimize the warming cores experienced,

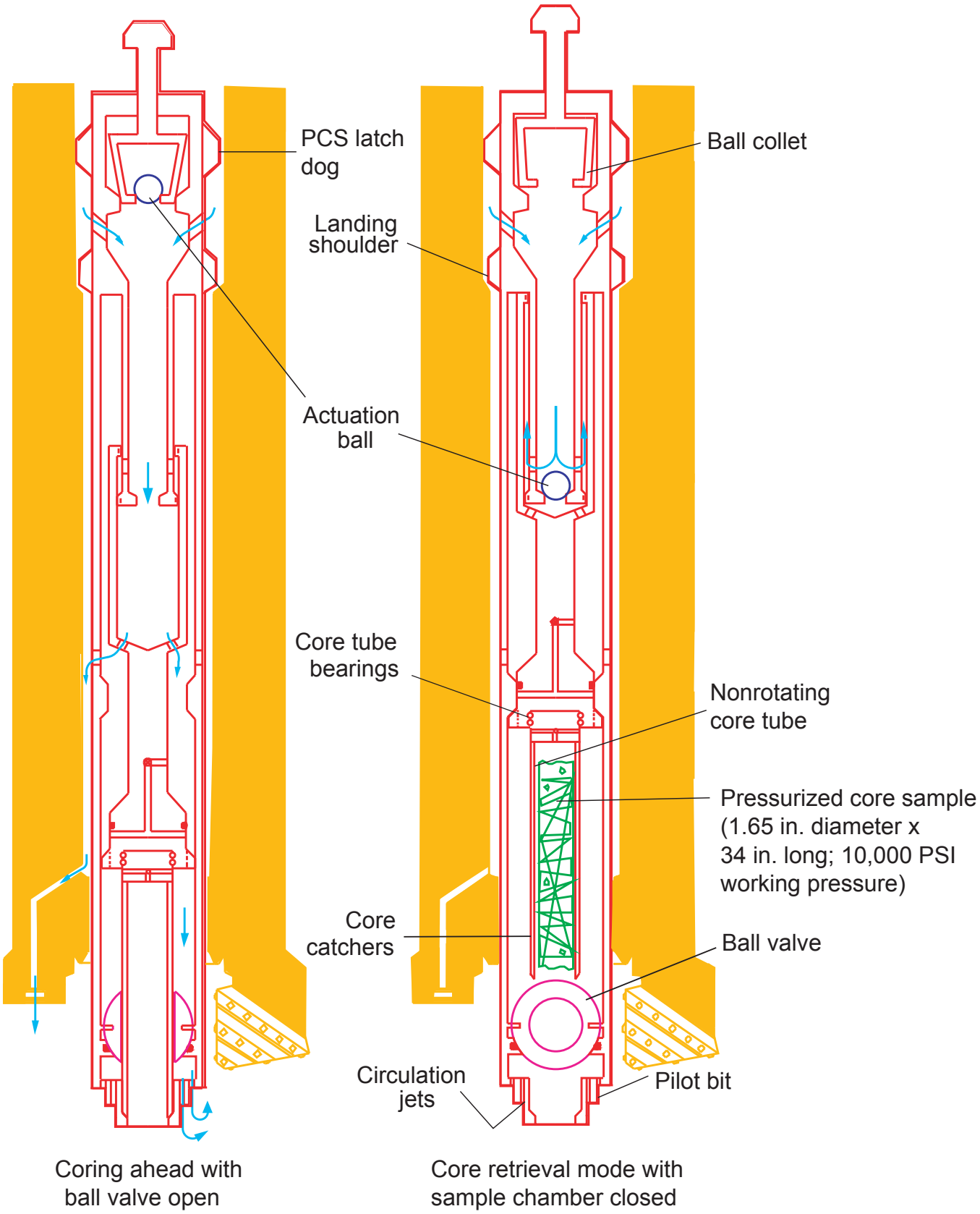

Figure 21. Diagram of Pressure Core Sampler (PCS) from Graber and others., 2002. [in., inches]

the PCS was chilled prior to deployment in the ice shuck, cooled at the mudline for 20 minutes after the core was collected, and recovered to the rig floor on the wire line "as fast as practically possible"— normally at a speed of 100 m/min, but up to 250 m/min. When the core was retrieved from the drill pipe, it was immediately inserted into the ice shuck for 30 minutes to cool it as fast as possible and counteract any warming during the wire-line trip. The cooled PCS autoclave was removed from the rest of the tool on the rig floor and delivered to the refrigerated pressure-coring van on top of the core tech shop for nondestructive measurements and depressurization experiments. When depressurization experiments were completed, the core was moved to the core tech shop for core removal. The inner barrel was removed from the rest of the PCS autoclave and x rayed a final time in the pressure coring van for an image of the entire core. Final extrusion of the core into a half-liner took place in the core tech shop by sealing the end of the core with a metal plug and forcing the core most of the way out with a hydraulic pump; the extrusion was completed by pushing the plug with a broom handle to avoid water contamination of the core.

HYACINTH Coring Systems

Two types of wire-line pressure-coring tools were developed in the European-Union-funded HYACE/HYACINTH programs: a percussion corer and a rotary corer, which were designed to cut and recover core in a wide range of lithologies where gas-hydrate-bearing formations might exist (Schultheiss and others, 2006). Both tools have been designed for use with the same IODP bottom-hole assembly (BHA) as the PCS (that is, the APC/XCB BHA). The HYACINTH pressure-coring systems were used successfully on ODP Leg 204 and IODP Expedition 311 to recover gas hydrate and surrounding sediments (Tréhu and others, 2003; Expedition 311 Scientists, 2005).

The design and operation of the HYACINTH tools differs in five significant respects from that of the PCS:

1. The HYACINTH tools penetrate the sediment using downhole driving mechanisms powered by fluid circulation rather than by top-driven rotation with the drill string. This allows the drill string to remain stationary in the hole while core is being cut, which significantly improves core quality.

2. The coring portion of the HYACINTH tools moves relative to the main bit during the coring process, which also improves core quality. However, the extension of the core barrel up to one meter past the drill bit makes these tools far more susceptible to ship heave than other coring tools, and it is essential that the bit remain stationary on the bottom of the hole during coring.

3. Both HYACINTH tools use "flapper valve" sealing mechanisms at the bottom end above the cutting shoe, rather than a ball valve, to maximize the diameter of the recovered core.

4. The HYACINTH pressure autoclaves are attached to a pressure accumulator filled with gas which can compensate for drops in core pressure due to tool volume expansion during core retrieval. This used to be a feature of the PCS but was removed at the end of Leg 201 because of operational complexities and to make way for the temperature and pressure logging system referred to as the "methane tool".

5. The recovered HYACINTH cores are contained in an inner plastic liner that enables them to be manipulated and transferred into other chambers for analysis, storage and transportation under full pressure.

Fugro Pressure Corer (FPC)

The HYACINTH percussion corer was developed by Fugro Engineers BV and is known as the Fugro Pressure Corer (FPC; fig. 22). The FPC uses a water hammer, driven by the circulating fluid pumped down the drill pipe, to drive the core barrel into the sediment up to one meter ahead of the drill bit. The core diameter is 57 mm (liner outer diameter is 63 mm). On completion of coring, the drill string is lifted to extract the core barrel from the sediment. Once the core barrel is free from the sediment the wire line pulls the core barrel liner containing the core into the autoclave. A specially designed flapper valve is used to seal the bottom end of the autoclave after the core has been retrieved. The FPC is designed to retain a pressure of up to 25 MPa. It is suitable for use with unlithified sediments ranging from soft through stiff clays to sandy or gravelly material. In soft sediments it acts like a push corer prior to the hammer mechanism becoming active. It has operated effectively in sediments with shear strengths up to 500 kPa or even higher.

HYACE Rotary Corer

The HYACINTH rotary corer was developed by the Technical University of Berlin and the Technical University of Clausthal and is known as the HYACE Rotary Corer (HRC; fig. 22). The HRC uses an Inverse Moineau Motor driven by the circulating fluid pumped down the drill pipe to rotate the cutting shoe up to 1 m ahead of the roller cone bit. The original bit used with the HRC was a narrow kerf, dry auger design cutting shoe, with polycrystalline diamond cutting elements (fig. 23). This design allows the core to enter into the inner barrel before any flushing fluid can contaminate the material being cored. The core diameter is 51 mm (liner outer diameter is 56 mm). On completion of coring, the tool is lifted off bottom with the drill string and then the core is retracted into the autoclave by pulling in on the wire line in a similar manner to the FPC, and the pressure is sealed by a specially designed flapper valve. The HRC is designed to retain a pressure of up to 25 MPa and was primarily designed for use in sampling lithified sediment or rock. In practice we have found

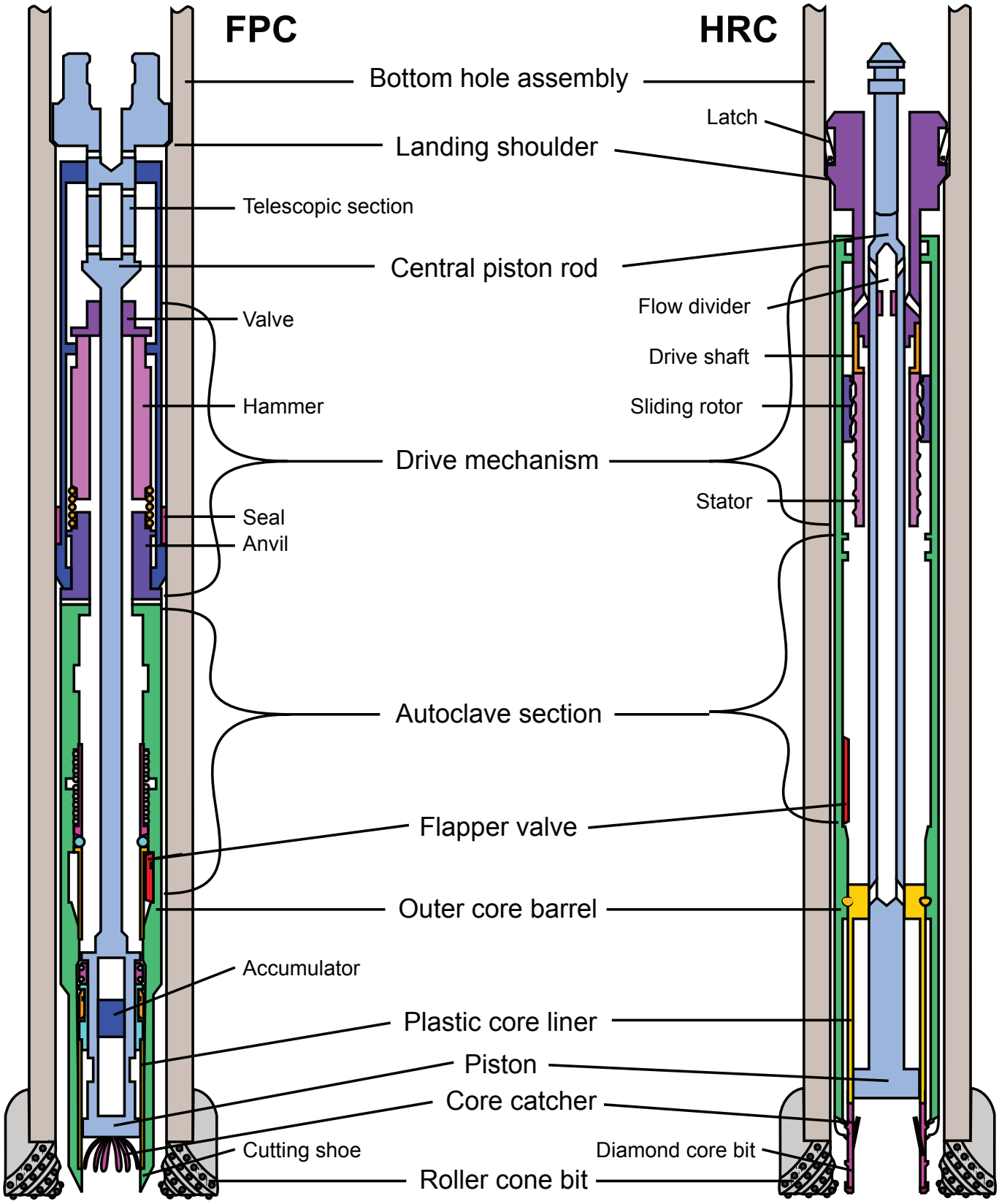

Figure 22. Diagram of HRC (HYACE Rotary Corer) and FPC (Fugro Pressure Corer) showing common components where possible.

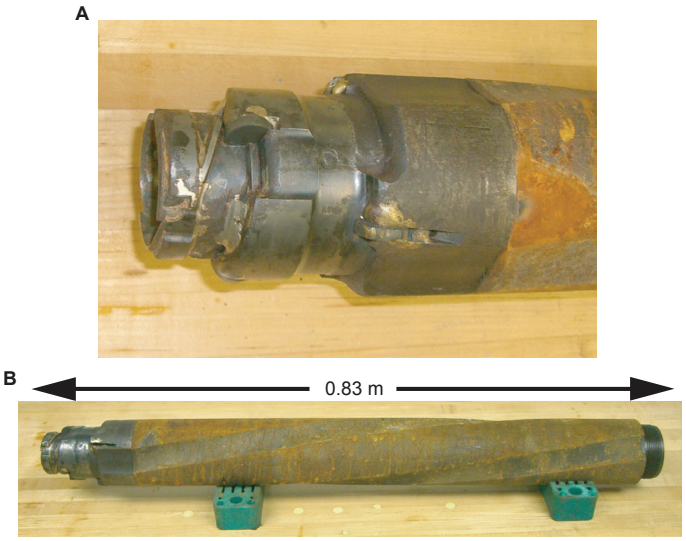

Figure 23. Picture of (A) original HRC diamond bit and (B) dry auger, designed for cutting core in lithified sediments.

that the HRC can sample much softer formations, presumably acting as a push corer with minimal rotation. However, it has not been very effective in common sticky clay formations, and during this expedition we manufactured a new cutting bit with an enhanced auger to enhance penetration (fig. 24). This new bit proved very successful during the latter stages of the expedition.

HYACINTH Coring Operations

As on ODP Leg 204 and IODP Expedition 311, the HRC and the FPC were prepared and assembled on tool trestles located on the port side of the pipe racker. The normal tool assembly area above the core tech shop was in use for PCS tool assembly. Stands of drill pipe normally used from the port side were moved to the starboard side to reduce disruption to the tool preparations.

Both tools followed similar operational procedures on the rig floor. They were initially transferred from the piperacker working area into the vertical position. To achieve this, a tugger line from the derrick was attached to the upper end of the tool while the base of the tool was lowered onto the piperacker skate using the port side racker crane. The tool was then hauled into a vertical position using the tugger line and lowered into the rig floor shuck as the strongbacks were removed by hand. Finally the tool was deployed in the open drill string, which was then closed and the tools were lowered on the wire line while pumping and rotating. The corer was cooled at the mudline for 20 min both before and after the core was collected, and, as with the PCS, the corer was recovered to the surface "as fast as practically possible." As soon as the tools were recovered to the rig floor, they were placed into the ice-water-filled shuck in the moon pool for 30 minutes. Once removed from the ice shuck, both the FPC and the HRC followed a reverse procedure back to the trestles on the piperacker, including replacing the strongbacks. Bags of ice were placed on the autoclaves as they were removed from the body of the tool to prevent them from warming. Autoclaves were removed from the tools in a timely manner (less than 15 minutes) and placed in the refrigerated van over the core tech shop for analysis.

HYACINTH Core Transfer

Core transfer procedures were similar to those used on IODP Expedition 311 (Expedition 311 Scientists, 2005) and took place in the refrigerated van over the core tech shop. To remove the core from the pressure corer autoclave, the autoclave was connected to the manipulator/shear transfer chamber (STC) with quick-clamps (fig. 25) and then pressure balanced with the autoclave before opening the ball valves. The top half of the pressure core, containing the piston and other components, was captured by a catcher on the end of the manipulator, and the full core was withdrawn from the autoclave into the shear transfer chamber, the ball valves closed, and the autoclave removed from the system.

The manipulator/STC, now containing the core at full *in situ* pressure, was attached to the MSCL–P (see **"**MSCL–P measurements on HYACINTH co"), pressures were balanced, and ball valves were opened (fig. 25B). The core was pushed and pulled through the sensors using the manipulator under computer control (fig. 25D). Once the analyses were completed, some cores were depressurized in place, with the core catcher under the gas collection port (fig. 25E–I). Cores to be saved for subsampling or further analysis were transferred into storage chambers. To transfer a core, the bottom half (containing the sediment) must be severed from the re-usable top half of the core. The core was withdrawn to the cutting position (fig. 25E-ii) and the sediment-containing bottom half of the core was cut free from the mechanical top half of the core with

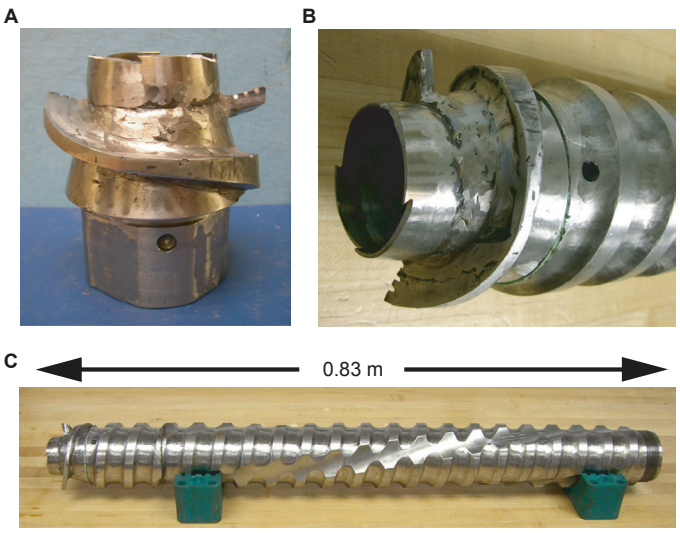

Figure 24. Picture of modified HRC auger bit (the "Viking"), designed to penetrate soft or sticky formations (A and B). Picture of HRC auger bit and auger (C).

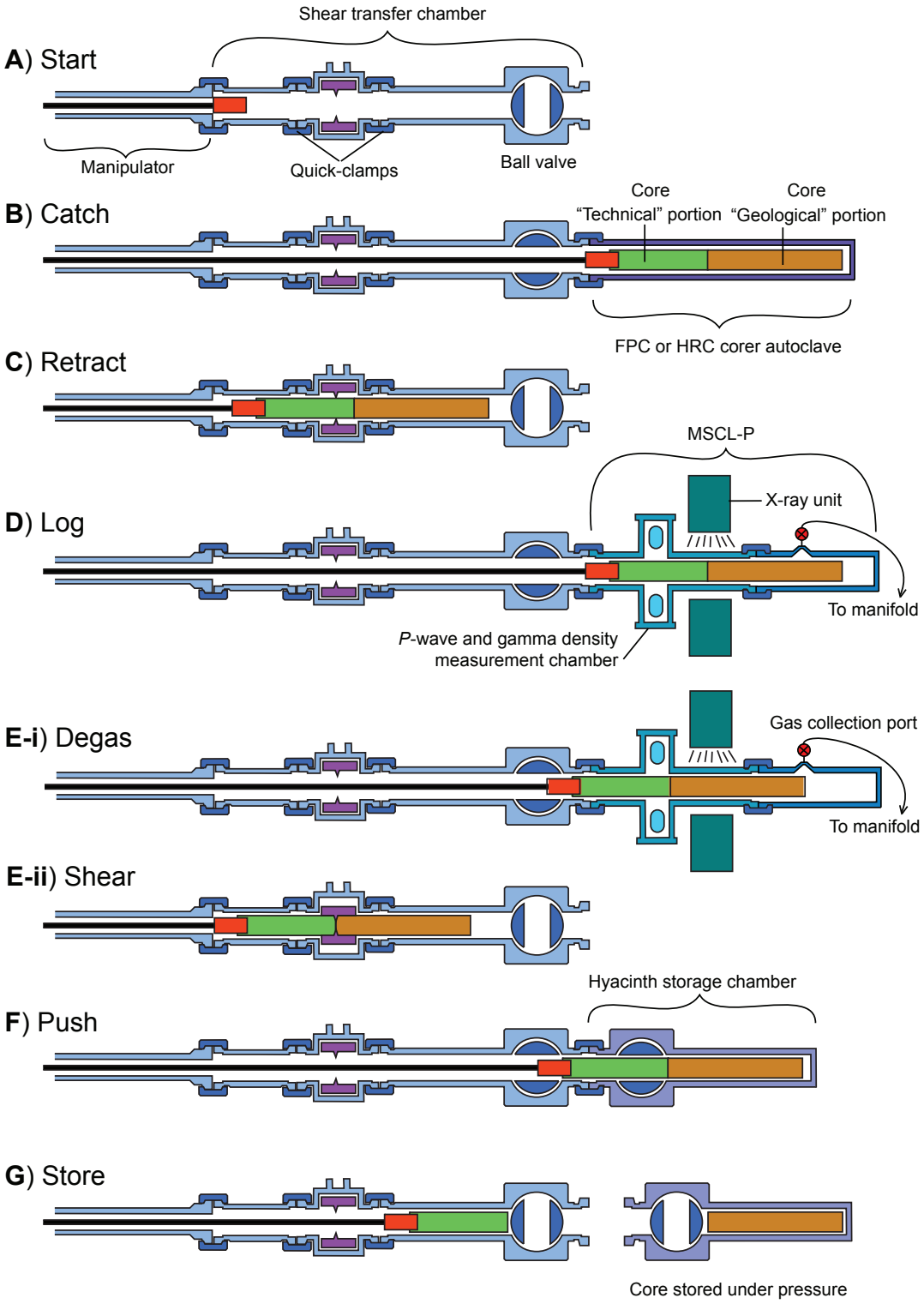

Figure 25. Illustration of pressurized HYACINTH core manipulation. (A) "start" position, (B) the "catch" position after the autoclave has been attached with core under pressure, (C) "retract" position showing the core removed from the autoclave, (D) "core log" position with the MSCL–P in place. Core can then proceeed to (E-I) "degas" position with the core catcher under the gas escape port (core is removed when pressure drops to atmospheric pressure), or (E-II) "shear" position in the shear transfer chamber where the core liner is cut under full pressure, (F) "push" position where the core is pushed into the storage chamber, and G) "store" position where the manipulator rod is retracted, the ball valve closed, and the core free to be transported in the storage chamber at full *in situ* pressure.

the shear blades. A storage chamber was then attached to the manipulator/STC and pressures balanced. The bottom half of the core was pushed into this storage chamber (figs. 25F and 25G) for storage at *in situ* pressure and temperature-controlled conditions (5–7 °C) for shorebased analyses.

Pressure Core Performance and Assessment

Recovering high-quality conventional sediment cores from beneath the ocean floor is not always simple; recovering high-quality sediment cores at *in situ* hydrostatic pressures is intrinsically difficult. However, the ability to quantify the amount of gas hydrate in the formation and determine the *in situ* distribution and morphology of gas hydrate makes pressure coring a worthy pursuit. The overall criteria in evaluating the success of any pressure coring attempt is to ask if the pressure core provided information that could not have been obtained with a conventional (nonpressure) core. If the answer is "yes," then the run can be deemed successful. There are of course degrees of success and these depend primarily on

- The amount and quality of core material recovered, and
- The pressure and temperature at which the core was sealed in the autoclave relative to both the *in situ* P/T conditions and the gas-hydrate stability P/T conditions.

The success of any given pressure coring run requires not only that the tool intrinsically works well but also that the coring operation (for example, operations with the drill pipe, wire line, and mud pumps) proceeds according to plan, the hole conditions and lithology are suitable, and that the weather is favorable. All these factors affect the success of a pressure coring operation and, in the event of a failure, it can be challenging to pinpoint the cause.

During NGHP Expedition 01, we attempted 97 pressure core operations and had an overall success rate of 41 percent (table 2). However, at the last site (Site NGHP-01-21) this success rate improved to 75 percent after modifications were made to the tools to improve operation on this platform and in these formations. In order to quantify success, we have defined "success" as a pressure core with >30 percent recovery and >50 bar pressure. "Successful" cores provided a good assessment of the concentration of gas hydrate in the core, as the core was unlikely to have lost any significant constituents. The cores could also be used to examine sediment-hydrate structures, but this morphological and physical property data may have been compromised by either the lack of sediment or partial release of pressure. Cores that provided the highest quality data about both gas-hydrate morphology and distribution as well as the concentration of gas hydrate within the sediment were termed "excellent" pressure cores, which we define as > 60 percent sediment recovery, >70 percent *in situ* pressure, and > 50 bar pressure. Cores that retained this percentage of *in situ* pressure were likely to have sealed near the seafloor and retained all constituents.

Out of 42 deployments, the PCS returned 12 successful cores (29 percent; table 2), 8 of which were considered excellent cores (19 percent; table 2). Because the PCS no longer contained a pressure accumulator, as the FPC and HRC did, the pressure criterion for excellence was relaxed to >50 percent *in situ* pressure. Overall, the PCS was very reliable in recovering full core in most formations cored on this Expedition. The core quality in stiff formations was quite good (formations in which the XCB recovered good core), but the core quality suffered in softer formations, which could be seen in x rays and seawater infiltration as measured by sulfate concentration. The low pressures on recovery were due to the closing mechanism on the ball valve, which was not as positive or as reliable as it might have been and which often closed late during the wire line trip back up the drill string. The lack of an accumulator probably also contributed to the low recovered pressures.

Out of 31 deployments, the FPC returned 12 successful cores (39 percent; table 2), all of which were considered excellent cores (39 percent; table 2). Overall the FPC hammer mechanism recovered high-quality, full cores in most formations cored on this Expedition, but the retraction mechanism (where the inner core is retracted into the autoclave) was susceptible to rapid movements on the sandline. The slow constant speed of the sandline winch required for reliable retraction was hard to achieve and required a delicate touch of the operator when balancing the control valve and the brake. The requirement for slow, controlled retraction made the FPC more susceptible to weather-related operational issues (for example, increased heave) than other tools. Even with a slow winch speed, as ship heave increases the motion of the inner rod (some 1 to 1.5 km down the drill pipe) is likely to be oscillatory in nature due to the inertia and elasticity of the wire. On a previous commercial operation (one month earlier than NGHP Expedition 01) in similar formations, the FPC had a pressure success rate over 70 percent using a winch with smooth slow speeds in extremely calm weather. After Site NGHP-01-19, a hydraulic "choke" was incorporated into the FPC that was designed to slow down the retraction of the inner rod, irrespective of the actual speed and motion of the sandline. This new mechanism was tested in the pipe and at the rig floor during

Table 2. NGHP Expedition 01 pressure core deployment summary.

[PCS, Pressure Core Sampler; FPC, Fugro Pressure Core; HRC, Hyacinth Rotary Core]

Corer type	Total deployments	>20% Sediment recovery		>60% Sediment recovery		>50 Bar pressure		>70% Pressure recovery*		Successful pressure cores		Excellent pressure cores	
PCS	42	30	71%	26	62%	15	36%	11	26%	12	29%	8	19%
FPC	31	28	90%	26	84%	12	39%	12	39%	12	39%	12	39%
HRC	24	20	83%	10	42%	17	71%	17	71%	16	67%	10	42%

Note: *50% of *in situ* pressure for the PCS.

transit to Site NGHP-01-20. This new arrangement was used for the last six FPC cores of the Expedition and eliminated the problems with heave and sandline winch speed.

Out of 24 deployments, the HRC returned 16 successful cores (67 percent; table 2), 10 of which were considered excellent cores (42 percent; table 2). The HRC was not originally designed to recover cores in most of the materials encountered during the NGHP Expedition 01; it uses a downhole rotary mechanism and diamond bit that is designed to cut hard lithified sedimentary rocks (fig. 23) and tended to recover short cores in sticky clay formations. The new auger-style "Viking" cutting bit (fig. 24) fabricated and used successfully in the later stages of the Expedition significantly improved recovery lengths in soft sediments, with 8 excellent cores taken out of 11 total runs (72 percent). The HRC has a reliable flapper valve seal and the inner retraction mechanism appears to be insensitive to variations in the winch speed during retraction. Consequently, the HRC has a very good record of recovering cores under pressure, the lengths of which have improved.

Pressure, Temperature, and Pressure Coring

All three pressure coring tools had pressure and temperature (P/T) data loggers that recorded the complete deployment of the tool and enabled the P/T history of the deployment to be analyzed. In particular we were interested to know when the tool sealed and what temperatures and pressures the core was subjected to during recovery. In addition to the tool data loggers, we had a fortuitous opportunity to test a micro P/T data logger made by Star-Oddi (see *www.star-oddi.com*). These DST (Data Storage Tag) micro data loggers were only 3.3 mm in diameter and 25.4 mm long and fit as comfortably inside the pressure-coring tools as in the fish guts for which they were designed. In the FPC and HRC they were fixed inside the piston at the top of the core and in the PCS they were fixed to the outside of the inner barrel. These small data loggers provided a much improved assessment of the temperature of the core because the tool data loggers were somewhat remote from the core and heavily influenced by the large thermal mass of the tool itself. The disadvantage with the DST micro data loggers was that they were only pressure rated to about 120 bar and could only be used on the shallower deployments during the Expedition. When both the DST micro and the tool data loggers could be used, the comparison between the pressures and temperatures of the two records put tool data logger P/T data at deeper sites into perspective.

Figure 26 illustrates the pressure and temperature history during the course of a typical deployment. Initially during a deployment, the pressure rose rapidly as the tool was lowered in the pipe to the mudline, which in this case took about eight minutes. The pressure was then constant for 20 minutes at 105 bar during the mudline stop before being lowered to the coring depth. Pressure perturbations were recorded during the coring process itself before the tool was raised to the mudline for a 20-minute stop where pressure was again stable at 105 bar. At the end of this period, the tool was raised rapidly to the surface and the pressure inside the tool often dropped slightly to markedly, in this case to about 90 bar. The drop in pressure was generally thought to be caused by tool volume changes but could also be caused by late sealing of the tool autoclave. The tool temperature generally rose rapidly during the approximately five-minute handling period on deck, and the pressure also rose slightly before dropping again when the tool was plunged into the ice shuck.

The pressure history of a pressure core and its final recovered pressure are very sensitive to changes in the external pressure on the autoclave and the internal temperature of the autoclave and contents. The change in the internal volume of the corer during sealing, as valves seat and "O" rings compress, is also a major effect (fig. 27). To illustrate the problem we have performed a simple calculation to show the pressure changes that might occur to a core recovered from 1,000 m water depth. Figure 27 shows an idealized plot of temperature and pressure for a pressure-coring operation using a tool with an internal volume of 5 liters. It shows simplified temperature profiles for both the steel autoclave and the internal water and core, which are significantly different. Initially, the core is sealed inside the core with a pressure of 100 bar at 10 °C and from that point on there is no transfer of mass (that is, it does not leak). After the tool has reached the rig floor, the temperature of the steel autoclave has increased to near ambient temperature but the temperature of the contents has only increased slightly. We have estimated that there is a 0.1 percent increase in volume of the autoclave caused by drop in external pressure, both due to expansion of the steel autoclave and volume changes from tool sealing. We then calculated the additional increase in autoclave volume caused by the thermal expansion of the steel container (linear thermal expansion coefficient 17.3×10^{-6}/K). The change in density of water was calculated using the new volume and the resulting pressure determined from the equation of state for water (UNESCO, 1981) using a salinity of 35 ppt. This procedure was repeated for the condition when the autoclave is first plunged into ice and finally when it reaches equilibrium. This exercise, while not completely rigorous, shows how large pressure changes could occur even if a pressure-coring system worked perfectly. A core that sealed at 100 bar *in situ* might reach the laboratory at only 60 percent of that pressure unless an accumulator (pressure capacitor) were installed to mitigate against these effects. This effect is probably the primary reason why the FPC and HRC return with higher pressures than the PCS, which no longer incorporates a pressure accumulator.

The HRC, FPC, and PCS tool P/T logger and the DST micro logger pressure records agreed very well. However, there was an important difference in the temperature profiles for the tool and DST micro data loggers. The DST logger (situated in the piston) more accurately reflected the temperature of the core. The small DST logger cooled rapidly on descent and showed far less heating during the recovery and handling process than the tools' data loggers. This observation was pertinent because it was important to know if the pressurized sample spent any time outside the gas-hydrate stability field, and if so how long. Figure 28 shows P/T trajectories for the same

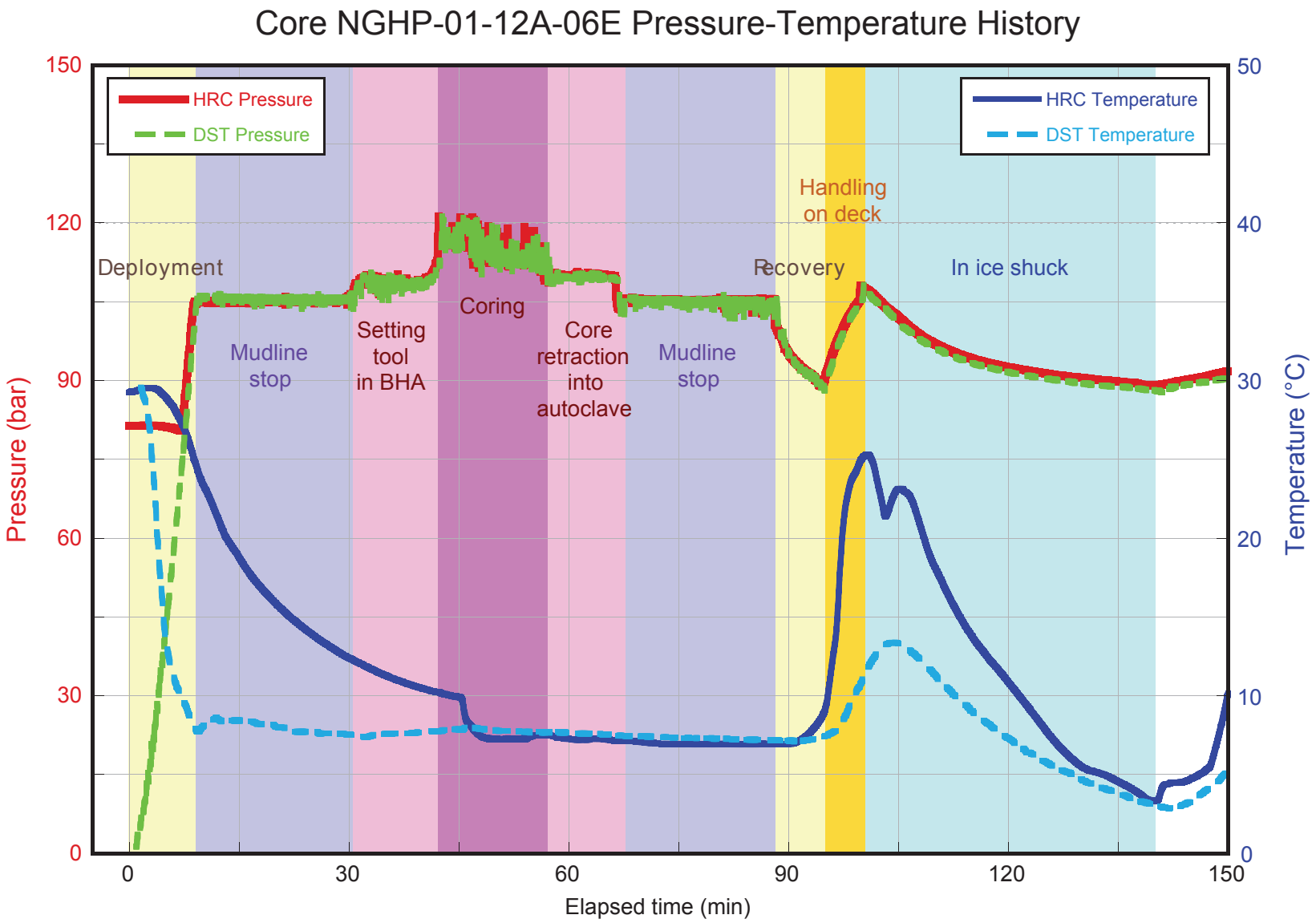

Figure 26. Annotated plot of pressure and temperature vs. time from the tool data logger and the DST data logger for HRC Core NGHP-1-12A-06E. The HRC tool pressure logger starts at the accumulator pressure. [min, minutes]

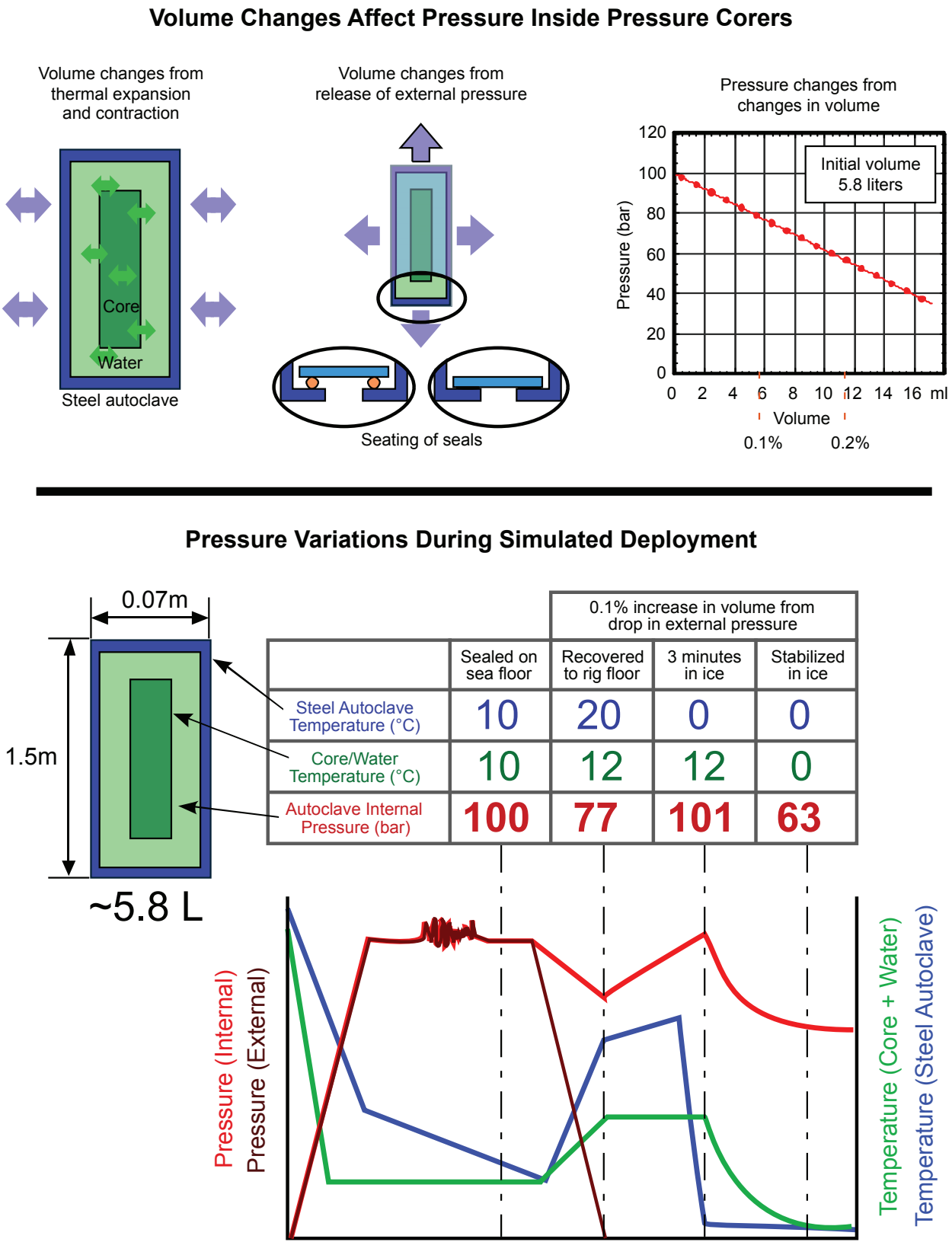

Figure 27. Diagrams showing effects of temperature and pressure on the internal pressure of pressure cores. Top: changes in volume produced by temperature or pressure (including compression of compliant components) produce changes in internal pressure. Bottom: simulated pressure core deployment taking into account both temperature and pressure effects on internal pressure of corer.

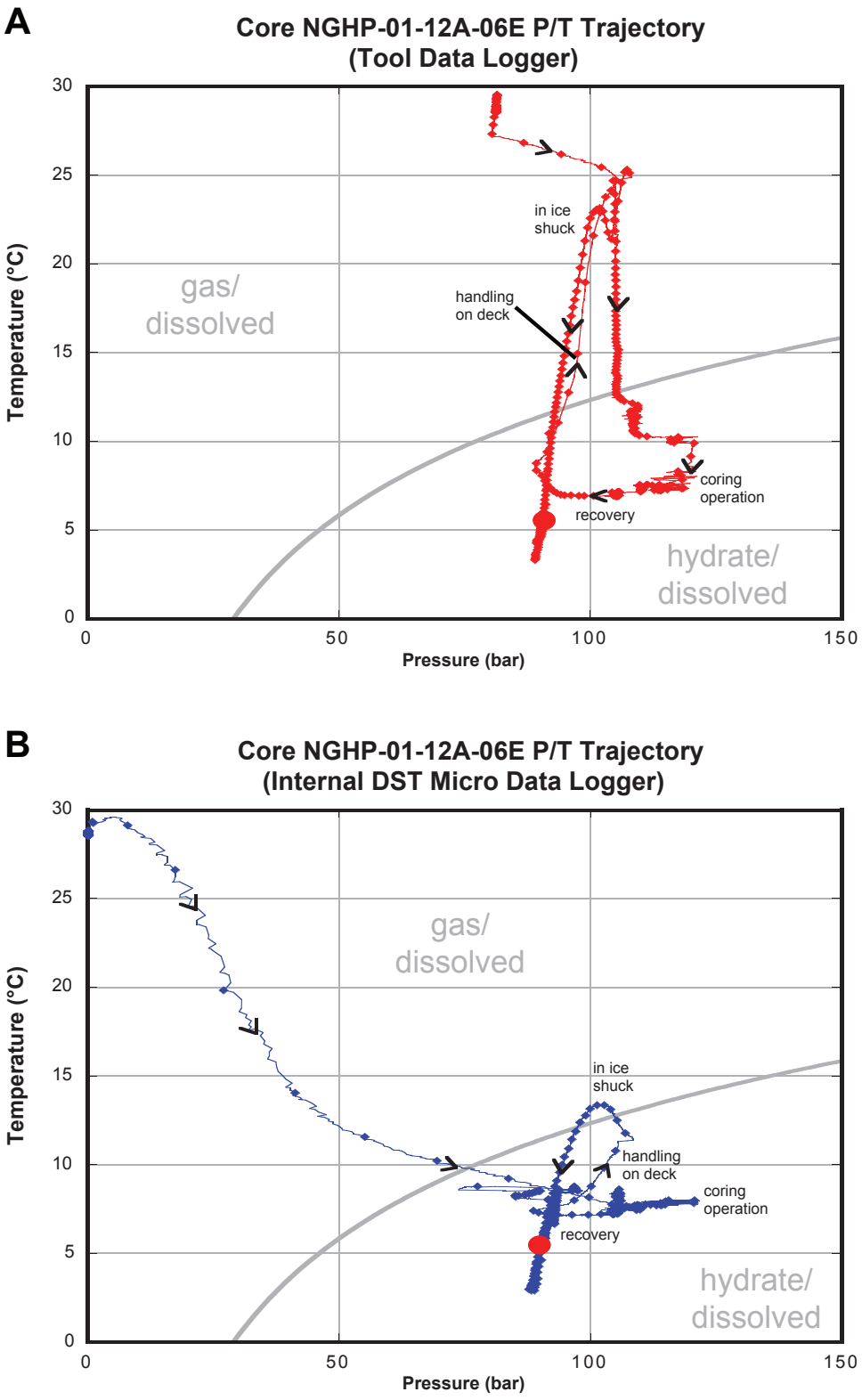

Figure 28. Annotated plot of pressure & temperature vs. time from the (A) tool data logger and the (B) DST data logger for HRC Core NGHP-01-12A-06E, showing trajectory relative to gas-hydrate stability (35 ppt salinity) as calculated from Xu (2002, 2004). The HRC tool pressure logger starts at the accumulator pressure

pressure-core deployment (Core NGHP-01-12A-6E) on which is also plotted the gas-hydrate phase boundary. In figure 28A, which shows the trajectory for the HRC tool data logger, it appears at first sight that core has spent a significant amount of time outside the gas-hydrate stability zone. However, this is in fact a misrepresentation of what actually happened to the core, which is more accurately represented by the P/T trajectory created from the DST data (fig. 28B). The DST data indicated that the core piston only spent a small amount of time outside the gas-hydrate stability zone and it is likely that the core itself remained inside the gas-hydrate stability zone, as the thermal conductivity of the sediments is significantly less than the tool itself. These comparisons have confirmed that the precautions that we have taken, designed to keep the core temperatures as low as practically possible, generally maintain the sample inside the gas-hydrate stability zone.

Nondestructive Measurements on Pressure Cores

Although pressure cores are particularly valuable for providing accurate methane volumes for gas-hydrate concentration calculations, nondestructive measurements made before or during the depressurization process can provide additional information on the nature and distribution of gas hydrate within the sediment and rare data on near-*in-situ* physical properties of gas-hydrate-bearing sediments. X-ray images of the pressure cores show the overall structure of the core and gas hydrate within them (as well as contributing to the core length estimate), gamma ray attenuation provides accurate densities of sediment/gas-hydrate structures, and measurement of *P*-wave velocity on undisturbed gas-hydrate-bearing core at *in situ* pressure provides acoustic parameters valuable for analysis of seismic data. During NGHP Expedition 01, data were collected on pressure cores using the Geotek Pressure Multisensor Core Logger (MSCL–P), located in the refrigerated pressure-coring van, in two modes, one for HYACINTH cores and one for the PCS cores.

MSCL–P Measurements on HYACINTH Cores

The MSCL–P (fig. 29) is an automated measurement system for the collection of acoustic P-wave velocity, gamma ray attenuation, and X-ray image data on HYACINTH pressure cores under pressures up to 25 MPa. The MSCL–P pressure chamber is constructed of aluminum and contains an internal set of ultrasonic transducers. X-ray and gamma ray sources and detectors are situated outside of the pressure chamber. The system moves pressurized HYACINTH cores incrementally past these sensors under computer control with a positional precision of better than one millimeter, allowing detailed gamma density and acoustic velocity profiles to be obtained rapidly and automatically along the core as well as creating automated full-core X-ray montages. The manipulator mechanism ensures that the core does not rotate during the linear translation.

Core logging under pressure using the MSCL–P is in principle very similar to core logging with the IODP MST or a standard Geotek Multisensor Core Logger (MSCL–S). One exception is the increased distance and varied material between the sensors and the core. Sensors are separated from the core by the plastic liner, the pressurizing fluid (seawater), and, in the case of the gamma and X-ray sensors, the aluminum pressure chamber. To calibrate for measurements of acoustic velocity and gamma density, similar techniques are used to those developed for the MST and MSCL (see "Multisensor Core Logger (MSCL)" in "Physical Properties"), which use distilled water and aluminum as standards. During logging of pressure cores, the inner liner is assumed to have a constant diameter because it cannot be directly measured under pressure.

Gamma density was measured using a ^{137}Cs source and NaI detector identical to those used on the MSCL–S (see "Multisensor Core Logger (MSCL)" in "Physical Properties"). Errors are proportional to the square root of the total counts (generally around 5,000 cps, giving a density precision of 2 percent). Calibration of the gamma density measurement was performed by measuring the intensity of the gamma beam through a stepped aluminum bar of varying thickness sitting centrally in a core liner filled and surrounded with salt water of known salinity. This calibration procedure, using aluminum and water, provides a good approximation for a water-saturated sediment (minerals and water) and has proven to be

Figure 29. Inside of the pressure coring van over the core tech shop showing the long shear transfer system in the center with the MSCL–P being adjusted at the far end. Photo credit: IODP.

an excellent calibration protocol for determining density from the attenuation of gamma rays. Separate calibrations were performed for FPC and HRC liners and no effect was seen with increasing pressure. It should be noted that the density measurements on the cores made at one atmosphere after depressurization was complete may have been underestimates, due to the potential for trapped gas in the gamma beam outside the core. After Site NGHP-01-17, a bubble excluder was manufactured and installed, and the one-atmosphere measurements were no longer susceptible to bubble-induced lowering of density.

Ultrasonic P-wave velocity (V_p) was measured using two 500 kHz acoustic transducers mounted inside the pressure chamber, perpendicular to the core and the gamma ray beam. Travel times were measured with a precision of 50 ns, and the error associated with the velocity was ±3 m/sec assuming a core thickness of around 6 cm. To calibrate V_p, the total P-wave travel time was measured when both the core liner and the pressure chamber were filled with water of known velocity (from temperature, pressure, and salinity). The measured variation in V_p with pressure in the MSCL–P with empty HYACINTH core liners has previously been found to be close to the theoretical variation for water (Tréhu and others, 2003; Expedition 311 Scientists, 2005), and thus the travel times in the liner material were essentially constant with changing pressure.

Occasionally, cores were repressurized to examine the P-wave velocity of sediments after full depressurization. When gas-rich cores are depressurized, many small gas bubbles are formed in the sediment matrix which do not escape. These small bubbles cause the high attenuation of the P-wave signal that prevents velocities from being measured. When the core is repressurized, these small gas bubbles are forced back into solution and hence the *P*-wave velocity can once again be measured throughout the core.

X-ray images were obtained using a linear X-ray device consisting of a lead-shielded microfocal X-ray source and phosphor image intensifier. An aluminum compensator was used to minimize the intensity variations which are caused when illuminating round objects. With the geometrical arrangement used and with a typical X-ray spot size used of around 8–12 mm, the intrinsic spatial resolution of the images is about 150 mm. All final core images were obtained by creating montages from a series of area images taken along the core. The spatial interval used for all the final images was 0.5 cm, which creates a relatively flat image along the core without any apparent significant spherical distortion. The montages were slightly affected by an electromagnetic distortion in the image intensifier. The X-ray images were not density calibrated because the gamma attenuation measurements give higher accuracy than the polychromatic x rays. Instead, we varied the X-ray energy and power levels to maximize the qualitative resolution of the image in an effort to examine subtle structures within the core. X-ray energies up to 110 kV were used depending on the density of the cores being measured.

Measurements on PCS Cores

Gamma density measurements and X-ray imaging of PCS cores prior to depressurization were critical for the calculation of gas hydrate content as they provide the original length (and hence volume) of the core. Additionally, the density and X-ray measurements taken during depressurization provided information similar to that collected on HYACINTH cores during ODP Leg 204 and IODP Expedition 311 (Tréhu and others, 2003; Expedition 311 Scientists, 2005), where low-density, potential gas-hydrate-bearing layers could be monitored as the core was depressurized to observe hydrate dissociation and gas evolution.

The MSCL–P was modified to accept the PCS autoclave by removing the MSCL–P pressure chamber that mates to the HYACINTH transfer system and attaching the top of the PCS autoclave to the end of an unpressurized HYACINTH manipulator, allowing the MSCL–P software and manipulator to push the PCS autoclave through the sensor array (fig. 30). Gamma attenuation measurements and X-ray images can be collected on PCS autoclaves using this system. P-wave velocity measurements cannot be made through the autoclave of the PCS.

The PCS autoclaves were always oriented the same way in the MSCL–P, with the transducer port facing upward, and gamma attenuation for the PCS autoclaves, filled with water, was measured so that the data could be corrected as a function of vertical position (fig. 31). The densities measured on core in the upper half of the PCS autoclave had an estimated error of ±0.05 g/cm^3, but because the lower half of the autoclave outer barrel contains a spring and other steel moving parts, the density could not be determined as accurately. The steel in the PCS body also created an "S" distortion in the X-ray image intensifier, and as the PCS was moved past the image intensifier, the character of the S-distortion changed (fig. 32), probably due to the moving steel interacting with the magnetic fields in the image intensifier. The lower half of the barrel was completely obscured by a steel sleeve (fig. 31).

Pressure-Core Depressurization Experiments

During NGHP Expedition 01, the bulk of pressurized sediments were available for onboard depressurization experiments. Controlled release of pressure from pressure cores through a manifold permitted

- Collection of the gas discharged from the sediment's dissolved gas, free gas, and gas-hydrate phases for quantitative and qualitative analysis;
- Estimation of the *in situ* abundance of gas hydrate or free gas based on mass balance, methane solubility, and gas-hydrate stability considerations (Dickens and others., 1997; see "Calculating the quantity of gas hydrate or free gas in a pressure core");

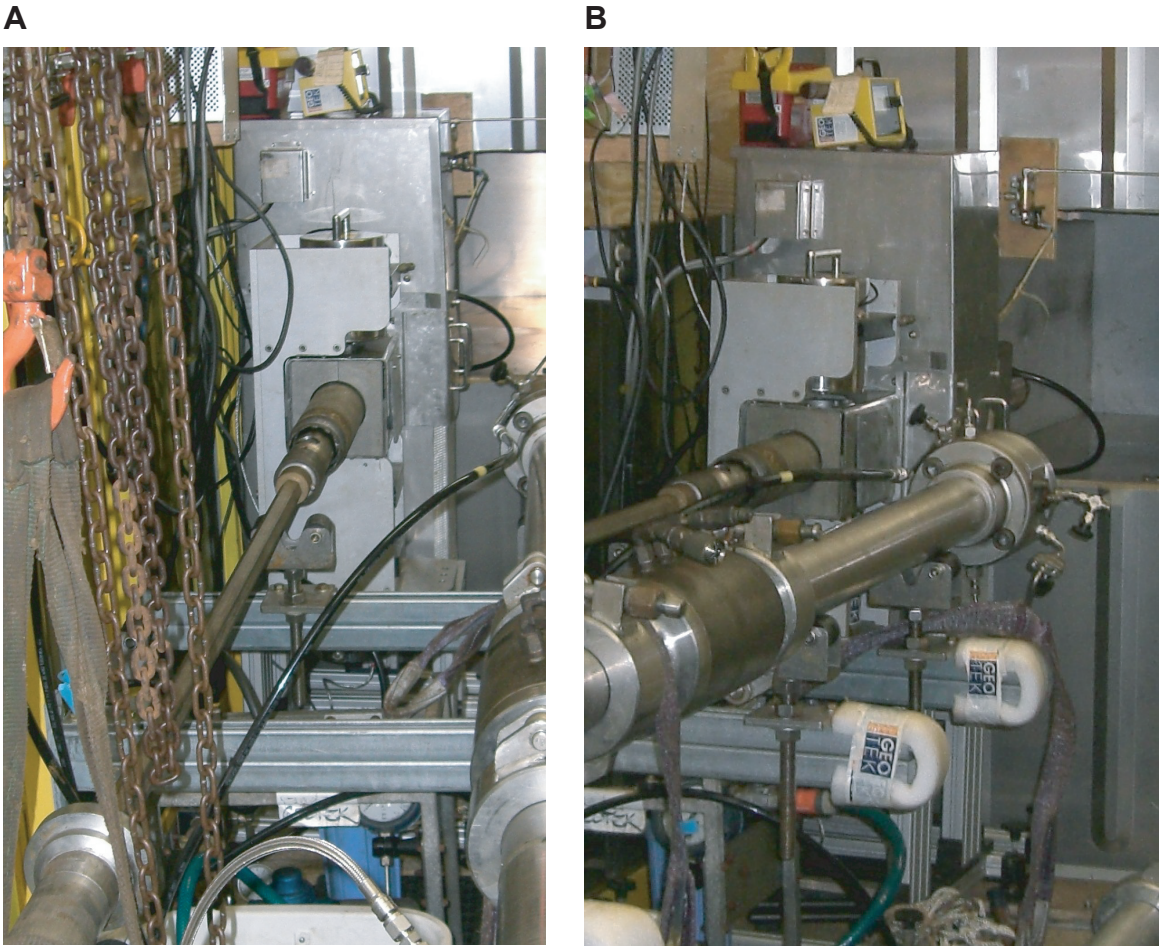

Figure 30. Inside of the pressure coring van over the core tech shop showing two views of the PCS autoclave within the MSCL–P sensor array.

- Identification of the presence of gas hydrate from volume-pressure-time relations (Hunt, 1979; Dickens and others., 2000b; Milkov and others, 2004); and
- Visualization of the controlled decomposition of gas hydrate with nondestructive methods in the course of the depressurization experiment.

Depressurization experiments began with an initial baseline set of nondestructive measurements consisting of x rays and gamma density for PCS cores and x rays, gamma density, and P-wave velocity (full MSCL–P scan) for HYACINTH cores. The gas collection manifold and bubbling chamber (fig. 33) were filled with fluid and attached to the PCS autoclave or MSCL–P gas collection port. Pressure was released from the pressure core in a stepwise fashion and the fluid and gas that collected in the bubbling chamber were measured and recorded. Depressurization experiments on cores brought back near *in situ* pressures (100–200 bar) began with depressurization increments of approximately 10 bar. As depressurization progressed, increments were based on gas volume (1,100 mL maximum increment) and fluid volume (250 mL maximum increment). Cores were monitored for pressure increases after a depressurization step ("pressure rebounds"), which can arise from slow escape of dissolved gas (one pressure rebound at any given pressure) or from gas-hydrate dissociation (pressure recovers multiple times to similar pressure, near gas-hydrate stability pressure at lab temperature). Additional MSCL–P scans were made during depressurization to monitor gas-hydrate dissociation and evolution of gas voids and pathways.

Final MSCL–P scans were also made after the cores were fully depressurized. Gas remaining in the pressure core/manifold system was estimated from the volume of fluid expelled during the experiment and assigned the composition of the final gas sample for purposes of total methane calculation.

During each depressurization experiment, the pressure was monitored by analog pressure gauges and recorded by digital pressure transducers recorded on a personal computer. The released gas was collected in a 1 liter bubbling chamber consisting of an inverted graduated cylinder and a plexiglass tube filled with water (fig. 33). After measuring the volume of collected gas, gas aliquots were sampled from a valve at the top of the cylinder using a syringe/valve assembly. Sampled gases were given to the organic geochemistry laboratory for analysis and archival (see "Organic geochemistry").

Graphs showing gas and liquid volume expelled during depressurization of pressure cores also showed "estimated"

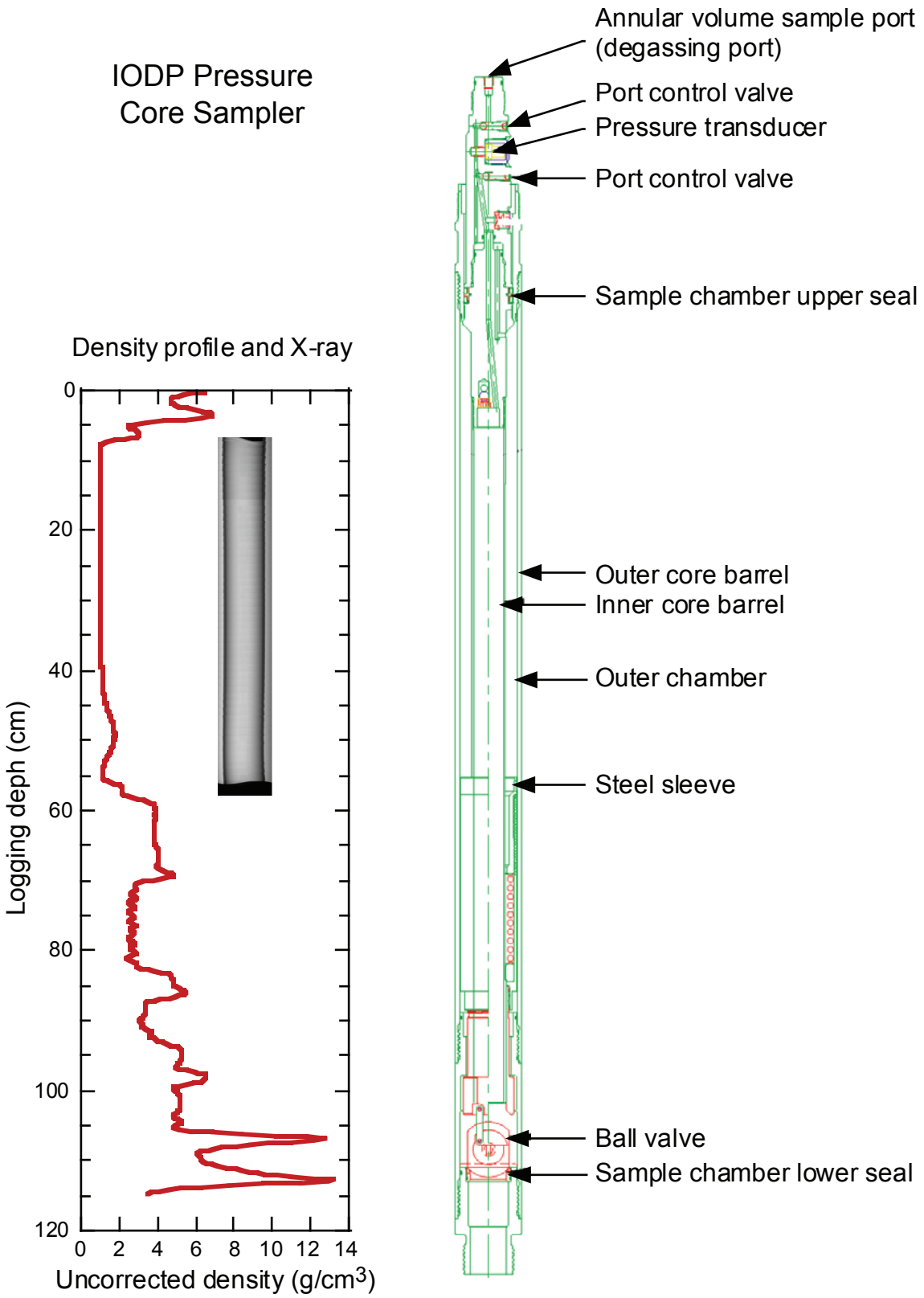

Figure 31. Diagram of Pressure Core Sampler (PCS) with the gamma density profile and X-ray collected using the MSCL–P, to scale. X-ray below 51 cm core depth is not possible because of the steel components inside the outer barrel. Diagram of PCS modified from Pettigrew and others, 1992.

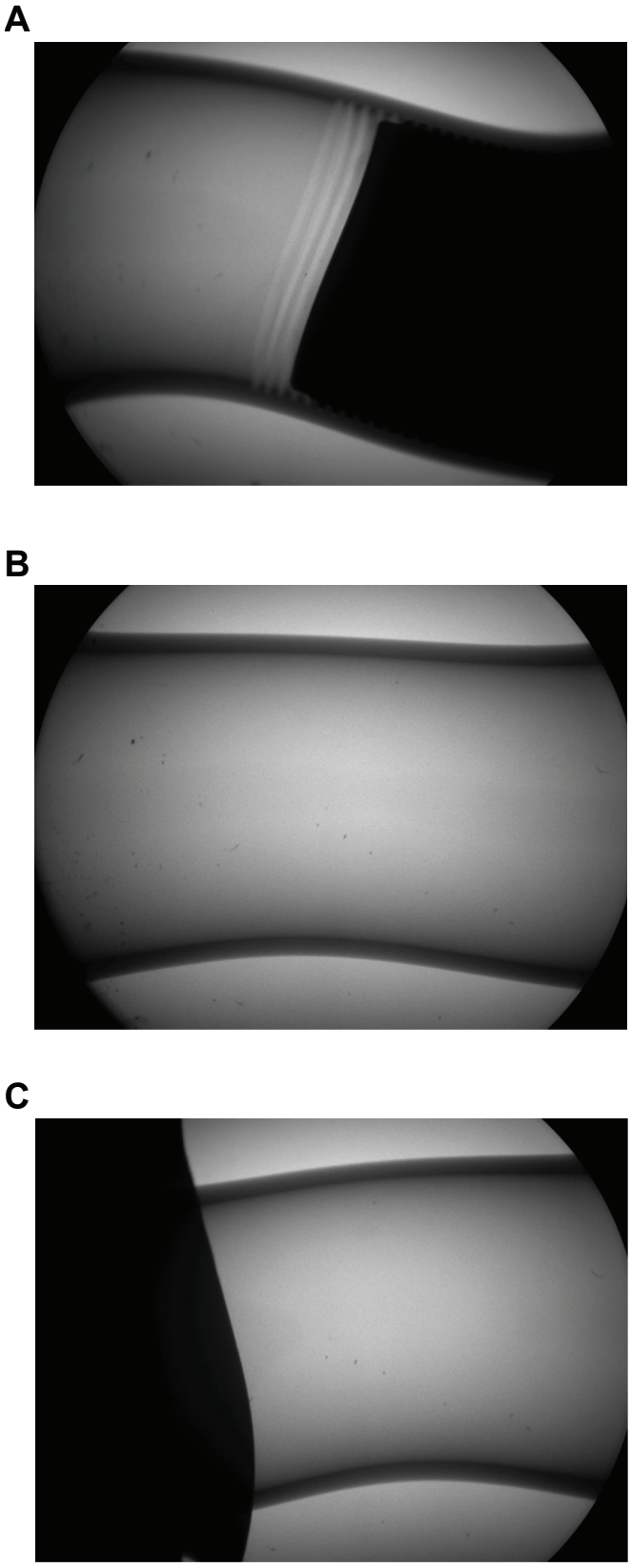

Figure 32. Several (A, B, and C) X-ray images of the inner aluminum liner in the PCS illustrating the "S"-distortion of these images caused by the massive steel components in the PCS.

gas (for example, fig. 34). The estimated gas released by the system at any given pressure was calculated by adding the total amount of gas released up to that point to the total amount of gas remaining in the system. The gas remaining in the system was estimated by multiplying the fluid released up to that point by the pressure. The estimated gas method was very valuable for recognizing pressure plateaus with respect to volume, which would go unnoticed if searched for in actual released gas volume alone (fig. 34A), or the simple expansion of gas (fig. 34B). This measure of "estimated" gas did not take into account the compliance of the system and at high pressure (at the beginning of an experiment) occasionally overestimated the final gas volume.

Calculating the Quantity of Gas Hydrate or Free Gas in a Pressure Core

Pressure core depressurization experiments allowed quantification of the total amount of methane that was present in a given pressure core and estimation of the quantity of methane hydrate or free methane gas, assuming the methane phases were in thermodynamic equilibrium. Excess methane was estimated by comparing the total quantity of methane contained in the core to the quantity of methane that would be expected for a core of that volume and porosity, assuming the porewaters were saturated in methane. This excess methane was assumed to be either methane hydrate or free methane gas, depending on the location of the hydrate/gas phase stability boundary in relation to the temperature, pressure, and salinity at core depth. The calculations for Structure I methane hydrate are detailed below.

Calculation of total moles of methane from a pressure core:

- **Total moles of methane in the core** were calculated from the **volume of methane released from the core** using the ideal gas law (n=PV/RT), assuming one atmosphere pressure and using the actual van temperature at the time of depressurization (7 °C unless otherwise stated), plus the **moles of methane remaining dissolved in pore fluids**.
- **Total volume of methane released from the core** was calculated by summing the collected gas volumes multiplied by their respective mole fractions of methane (from the gas chromatographic analysis) and adding the **volume of methane remaining in the pressure core/manifold system** at the end of the depressurization experiment.
- **Volume of methane remaining in the pressure core/manifold system** was calculated from the **volume of gas remaining in the pressure core/manifold system** multiplied by the mole fraction of methane corresponding to the final measured gas sample.

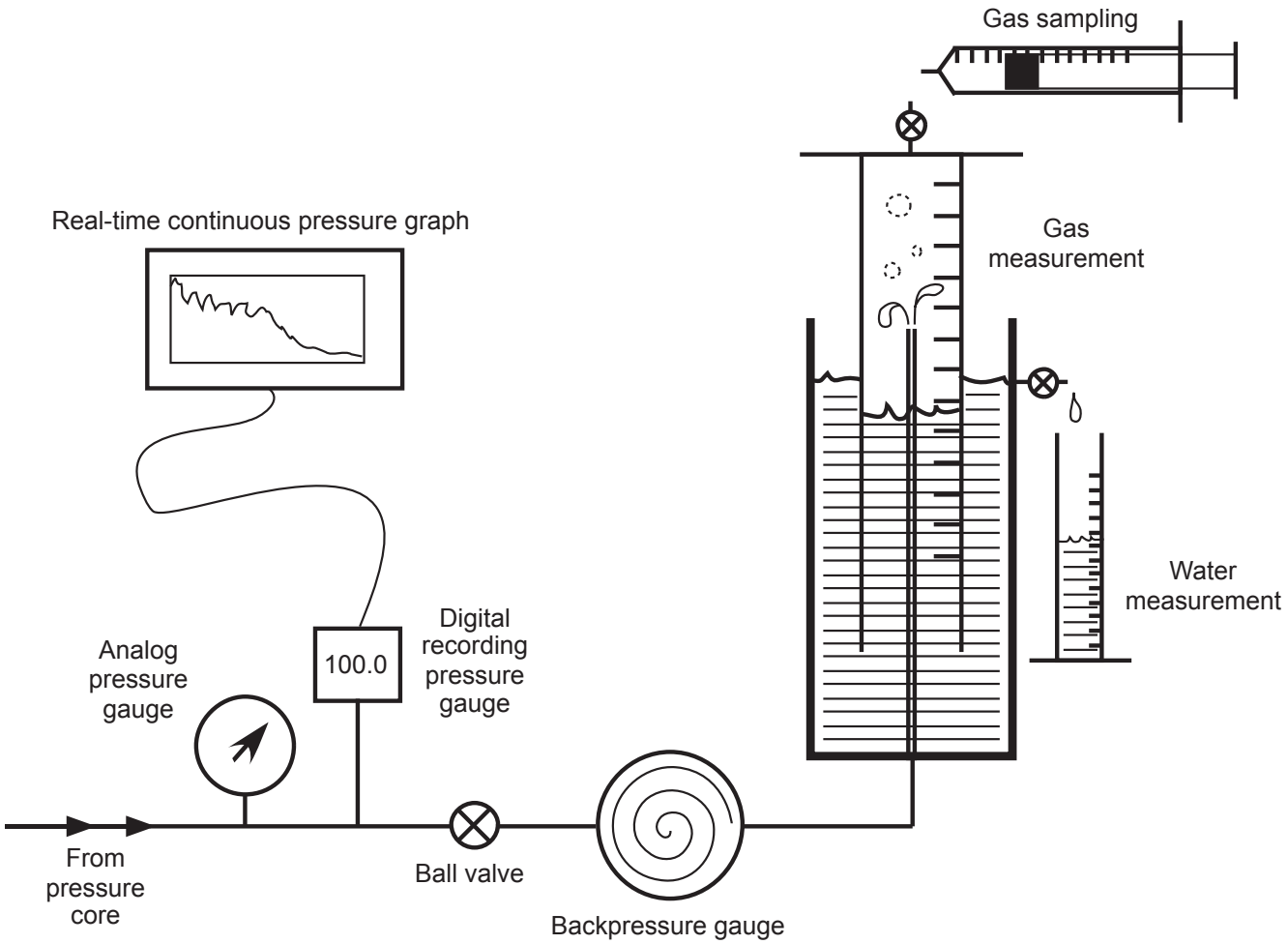

Figure 33. Diagram of depressurization manifold and bubbling chamber, modified after IODP Leg 311.

- **Volume of gas remaining in the pressure core/manifold system** at the end of the experiment was estimated from the volume of fluid displaced during the depressurization minus the change in volume of the system with pressure. The change in volume of the MSCL–P system was measured as 350 mL for the pressure drop of 110 bar to atmospheric pressure. The change in volume of the PCS depressurization system was assumed to be zero.
- **Mole of methane remaining dissolved in the pore fluids** were calculated by measuring the methane concentration of the pore fluids by the headspace technique (see "Organic geochemistry") and multiplying this concentration by the **pore volume**. If no measurement was made, this value was taken to be zero, which gives a conservative (minimum) estimate of total methane.
- **Pore volume** was calculated from the **core volume** multiplied by the **porosity**, which was calculated from the initial gamma density assuming a mixture of only porewater and sediment, with a grain density of 2.7 g/mL.
- **Core volume** was calculated from initial core length, estimated from initial x rays and gamma density scans, multiplied by the core area, calculated from the core diameter (4.32, 5.7, and 5.1 cm for the PCS, FPC, and HRC, respectively);

Calculation of total moles of excess methane in a pressure core:

- **Total moles of excess methane** were calculated by subtracting the **maximum equilibrium dissolved methane** in the pressure core, *in situ*, from the **total moles of methane in the core** (calculated above).
- **Maximum equilibrium dissolved methane** in the pressure core was calculated from the **maximum equilibrium concentration of dissolved methane** multiplied by the **pore volume** (calculated above).
- **Maximum equilibrium concentration of dissolved methane** (that is, methane saturation) was calculated according to Xu (2002, 2004), using the *in situ* **temperature**, pressure (hydrostatic pressure at core depth), and **salinity**.

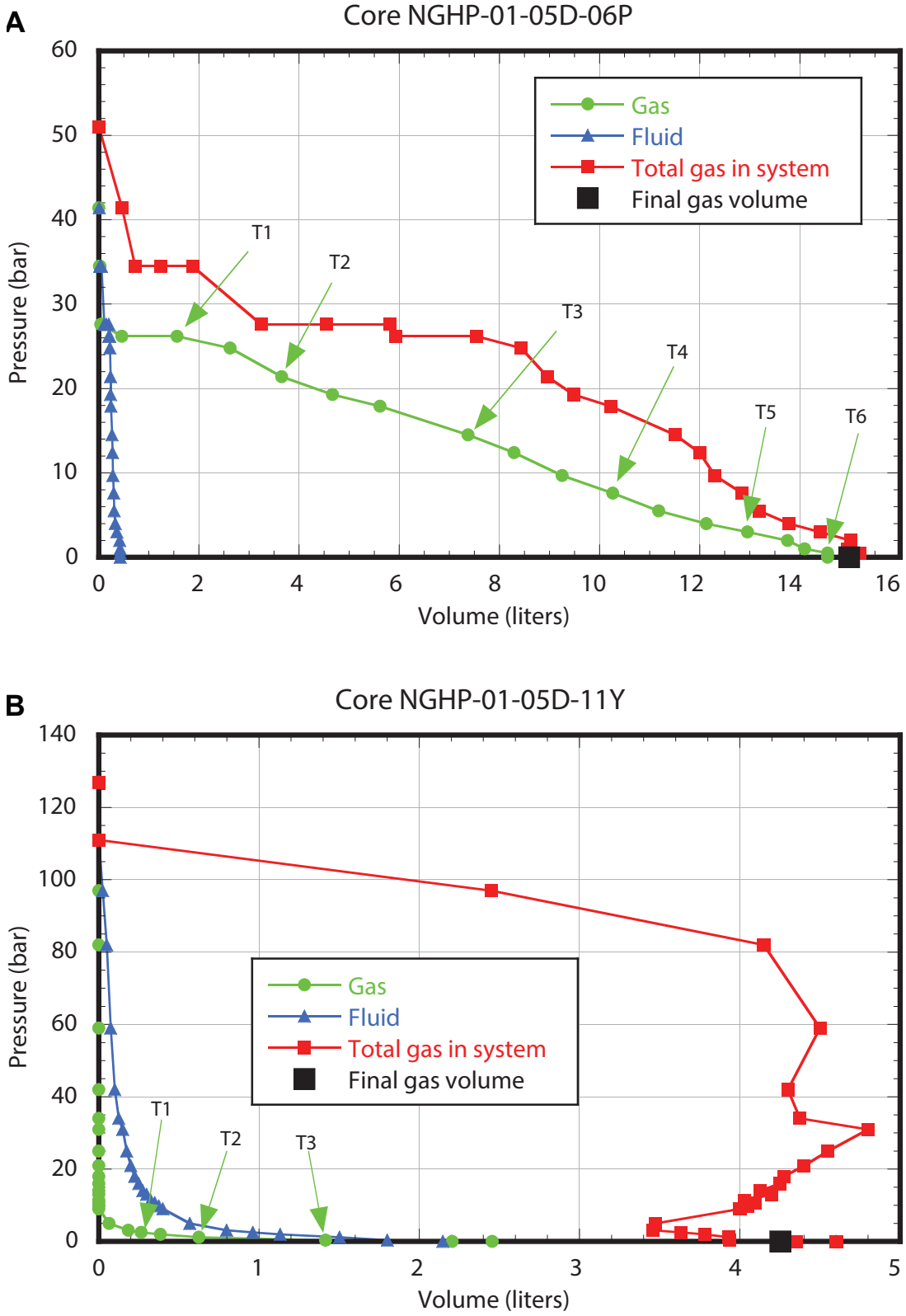

Figure 34. Plot of cumulative volume of gas and fluid released vs. pressure from (A) Cores NGHP-01-05D-06P and (B) NGHP-01-05D-11Y. The depressurization of Core NGHP-01-05D-6P showed a pressure plateau indicating gas hydrate that can be seen in the estimated gas ("total gas in system;" red) but not in the released gas (green). During depressurization of Core NGHP-01-05D-11Y, gas was evolved at a very high pressure (~100 bar) and simply expanded within the pressure system, expelling water. The estimated gas volume ("total gas in system") ceased to change after 80 bar.

- *In situ* **temperature** at the core depth was calculated using the thermal gradients calculated from *in situ* temperature measurements made for the appropriate Site (see "Physical properties").
- *In situ* **salinity** was taken from the estimated baseline salinity at the core depth (see "Inorganic geochemistry").

Calculation of methane hydrate volume in a pressure core:

- **Methane hydrate volume** in a core was only calculated if the *in situ* temperature, pressure, and salinity of the core placed it within the gas-hydrate stability zone.
- **Methane hydrate volume** in a core was calculated from the moles of excess methane, multiplied by the theoretical molecular weight of pure methane hydrate (124 g/mol), divided by the theoretical density of pure methane hydrate (0.91 g/mL).

Calculation of free methane gas volume in a pressure core:

- **Free methane gas volume** in a core was only calculated if the *in situ* temperature, pressure, and salinity of the core placed it outside the gas-hydrate stability zone.
- **Free methane gas volume** in a core was calculated from the moles of excess methane using the ideal gas law (V=nRT/P) and the *in situ* temperature and pressure.

Downhole Logging

The downhole logging program during NGHP Expedition 01 was specifically designed to assess the presence and concentration of gas hydrates on the continental margin of India and of the Andaman Islands. Several logging while drilling and wire-line logging devices were deployed, as described below. Not all tool strings were run in each hole; refer to individual site chapters for details of the tool strings deployed at each site.

Logging While Drilling

During NGHP Expedition 01, five logging-while-drilling (LWD) and measurements while drilling (MWD) tools were deployed in the holes drilled on the eastern continental margin of India. Schlumberger Drilling and Measurements provided these tools under contract with the Lamont-Doherty Earth Observatory Borehole Research Group (LDEO–BRG).

LWD tools measure *in situ* formation properties with instruments that are located in the drill collars immediately above the drill bit. MWD tools are also located in the drill collars and measure downhole drilling parameters (for example, weight on bit, torque). The difference between LWD and MWD tools is that LWD data are recorded into downhole computer memory and retrieved when the tools are brought to the surface, whereas MWD data are transmitted through the drilling fluid within the drill pipe by means of a modulated pressure wave, or "mud pulsing," and monitored in real time (see below). MWD tools enable both LWD and MWD data to be transmitted up-hole when the tools are used in conjunction. The term LWD is often used more generically to cover both LWD- and MWD-type measurements.

LWD measurements are made shortly after the formation is drilled and before the adverse effects of continued drilling or coring operations. Erosion of the borehole wall due to prolonged circulation and drilling fluid invasion into the formation are reduced relative to wire-line logging because of the shorter time elapsed between drilling and taking measurements. LWD logs complement wire-line logs and other measurements in an integrated interpretation of gas-hydrate saturations.

The LWD equipment is powered by batteries or mud turbines and uses erasable/programmable read-only memory chips to store logging data until they are downloaded; a limited amount of data is sent to the surface in real time by the MWD tool. The LWD tools take measurements at evenly spaced time intervals and are synchronized with a system on the drilling rig that monitors time and drilling depth. After drilling, the LWD tools were retrieved and the data downloaded from each tool. Synchronization of the up-hole and downhole clocks allows merging of the time-depth data (from the surface system) and the downhole time-measurement data (from the tools) into depth-measurement data files. The resulting depth-measurement data were transferred to the Schlumberger Drilling and Measurements Integrated Drilling Evaluation and Logging system (IDEAL) on the *JOIDES Resolution* for processing. For a detailed description of the depth tracking systems, see the Explanatory Notes for ODP Leg 204 (Tréhu and others, 2003).

The Schlumberger LWD and MWD tools used during NGHP Expedition 01 include

- the GeoVISION tool (formerly known as the resistivity-at-bit, or RAB tool),
- the EcoScope tool,
- the SonicVISION tool,
- the TeleScope MWD tool, and
- the ProVISION (NMR) tool.

The collar of all these LWD/MWD tools had an outside diameter (OD) of 6.75 in, and we used a 9 7/8 in drilling bit. Some tools had a stabilizer to centralize the collar in the borehole

- GeoVISION (OD of collar 9 3/8 in),
- EcoScope (OD of collar 9 1/8 in), and
- ProVISION (OD of collar 9 7/8 in).

Figure 35 shows the configuration of the LWD/MWD bottom hole assembly (BHA), and table 3 lists the set of measurements recorded. The ProVISION tool that was originally on the ship did not function properly, and we did not use it in Holes NGHP-01-02A through NGHP-01-09A, where the LWD BHA was as in figure 35 without the ProVISION tool at the top. We received a replacement ProVISION that was deployed in Holes NGHP-01-10A, NGHP-01-11A, and NGHP-01-05B.

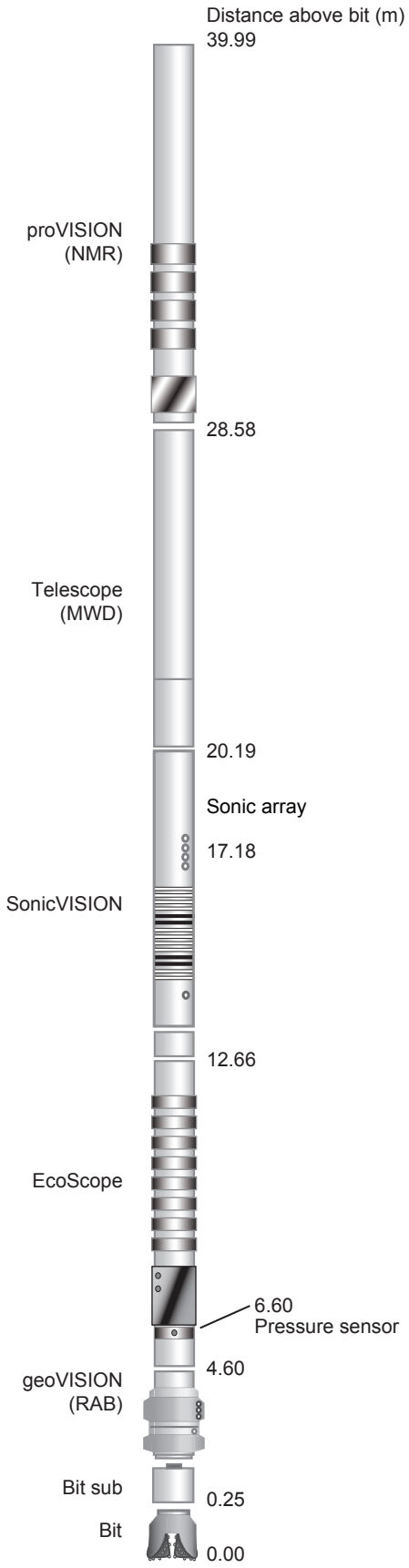

Figure 35. Bottom-hole assembly (BHA) used for LWD operations.

GeoVISION Resistivity Tool

The GeoVISION resistivity, or GVR tool provides resistivity measurements of the formation and electrical images of the borehole wall that are similar to the wire-line Formation MicroScanner but with complete coverage of the borehole walls and lower vertical and horizontal resolution. In addition, it contains a scintillation counter that provides an azimuthal total gamma ray measurement.

The tool is located directly above the drill bit and uses two transmitter coils and a number of electrodes to obtain several resistivity measurements (Bonner and others, 1996):

- *Bit resistivity*.—The lower transmitter coil generates a current that flows through the bit and into the formation, returning to the drilling collar higher in the tool string. By measuring the axial current through the bit for a given voltage, resistivity near the bit is determined by Ohm's law.
- *Ring resistivity*.—The upper and lower transmitter coils produce currents in the collar that meet at the ring electrode. In a homogeneous medium, these currents would flow perpendicularly to the tool at the ring electrode. In a heterogeneous formation, this radial current flow is distorted, and the current required through the ring electrode to focus current flow into the formation is related to the formation resistivity. The ring electrode is only 4 cm thick and provides a high resolution resistivity measurement.
- *Button resistivity*.—The same focusing process used in measuring the ring resistivity is applied to determine the resistivity at three 2.5-cm-wide button electrodes. Button resistivity measurements made about every 6° as the tool rotates in the borehole are stored and processed to produce a resistivity image of the borehole wall. The button electrodes measure resistivity at three depths of investigation, and thus generate three resistivity images: shallow, medium, and deep. The tool uses the Earth's magnetic field to reference the resistivity images to magnetic north.

For quality control reasons, the GeoVISION minimum data recording rate is one measurement per 6-in (15.2-cm) interval; hence, a balance must be determined between the rate of penetration (ROP) and the sampling rate. This relationship depends on the recording rate, the number of data channels to record, and the memory capacity of the tool. During the NGHP Expedition 01 LWD program, we used a data acquisition sampling rate of 5 seconds for high-resolution resistivity images. The maximum ROP allowed to produce one sample per 6-in interval is given by the equation: ROP (m/h) = 548/sample rate. This relationship gives 110 m/h maximum ROP for the GeoVISION. In NGHP Expedition 01, the target ROP was 25 m/h, well below the maximum allowable for the GeoVISION tool. Low penetration rates improve the vertical resolution of the resistivity images to 5–10 cm per rotation. Under this configuration the GeoVISION tool has enough

Table 3. Measurement acronyms and units, vertical resolutions and depths of investigation (where available) of the LWD tools used in NGHP Expedition 01.

[cm, centimeters]

Tool	Output	Explanation	Units	Vertical resolution (cm)	Depth of investigation (cm)
		Multifunction tool			
EcoScope	AXXH, AXXL, AXXB	Attenuation resistivity at source-receiver spacing XX, where XX = 16, 22, 28, 34, 40 in	Ω m	55–122	48–102
	PXXH, PXXL, PXXB	Phase-shift resistivity at source-receiver spacing XX, where XX = 16, 22, 28, 34, 40 in	Ω m	21–30	33–79
	In the output acronyms above, H=2 MHz resistivity; L=400kHz resistivity; B=Blended resistivity				
	GRMA_FILT	Calibrated, filtered gamma ray	gAPI	46	
	DCAV	Density caliper	in		
	UCAV	Ultrasonic caliper	in		
	IDPE	Image-derived photoelectric factor	b/e^-		
	TNPH	Thermal neutron porosity	%	31	
	BPHI	Best thermal neutron porosity	%		
	RHOB	Density	g/cm^3	15	
	IDRO	Image-derived density	g/cm^3		
		Oriented density images of borehole wall			
		Resistivity at the bit tool			
GeoVISION	GR_RAB_FILT	Calibrated, filtered gamma ray	gAPI	46	
	RBIT	Bit resistivity	Ω m	30–61	30
	RING	Ring resistivity	Ω m	5–8	18
	BDAV	Deep button resistivity average	Ω m	5–8	13
	BMAV	Medium button resistivity average	Ω m	5–8	8
	BSAV	Shallow button resistivity average	Ω m	5–8	2.5
		Oriented resistivity images of the borehole wall		5–8	
		Nuclear magnetic resonance tool			
ProVISION	MRP	Magnetic resonance porosity	%	15–120	7
	BFV	Bound fluid volume	%		
	FFV	Free fluid volume	%		
	T2LM	Log mean T2 relaxation time	ms		
	T2	T2 distribution (30 values at each depth)	%		
		Sonic tool			
SonicVISION	DTCC	Compressional wave slowness	µs/ft	61	~10

memory to record up to six days of data. This would be sufficient, under normal operating conditions, to complete the scheduled NGHP Expedition 01 LWD operations.

EcoScope Tool

The EcoScope multifunction tool (also known as the DVD) provides a suite of resistivity, thermal neutron porosity, and azimuthal gamma ray and density measurements. The resistivity measurements are propagation resistivities: electromagnetic waves are both attenuated and phase-shifted when they propagate in a formation of finite conductivity, and the degree of attenuation and phase shift depends on the resistivity of the formation (Bonner and others, 1995, 1996). Phase-shift resistivity has relatively high vertical resolution and a shallow depth of investigation, while attenuation resistivity has lower vertical resolution and a deeper depth of investigation. The dual-frequency (2 MHz and 400 kHz) array of coils in the EcoScope makes 10 phase-shift and 10 attenuation measurements at five transmitter-receiver spacings (16, 22, 18, 34, and 40 in), which correspond to several depths of investigation. For a given frequency, the vertical resolution of phase-shift resistivities measured at different transmitter-receiver separations is similar. Values for vertical resolution and depth of investigation are listed in table 3.

For neutron generation the EcoScope uses a pulsed neutron generator (Minitron), which eliminates the need for a chemical neutron source; the EcoScope still uses a ^{137}Cs gamma ray source for density logging. In addition, the EcoScope provides measurements of elemental capture spectroscopy, neutron gamma density, photoelectric factor, and neutron capture cross-section, or sigma. Drilling optimization measurements include annular pressure while drilling (APWD), ultrasonic and density caliper, and shock detection. We used the APWD measurement to monitor gas in the annulus in real time.

SonicVISION Tool

The SonicVISION tool records monopole acoustic waveforms in downhole memory and transmits up-hole in real time P-wave slowness obtained by processing the recorded

waveforms. The principle of the SonicVISION tool is similar to that of wire-line array sonic tools (Schlumberger, 1989). The monopole source produces energy around 13 kHz that travels into the formation and refracts back into the borehole. In the shallow holes drilled during NGHP Expedition 01, the tool was reconfigured to use a frequency of 7.5 kHz. Sonic waveforms are recorded at four receivers located at 10 ft (3.05 m), 10.67 ft (3.25 m), 11.33 ft (3.45 m), and 12 ft (3.65 m) above the source.

Sonic measurements made while drilling are affected by drilling noise. Because the upward propagation of energy in the formation is synchronized with the transmitter firing and any residual drilling noise is not, averaging the waveforms from various consecutive firings will increase the relative amplitude of coherent signals. A stack size of approximately eight waveforms is deemed appropriate for these conditions. The SonicVISION tool must also be kept centralized in the borehole in order to maximize the strength of the formation signal for stacked waveforms. In large holes and slow sediments, both the formation itself and asymmetry of the annular space in the hole will attenuate the signal.

To monitor for gas, the SonicVISION tool was configured to process and transmit up-hole in real time arrivals within a velocity range appropriate for the drilling fluid (180–230 microseconds/foot). The SonicVISION tool is configured so that waveform data are stored at 10 s intervals, allowing for 83 hr of drilling before the downhole memory is filled. This was sufficient to reach the target depth at each of the NGHP Expedition 01 sites at a typical ROP of 25 m/h. The maximum ROP allowable to achieve one sample per 6-in interval is estimated as ROPmax = 1,800/8 = 225 ft/hr (about 68 m/h). SonicVISION waveform data were downloaded from the tool, converted to depth, and processed to estimate *P*-wave slowness in the formation and waveform coherence using the Schlumberger Drilling and Measurements IDEAL system on the JOIDES Resolution.

TeleScope MWD Tool

The TeleScope tool transmits MWD data up-hole through the fluid in the drill pipe. In practice, TeleScope generates a continuous wave within the drilling fluid (12 or 24 Hz) and changes the phase of this signal (s in frequency modulation) to transmit relevant bit words representing information from various sensors. Two pressure sensors were attached to the standpipe (one near the top and the second near the bottom) on the rig floor and were used to measure the pressure wave in the drilling fluid when information is transmitted up the drill pipe by the MWD tool. Transmission rates are 6 or 12 bits/s, depending primarily on water depth and mud density.

ProVISION NMR Tool

The basic technology behind the ProVISION nuclear magnetic resonance tool is similar to wire-line NMR technology, and is based on measuring the relaxation time of the magnetically induced precession of polarized protons. A combination of magnets and directional antennas are used to focus a pulsed, polarizing field into the formation. The ProVISION tool measures the relaxation time of polarized hydrogen nuclei in the formation, which provides information on the formation porosity. By exploiting the nature of the chemical bonds within pore fluids, for hydrogen in particular, the ProVISION tool can provide estimates of the total porosity and bound fluid volume, and thus be useful to determine whether water, gas, or gas hydrate are present in the formation.

During NGHP Expedition 01, the ProVISION tool recorded downhole relaxation time spectra and transmitted to the surface in real time total porosity estimates. These spectra were stacked in postprocessing to improve the measurement precision. The signal probes a 14-inch cylindrical volume around the borehole, and for an 8-1/2-inch bit size, the depth of investigation of the measurement is ~7 cm into the formation. When the tool is static, the vertical resolution is 6 inches (about 15 cm); when the tool moves, vertical resolution is decreased due to the need to maintain accuracy by vertical stacking of relaxation time spectra. For example, at a logging speed of 30 m/h, the vertical resolution is 1.2 m. Lateral tool motion may reduce ProVISION data quality in some circumstances. Therefore, accelerometers and magnetometers contained in the downhole tool are used to evaluate data quality and determine the maximum relaxation times that can be resolved.

LWD Logging Data Flow and Processing

Data for each LWD logging run were monitored and displayed in real time using the Schlumberger IDEAL system. After logging was completed in each hole, data were downloaded from the tools, processed by Schlumberger to translate acquisition time into depth, and transferred to the shipboard downhole measurement laboratory for preliminary interpretation. GeoVISION and EcoScope image data were interpreted using Schlumberger's GeoFrame software package.

Logging data were also transmitted to LDEO–BRG using a satellite high-speed data link for processing soon after each hole was logged. Data processing at LDEO–BRG consisted of

- Depth-shifting all logs relative to a common datum (in meters below sea floor),
- Corrections specific to individual tools, and
- Quality control and rejection of unrealistic or spurious values.

Once processed at LDEO-BRG, log data were transmitted back to the ship, providing near real-time data processing. Processed data were then replotted on board (see "Downhole logging" section in each site chapter). Further postcruise processing of the log data was performed at LDEO–BRG.

Gas Monitoring with Real Time LWD Data

The LWD logs in NGHP Expedition 01 were acquired in the first hole drilled at each site to plan coring and pressure coring operations in subsequent holes. As the LWD holes were drilled without coring, the data had to be monitored to detect gas entering the wellbore. This new procedure supersedes the old standard of using gas ratio measurements for hydrocarbon safety analysis. Results of previous gas-hydrate drilling programs, such as ODP Legs 146 (Westbrook and others, 1994), 164 (Paull and others, 1996), and 204 (Tréhu and others, 2003), and more recently the Chevron/Texaco Gulf of Mexico Gas Hydrate JIP Drilling Program and IODP Expedition 311, have shown that gas-hydrate-bearing sections do not represent a significant threat to drilling operations and that as long as the hole is advanced at relatively normal drilling rates with mud temperatures near that of the deeper water column there is no significant gas flow from gas-hydrate-bearing formations. However, the main concern of the LWD/MWD monitoring program was the recognition of free-gas zones that may flow.

LWD measurements sensitive to the presence of free gas include the borehole fluid pressure (decrease because of less dense fluids), the compressional velocity in the borehole fluid and the formation (strong decrease with free gas), the coherence of measured sonic waveforms (strong decrease with free gas), the electrical resistivity (increase with free gas), and the neutron and density logs (decrease of density and of neutron porosity, for example neutron/density crossover). In addition, the gamma ray log can help to indicate whether changes in the logs are due to changes in the lithology rather than in the pore fluid; the NMR porosity gives a reference porosity to calibrate the neutron/density crossover; and the caliper can be used to assess the reliability of the measurements and the possible influence of material falling in the borehole.

The primary measurement used in the gas monitoring was the “annular pressure while drilling” (APWD) measured by the EcoScope tool in the borehole annulus (the space between the drill string and the borehole wall). On the basis of a simple calculation of the effect of free gas on the borehole fluid density, it was determined that a pressure decrease of more than 100 psi (pounds per square inch) from the general trend of fluid pressure would indicate that a significant amount of gas had been released into the drilling fluid. For example, a pressure decrease of 100 psi corresponds to a 25-percent gas saturation in a borehole drilled to 300 mbsf. It was also decided to monitor sudden pressure increases of more than 100 psi, which had been reported as precursors to gas flow into the annulus (Aldred and others, 1998).

We also set the SonicVISION tool to process the borehole fluid velocity in real time because previous drilling experience in North Sea wells had shown that the presence of gas caused the coherence of the sonic waveforms to decrease and the computed value of fluid velocity to become erratic. In practice, we monitored the coherence of the sonic waveforms used to infer the fluid velocity: a low coherence may indicate the presence of gas. Although the pressure and acoustic sensors are located at some distance above the drilling bit (6.6 m and 17.2 m, respectively; see fig. 35), gas will rapidly move upward in the annulus from the point of entry at the bit and would be detected quickly.

Figure 36 shows the real-time screen that we used to monitor the LWD data during NGHP Expedition 01. The pertinent curves for gas monitoring are the annular pressure while drilling (APWD), the equivalent circulating density (ECD), and the sonic coherence. The annular pressure while drilling increases with depth approximately following the hydrostatic trend, while the equivalent circulating density (the equivalent density of a column of fluid that would give the measured annular pressure) remains approximately constant with a value near that of the water density (~8.65 lb/gal). The sonic coherence curve in figure 36 is the peak value of coherence of the sonic waveforms, and it normally is in the interval 0.5–0.9. The real-time screen also shows rate of penetration and data from the ultrasonic and density calipers, the gamma ray, resistivity, density, and neutron porosity.

The monitoring procedure we used followed the decision tree shown in figure 37, which is described below.

1. If a > 100 psi pressure decrease is observed, then drilling advancement will cease and relevant personnel will be notified. Seawater will be circulated in the hole and the APWD response will be monitored to obtain the baseline pressure. Duration of monitoring will depend on geologic and drilling conditions at a particular site and depth, based on shipboard personnel experience.
2. An observed pressure decrease of 150 psi will result in terminating the hole and following plug and abandonment procedures.
3. If a < 150 psi decrease is observed, drilling can advance at a reduced rate of penetration (ROP), with continued monitoring of pressure and other sensors. Pressure will be maintained within 150 psi of normal using weighted mud, as required. The ability to continue advancing the hole while controlling pressure changes with weighted mud is dependent upon onboard mud capacity and availability.
4. If pressure cannot be controlled with 10.5 pound per gallon (ppg) mud, the hole will be plugged and abandoned.
5. If pressure can be controlled with 10.5 ppg mud, then drilling advancement may continue.

A pressure decrease caused by gas flow into the borehole may be preceded by a pressure increase as the result of acceleration of fluids in the annulus (Aldred and others, 1998). If an increase >100 psi is observed, drilling will cease as a precautionary measure and relevant personnel will be notified. Seawater will be circulated in the hole and the APWD response will be monitored to obtain the baseline pressure. Because no overpressure water flow events are expected or likely in this environment, such a pressure increase could be the result of the aforementioned precursor or drilling-induced pressure increases. A drilling-induced pressure increase will be resolved by cleaning the hole whereas the precursor event will be followed by a pressure decrease, leading to appropriate response as dictated by the procedure above.

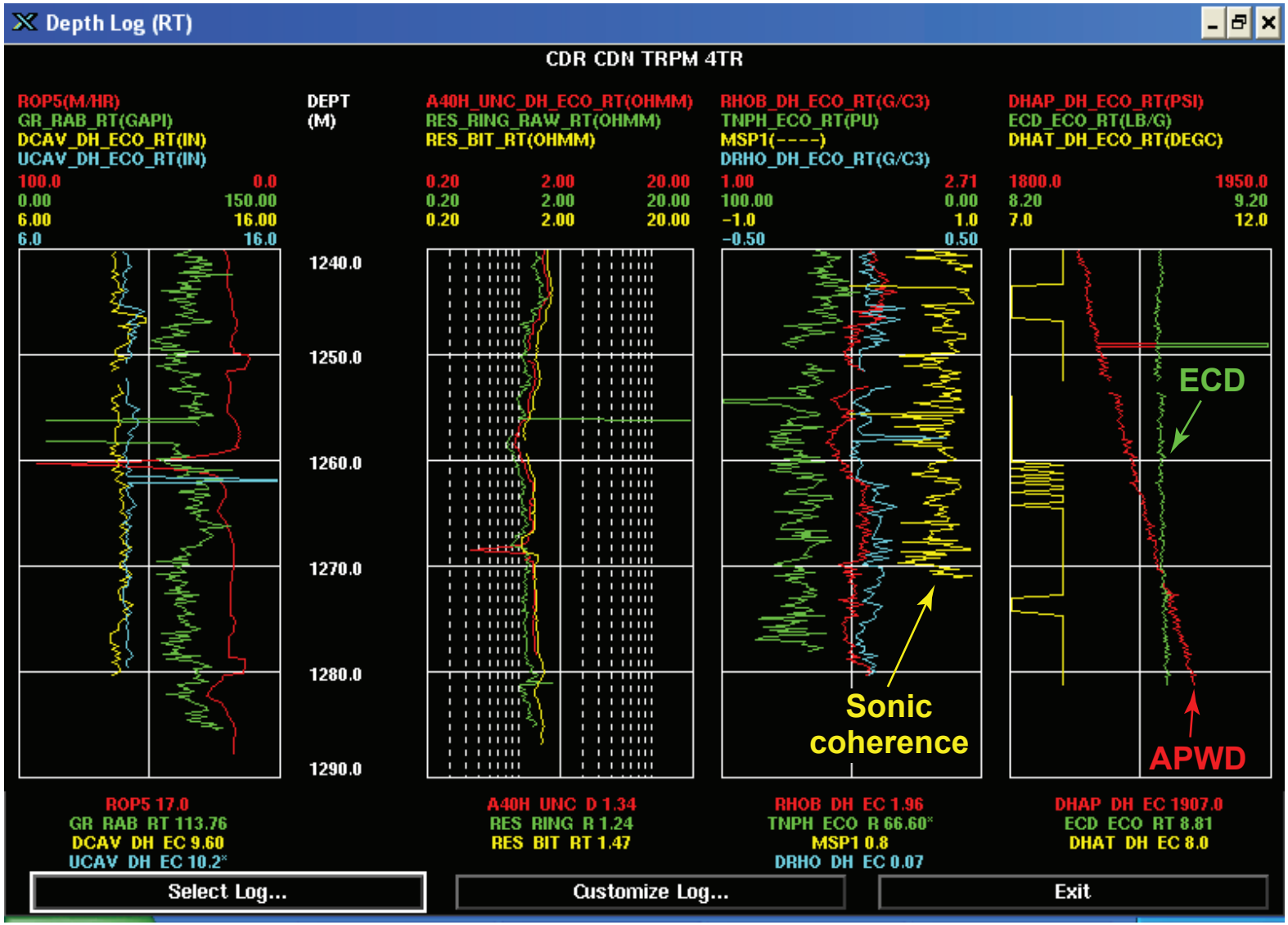

Figure 36. Example of real-time LWD monitoring screen. The curves useful for gas monitoring are the annular pressure while drilling (APWD, red), the equivalent circulating density (ECD, green), and the sonic coherence (yellow). ROP5 = Rate of penetration averaged over the last 5 ft; GR_RAB_RT = Gamma ray log (GeoVISION); DCAV_DH_ECO_RT = Density caliper (EcoScope); UCAV_DH_ECO_RT = Ultrasonic caliper (EcoScope); A40H_UNC_DH_ECO_RT = 2 MHz attenuation resistivity for a 40 in coil spacing (EcoScope); RES_RING_RAW_RT = Ring resistivity (GeoVISION); RES_BIT_RT = Bit resistivity (GeoVISION); RHOB_DH_ECO_RT = Bulk density (EcoScope); TNPH_ECO_RT = Thermal neutron porosity (EcoScope); MSP1 = Sonic waveform coherence (SonicVISION); DRHO_DH_ECO_RT = Density correction (EcoScope); DHAP_DH_ECO_RT = Annular pressure (EcoScope); ECD_ECO_RT = Equivalent circulating density (EcoScope); DHAT_DH_ECO_RT = Annular temperature (EcoScope).

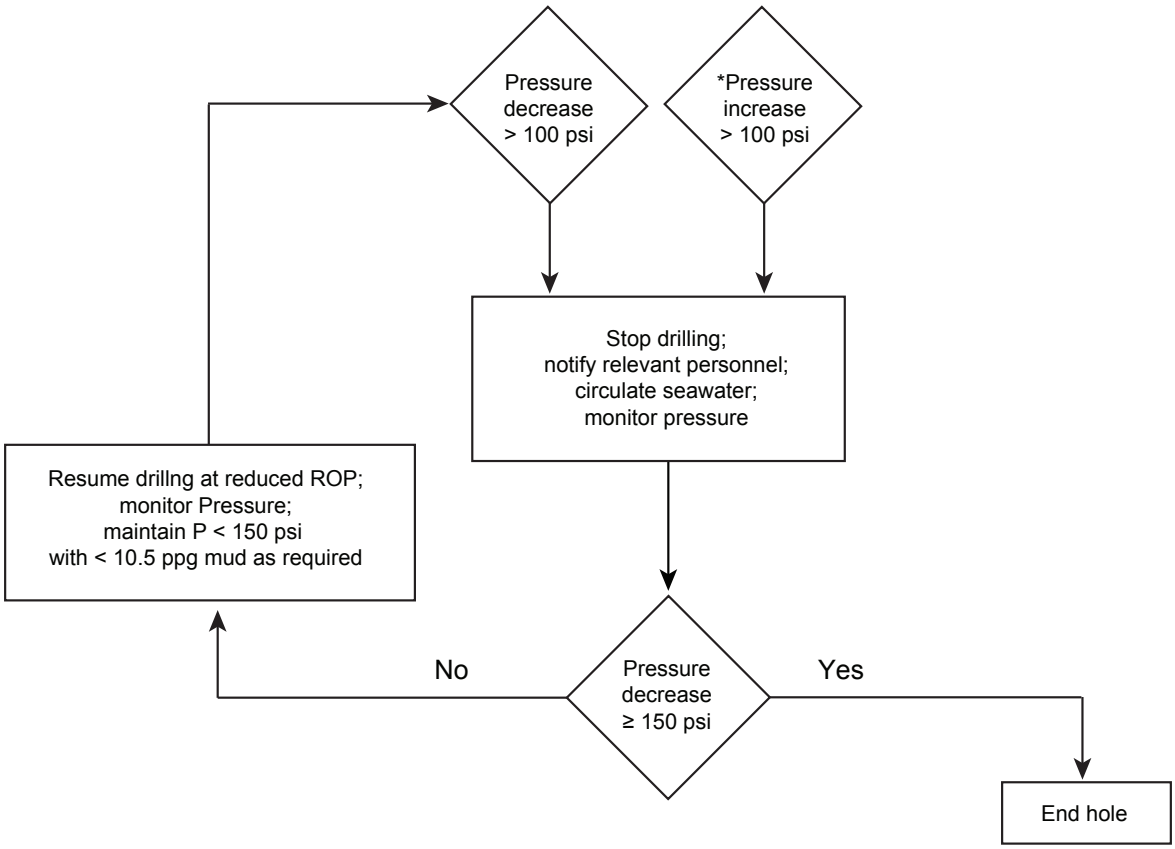

Figure 37. Decision tree used in gas monitoring based on LWD borehole fluid pressure measurements. Pressure increases were also monitored because they may be precursors to a gas flow pressure decrease. The ability to continue advancing hole while controlling pressure change at <150 psi with weighted mud will be dependent upon onboard mud capacity and availability. A mud weight >10.5 ppg required to control pressure results in hole abandonment. [psi, pounds per square inch; ppg, pounds per gallon]

Wire-line Logging Measurements

During NGHP Expedition 01, three wire-line logging tool strings were deployed (fig. 38 and table 4):

1. The triple combination (triple combo) string (resistivity, density, and porosity measurements), which consists of the Hostile Environment Gamma Ray Sonde (HNGS), the phasor dual induc-tion (DIT) tool, the Hostile Environment Litho-Density Tool (HLDT), and the Accelerator Porosity Sonde (APS).
2. The FMS-sonic tool string, which consists of the FMS, General Purpose Inclinometer Tool (GPIT), and Scintillation Gamma Ray (SGT) Tool, and the Dipole Sonic Imager (DSI).
3. The Vertical Seismic Imager (VSI).

Tool name acronyms, the parameters measured by each tool, the depth of investigation, and the vertical resolution are summarized in Table 4. More detailed descriptions of individual logging tools and their geological applications can be found in Ellis (1987), Goldberg (1997), Rider (1996), Schlumberger (1989, 1994), Serra (1984, 1986, 1989), and the LDEO–BRG Wire-line Logging Services Guide (2001).

Hostile Environment Spectral Gamma Ray Sonde (HNGS) and Scintillation Gamma Ray Tool (SGT)

The HNGS measures the natural gamma radiation from isotopes of potassium (K), thorium (Th), and uranium (U) and uses a five-window spectroscopic analysis to determine concentrations of radioactive K (in weight percent), Th (in parts per million), and U (in parts per million). The HNGS uses two bismuth germanate scintillation detectors for gamma ray detection with full spectral processing. The spectral analysis filters out gamma ray energies below 500 keV, eliminating sensitivity to bentonite or KCl in the drilling mud and improving measurement accuracy. The HNGS also provides a measure of the total gamma ray emission (in American Petroleum Institute units [gAPI]), and the uranium-free or computed gamma ray emission (CGR) (in gAPI units). The HNGS response is influenced by the borehole diameter and the weight and concentration of bentonite or KCl present in the drilling mud. KCl may be added to the drilling mud to prevent freshwater clays from swelling and forming obstructions. All of these effects are corrected for during processing of HNGS data at LDEO-BRG.

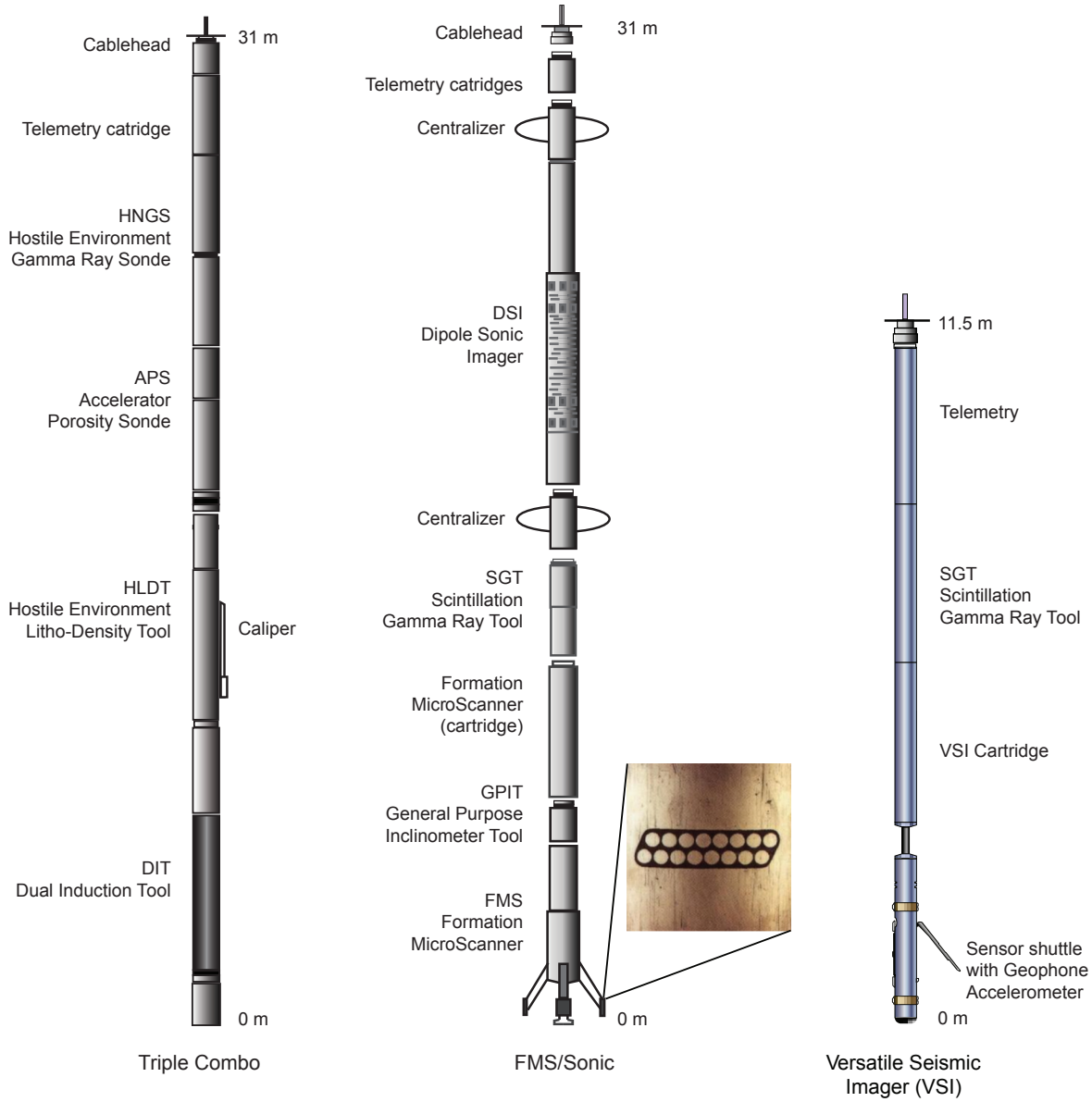

Figure 38. Tool strings used for wire-line logging operations.

The SGT tool uses a sodium iodide scintillation detector to measure the total natural gamma ray emission, combining the contributions of K, Th, and U concentrations in the formation. The SGT is not a spectral tool but provides high-resolution total gamma ray data for depth correlation between logging strings. It is included in all tool strings (except the triple combo, where the HNGS is used) to provide a reference log to correlate depth between different logging runs.

Hostile Environment Litho-Density Tool (HLDT)

The HLDT consists of a radioactive cesium (^{137}Cs) gamma ray source (622 keV) and far and near gamma ray detectors mounted on a shielded skid, which is pressed against the borehole wall by a hydraulically activated eccentralizing arm. Gamma rays emitted by the source experience both Compton scattering and photoelectric absorption. Compton scattering involves the ricochet of gamma rays off electrons in the formation via elastic collision, transferring energy to the electron in the process. The number of scattered gamma rays that reach the detectors is directly related to the number of electrons in the formation, which in turn is related to bulk density. Porosity may also be derived from this bulk density if the matrix density is known.

The HLDT also measures the photoelectric factor (PEF) caused by absorption of low-energy gamma rays. Photoelectric absorption occurs when gamma rays reach <150 keV after being repeatedly scattered by electrons in the formation. As the PEF depends on the atomic number of the elements in the formation, it is essentially independent of porosity, and varies according to the chemical composition of the sediment. Some examples of PEF values are pure calcite, 5.08; illite, 3.03;

Table 4. Measurement acronyms and units, vertical resolutions and depths of investigation (where available) of the wire-line logging tools used in NGHP Expedition 01.

[µs/ft, microsiements per foot; m/s^2, meters per seconds squared; g/cm^3, grams per cubic centimeter; wt%, weight percent; ppm, parts per million; gAPI, American Petroleum Institute gamma-ray units]

Tool	Output	Explanation	Units	Vertical resolution (cm)	Depth of investigation (cm)
APS		Accelerator Porosity Sonde			
	APLC	Near array porosity (limestone calibrated)	%	43	
	SIGF	Formation capture cross section	Capture units	31	
	STOF	Tool standoff (distance from borehole wall)	in		
DIT		Dual Induction Tool			
	IDPH	Deep induction resistivity	Ω m	246	122–158
	IMPH	Medium induction resistivity	Ω m	185	66–79
	SFLU	Spherically focused resistivity	Ω m	61	41
DSI		Dipole Sonic Imager			
	DTCO	Compressional wave slowness	µs/ft	107	~10
	DTSM	Shear wave slowness	µs/ft	107	~10
	DTST	Stoneley wave slowness	µs/ft	107	~10
FMS		Formation MicroScanner			
	C1, C2	Orthogonal hole diameters	in		
	P1AZ	Pad 1 azimuth	degrees		
		Oriented resistivity images of borehole wall		0.5	2
GPIT		General Purpose Inclinometer Tool			
	DEVI	Hole deviation	degrees		
	HAZI	Hole azimuth	degrees		
	Fx, Fy, Fz	Earth's magnetic field (3 orthogonal components)	Oersted		
	Ax, Ay, Az	Acceleration (3 orthogonal components)	m/s^2		
HLDT		Hostile Environment Litho-Density Tool			
	RHOB	Bulk density (corrected)	g/cm^3	46	
	PEF	Photoelectric effect	b/e^-		
	CALI	Caliper (borehole diameter)	in		
	DRHO	Bulk density correction	g/cm^3		
HNGS		Hostile Environment Gamma Ray Sonde			
	HSGR	Standard (total) gamma ray	gAPI	51	
	HCGR	Computed gamma ray (minus uranium contribution)	gAPI	51	
	HFK	Potassium	wt%	51	
	HTHO	Thorium	ppm	51	
	HURA	Uranium	ppm	51	
SGT		Scintillation Gamma Ray Tool			
	ECGR	Environmentally corrected gamma ray	gAPI	46	
VSI		Versatile Seismic Imager			

quartz, 1.81; and kaolinite, 1.49 b/e–. The PEF values can be used in combination with HNGS curves to identify different types of clay minerals. Coupling between the tool and borehole wall is essential for good HLDT logs. Poor contact results in underestimation of density values. Both density correction and caliper measurement of the hole are used to check the contact quality.

Accelerator Porosity Sonde (APS)

The APS consists of a minitron neutron generator that produces fast neutrons (14.4 MeV) and five neutron detectors (four epithermal and one thermal) positioned at different spacings along the tool. The tool is pressed against the borehole wall by an eccentralizing bow-spring. Emitted high-energy (fast) neutrons are slowed down by collisions with atoms. The amount of energy lost per collision depends on the relative mass of the nucleus with which the neutron collides. The largest energy loss occurs when the neutron strikes a nucleus of equal mass, such as hydrogen, which is mainly present in pore water. Once neutrons degrade to thermal energies (0.025 eV), they may be captured by the nuclei of silicon, chlorine, boron, and other elements, with the associated emission of a gamma ray. The neutron detectors record both the numbers of neutrons arriving at various distances from the source and the neutron arrival times, which are a measure of formation porosity. However, hydrogen bound in minerals such as clays or in hydrocarbons also contributes to the measurement, so the raw porosity value is often an overestimate of the formation porosity.

Phasor Dual Induction-Spherically Focused Resistivity Tool (DIT)

The DIT tool provides three different measurements of electrical resistivities, each with a different depth of penetration into the formation. Two induction devices (deep and medium resistivity) transmit high-frequency alternating currents through transmitter coils, creating magnetic fields that induce secondary (Foucault) currents in the formation. These ground-loop currents produce new inductive signals, proportional to the conductivity of the formation, which are measured by the receiving coils. The measured conductivities are then converted to resistivity. A third device, a spherically focused resistivity instrument that gives higher vertical resolution, measures the current necessary to maintain a constant voltage drop across a fixed interval.

Dipole Sonic Imager (DSI)

The DSI employs a combination of monopole and dipole transducers to make measurements of sonic wave propagation in a wide variety of formations. In addition to a robust measurement of *P*-wave velocity, the DSI uses the dipole source to generate a flexural mode in the borehole that can be used to estimate shear (*S*-wave) velocity even in highly unconsolidated formations. When the formation shear velocity is less than the sonic velocity of the borehole fluid, particularly in unconsolidated sediments, the flexural wave travels at the *S*-wave velocity and is the most reliable way to estimate a shear velocity log. Meanwhile, the monopole source generates *P*-, *S*-, and Stoneley waves into hard formations. The configuration of the DSI also allows recording of cross-dipole waveforms for anisotropy analysis. In many cases, the dipole sources can also provide estimates of *S*-wave velocity in hard rocks better than or equivalent to the monopole source. These combined modes can be used to estimate *S*-wave splitting caused by preferred mineral and(or) structural orientation in consolidated formations. A low-frequency (1 kHz) source enables Stoneley waveforms to be acquired as well.

The DSI measures the transit times between sonic transmitters and an array of eight receiver groups with 15-cm spacing, each consisting of four orthogonal elements that are aligned with the dipole transmitters. During acquisition, the output from these 32 individual elements are differenced or summed appropriately to produce in-line and cross-line dipole signals or monopole-equivalent (*P*- and Stoneley) waveforms, depending on the operation modes. The detailed description of tool configuration and data processing are described in the Leg 174B Initial Reports volume (Shipboard Scientific Party, 1998). The velocity data from the DSI together with the formation density can be used to generate a synthetic seismogram for correlation with seismic data.

Formation MicroScanner Tool (FMS)

The FMS produces high-resolution images of borehole wall microresistivity that can be used for detailed sedimentologic or structural interpretation. This tool has 4 orthogonally oriented pads, each with 16 button electrodes (5 mm diameter) that are pressed against the borehole wall (see inset in fig. 38). Good contact with the borehole wall is necessary for acquiring good-quality data. Approximately 30 percent of a borehole with a diameter of 25 cm is imaged during a single pass. Coverage may be increased by a second run. The vertical resolution of FMS images is ~5 mm, allowing features such as burrows, thin beds, fractures, veins, and vesicles to be imaged. The resistivity measurements are converted to color or grayscale images for display. FMS images are oriented to magnetic north using the GPIT (see below). This allows the dip and strike of geological features intersecting the hole to be measured from processed FMS images. FMS images can be used to visually compare logs with the core to ascertain the orientations of bedding, fracture patterns, and sedimentary structures (Serra, 1989; Luthi, 2001).

General Purpose Inclinometer Tool (GPIT)

The GPIT is included in the FMS-sonic tool string to calculate tool acceleration and orientation during logging. The GPIT contains a triple-axis accelerometer and a triple-axis magnetometer. The GPIT records the orientation of the FMS images and allows more precise determination of log depths than can be determined from cable length, as the accelerometer data can be used to correct for cable stretching, tool sticking, and ship heave. Detailed tool motion information is necessary to process the FMS data and obtain accurate images of the formation (Luthi, 2001).

Versatile Seismic Imager (VSI)

The VSI is a borehole seismic wire-line tool optimized for vertical seismic profiles (VSPs) and walkaway vertical seismic profiles (WVSPs) in both cased and open hole and vertical and deviated wells. It consists of multiple shuttles (each containing a three-axis geophone) separated by "hard wired" acoustically isolating spacers. During NGHP Expedition 01, we used the VSI tool with a single shuttle. The acoustic waves were generated by a 105 in^3 GI (Generator-Injector) air gun, positioned ~2 m below sea level, and offset by 50 m on the port side of the *JOIDES Resolution*. The VSI was clamped against the borehole wall at 5 to 10 m intervals, and the air gun was typically fired between five and fifteen times at each station. The recorded waveforms were stacked and a one-way travel time was determined from the median of the first breaks for each station, thus providing check shots for calibration of the integrated transit time calculated from sonic logs. Check shot calibration is required for well-seismic

correlation because P-wave velocities derived from the sonic log may differ significantly from the velocities determined by seismic data. Causes for this difference include

- Frequency dispersion (the sonic tool operates at 10–20 kHz, with seismic data in the 50–200 Hz range),
- Difference in travel paths between well sonic and surface seismic surveys, and
- Borehole effects caused by formation alterations (Schlumberger, 1989).

In addition, sonic logs cannot be measured through pipe, so the travel time down to the uppermost logging point has to be estimated by other means.

Wire-line Logging Data Flow and Processing

Data for each wire-line logging run were recorded and stored digitally and monitored in real time using the Schlumberger MAXIS 500 system. After logging was completed in each hole, data were transferred to the shipboard downhole measurement laboratory for preliminary processing and interpretation. FMS image data were interpreted using Schlumberger's GeoFrame software package.

Logging data were also transmitted to LDEO–BRG using a satellite high-speed data link for processing soon after each hole was logged. Data processing at LDEO–BRG consists of

- Depth-shifting all logs relative to a common datum (that is, mbsf),
- Corrections specific to individual tools, and
- Quality control and rejection of unrealistic or spurious values.

Once processed at LDEO-BRG, log data were transmitted back to the ship, providing near real-time data processing. Processed data were then replotted on board (see "Downhole logging" section in each site chapter). Further postcruise processing of the log data from the FMS was performed at LDEO–BRG. Downhole logging aboard was provided by LDEO–BRG in conjunction with Schlumberger Reservoir Evaluation Services, and Schlumberger Drilling and Measurements.

Wire-line Logging Data Quality

Logging data quality may be seriously degraded by changes in the hole diameter and in sections where the borehole diameter greatly decreases or the hole is washed out. Deep-investigation measurements such as resistivity and sonic velocity are least sensitive to borehole conditions. Nuclear measurements (density and neutron porosity) are more sensitive because of their shallower depth of investigation and the effect of drilling fluid volume on neutron and GRA. Corrections can be applied to the original data to reduce these effects. For very large washouts, however, data cannot be corrected. HNGS and SGT data provide a depth correlation between logging runs. Logs from different tool strings may, however, still have minor depth mismatches caused by either cable stretch or ship heave during recording. Ship heave is minimized by a hydraulic wire-line heave compensator designed to adjust for rig motion during logging operations.

Gas-Hydrate Detection and Evaluation with Down-Hole Logs

With growing interest in natural gas hydrate, it is becoming increasingly important to be able to identify the presence of *in situ* gas hydrate and accurately assess the volume of gas hydrate and associated free gas within gas-hydrate accumulations. Numerous publications (Mathews, 1986; Collett, 1993, 1998a, 1998b, 2000; Goldberg, 1997; Guerin and others, 1999; Goldberg and others, 2000; Helgerud and others, 2000) have shown that downhole geophysical logs can yield information about the presence of gas hydrate.

Because gas hydrates are characterized by unique chemical compositions and distinct physical properties, it is possible to obtain gas-hydrate saturation (percent of pore space occupied by gas hydrate) and sediment porosity data by characterizing the electrical resistivity, acoustic properties, and chemical composition of the pore-filling constituents within gas-hydrate-bearing reservoirs. Two of the most critical reservoir parameters to determine are porosity and gas-hydrate saturation. Downhole logs often serve as a source of porosity and hydrocarbon saturation data. Most of the existing gas-hydrate log evaluation techniques are qualitative in nature and have been developed by the extrapolation of petroleum industry log evaluation procedures. To properly test the adequacy of standard petroleum log evaluation techniques in gas-hydrate-bearing reservoirs would require numerous laboratory and field measurements. However, only a limited number of gas-hydrate occurrences have been sampled and surveyed with open-hole logging devices.

Reviewed below are downhole log measurements that together yield useful gas-hydrate-reservoir information. The downhole measurements considered include density, neutron porosity, nuclear magnetic resonance, electrical resistivity, and acoustic transit time. Most of these measurements are converted to porosity; because gas hydrate affects each measurement of porosity in a different fashion, the quantity of gas hydrate can be estimated by comparison of porosity measurements made using different techniques.

Density Logs

Density logs are primarily used to assess sediment porosities. The theoretical bulk density of a Structure I methane hydrate is ~0.9 g/cm^3 (Sloan, 1998). Gas hydrate can cause a small but measurable effect on density-derived porosities. At relatively high porosity (>40 percent) and high gas-hydrate saturation (>50 percent), the density log-derived porosities need to be corrected for the presence of gas hydrate (Collett, 1998b).

Neutron Porosity Logs

Neutron logs are also used to determine sediment porosities. Because Structure I methane hydrate and pure water have similar hydrogen concentrations, it can be generally assumed that neutron porosity logs, which are calibrated to pure water, are not significantly affected by the presence of gas hydrates. At high reservoir porosities, however, the neutron porosity log could overestimate porosities (Collett, 1998b).

Nuclear Magnetic Resonance Logs

NMR logs use the electromagnetic properties of hydrogen nuclei to analyze the nature of the chemical bonds within pore fluids. Relative to other pore-filling constituents, gas hydrate exhibits unique chemical structures and hydrogen concentrations. In theory, therefore, it should be possible to develop NMR well-log evaluation techniques that would yield accurate reservoir porosities and water saturations in gas-hydrate-bearing sediments. Gas hydrate cannot be directly detected with today's downhole NMR tools; however, these tools can yield very accurate gas-hydrate saturation estimates. Because of the short transverse magnetization relaxation times (T2) of the water molecules in the clathrate, gas hydrates are not "seen" by the NMR tool as fluid, and behave as part of the solid matrix. Thus, the NMR-calculated total porosity in a gas-hydrate-bearing sediment should be lower than the actual porosity. With an independent source of accurate total porosity, such as density- or neutron-porosity log measurements, it should be possible to accurately estimate gas hydrate saturations by comparing the apparent NMR-derived porosity to the total density-derived porosity (Kleinberg and others, 2005).

Electrical Resistivity

Water content (S_w) and pore water salinity are the most significant factors controlling the electrical resistivity of a formation. Other factors include the concentration of hydrous and metallic minerals, volume of hydrocarbons including gas hydrate, and pore structure geometry. Gas-hydrate-bearing sediments exhibit relatively high electrical resistivities in comparison to water-saturated units, which suggests that a downhole resistivity log can be used to identify and assess the concentration of gas hydrate in a sedimentary section. The relation between rock and pore fluid resistivity has been studied in numerous laboratory and field experiments. From these studies, relations among porosity (φ), pore fluid resistivity (R_w), and formation resistivity (R_t) have been developed. Among them, the empirical relation established by Archie (Archie, 1942) is used to estimate water saturations in gas-oil-water-matrix systems:

$$S_w = [(a\, R_w) / (\phi^m\, R_t)]^{1/n}.$$

where a, m, and n are called the "Archie coefficient", the "cementation exponent" and the "saturation exponent", respectively.

In this relationship, the term "$a\, R_w/\phi^m$" represents the resistivity R_o predicted by Archie (1942) in a water-saturated formation. Research has shown that the Archie relation yields useful gas-hydrate saturation data (reviewed by Collett, 2000). Gas-hydrate saturation (S_h) is the percentage of pore space in sediment occupied by gas hydrate, which is the complement of the water saturation S_w:

$$S_h = 1 - S_w.$$

It may seem necessary to use a modified version of Archie's equation (for example, Waxman and Smits, 1968) to account for the conductivity effect of clays in clay-rich marine sediments. Erickson and Jarrard (1998), however, showed that shallow, high-porosity marine siliciclastic sediments do not display any conductivity increase due to clay and it is appropriate to apply the simple Archie relationship above.

Gas Hydrate Saturation Estimation from Archie's Relationship

The formation resistivity (R_t) and the porosity used in Archie's relationship are directly provided by the logs. Water resistivity (R_w), can be derived from Fofonoff (1985), using the water salinity measured in core samples and the downhole temperature measurements that constrain the local geothermal gradient.

A common way to choose values for the Archie coefficient a and the "cementation exponent" m is to choose a logged interval where the sediments can be assumed to be water saturated and to fit a and m to a crossplot of measured resistivity versus the porosity, known as a "Pickett plot". In marine sediments, however, the range of porosity is relatively small and it is not possible to obtain a robust estimate of both a and m. We prefer to fix a to unity, which is physically the most realistic value, because it gives a resistivity equal to the formation water resistivity when the porosity is 100 percent. We then compute a log of "estimated m" given by

$$m_{est} = -\log F / \log \phi,$$

where

$F = R_t / R_w$ is the formation factor.

A reasonable value of m can be chosen from the baseline trend of this "estimated m" curve. The saturation exponent can be assumed to be n = 2 (Pearson and others., 1983).

Acoustic Transit Time

The velocity of P- and S-waves in a solid medium, such as gas-hydrate-bearing sediment, is usually significantly greater than the velocity of P- and S-waves in water or gas-bearing sediments. Studies of downhole acoustic log data from both marine- and permafrost-associated gas-hydrate accumulations have shown that the volume of gas hydrate in sediment can also be estimated by measuring interval velocities (Guerin and

others, 1999; Helgerud and others, 2000; Collett, 2000). Analysis of sonic logging waveforms has also shown that the presence of gas hydrate can generate significant energy loss in monopole and dipole waveforms (Guerin and Goldberg, 2002).

Interpreting Structure from GeoVISION (RAB) and Formation MicroScanner Images

Structural data were determined from GeoVISION electrical resistivity images using Schlumberger's GeoFrame software. GeoFrame presents GeoVISION data as a planar, "unwrapped" 360° resistivity image of the borehole with depth. The image orientation is referenced to north, which is measured by the magnetometers inside the tool, and the hole is assumed to be vertical. Horizontal features appear horizontal on the images, whereas planar, dipping features are sinusoidal in aspect. Sinusoids are interactively fitted to beds and fractures to determine their dip and azimuth, and the data are exported from GeoFrame for further analysis.

Methods of interpreting structure and bedding differ considerably between core analysis and wire-line Formation MicroScanner (FMS) images and GeoVISION image analysis. Resolution is considerably lower for GeoVISION image interpretation (5–10 cm at best, compared with millimeters within cores and 0.5 cm for FMS images), and therefore identified features are likely to be different in scale. For example, microfaults ("small faults," <1 mm width) and shear bands (1–2 mm, up to 1 cm width) can only be identified in FMS data. This should be considered when directly comparing FMS and GeoVISION images. GeoVISION provides 360° coverage at a lower resolution, FMS provides higher resolution data but coverage is restricted to only ~1/3 of the borehole wall. Fractures were identified within GeoVISION images by their anomalous resistivity or conductivity and from contrasting dip relative to surrounding bedding trends. Differentiating between fractures and bedding planes can be problematic, particularly if both are steeply dipping and with similar orientations.

References Cited

Aldred, W., Cook, J., Bern, P., Carpenter, B., Hutchinson, M., Lovell, J., Rezmer-Cooper, I., and Leder, P.C., 1998, Using downhole annular pressure measurements to improve drilling performance: Oilfield Review, Winter 1998, p. 40–55.

American Society for Testing and Materials (ASTM), 1997, Standard test method for specific gravity of soil solids by gas pycnometer D 5550–94, *in* American Society for Testing and Materials, Annual Book of ASTM Standards, v. 04.09, Soil and Rock: West Conshohocken, Penn., p. 380–383.

Archie, G.E., 1942, The electrical resistivity log as an aid in determining some reservoir characteristics: Journal of Petroleum Technology, v. 5. p. 1–8.

Balsam, W.L., and Damuth, J.E., 2000, Further investigations of shipboard vs. shore-based spectral data—Implications for interpreting Leg 164 sediment composition, *in* Paull, C.K., Matsumoto, R., Wallace, P., and Dillon, W.P., eds., Proceedings of the Ocean Drilling Program, Scientific Results, v. 164: College Station, Tex., Ocean Drilling Program, p. 313–324. [CD-ROM; available from: Ocean Drilling Program, Texas A&M University, College Station, Tex. 77845-9547, U.S.A.]

Balsam, W.L., Damuth, J.E., and Schneider, R.R., 1997, Comparison of shipboard vs. shore-based spectral data from Amazon-Fan cores—Implications for interpreting sediment composition, *in* Flood, R.D., Piper, D.J.W., Klaus, A., and Peterson, L.C., eds., Proceedings of the Ocean Drilling Program Scientific Results, v. 155: College Station, Tex., Ocean Drilling Program, p. 193–215. [CD-ROM; available from: Ocean Drilling Program, Texas A&M University, College Station, Tex. 77845-9547, U.S.A.]

Balsam, W.L., Deaton, B.C., and Damuth, J.E., 1998, The effects of water content on diffuse reflectance measurements of deep-sea core samples—An example from ODP Leg 164 sediments: Marine Geology, v. 149, p. 177–189.

Blum, P., 1997. Physical properties handbook—A guide to the shipboard measurement of physical properties of deep-sea cores: Ocean Drilling Program Technical Note 26. (Available at *http://www.odp.tamu.edu/publications/tnotes/tn26/INDEX.HTM*.)

Bonner, S.D., Tabanou, J.R., Wu, P.T., Seydoux, J.P., Moriarty, K.A., Seal, B.K., Kwok, E.Y., and Kuchenbecker, M.W., 1995, New 2-MHz multiarray borehole-compensated resistivity tool developed for MWD in slim holes. Paper presented at Annual Technical Conference Exhibition Society of Petroleum Engineers, Dallas, October 1995, Paper SPE 30547.

Bonner, S., Fredette, M., Lovell, J., Montaron, B., Rosthal, R., Tabanou, J., Wu, P., Clark, B., Mills, R., and Williams, R., 1996, Resistivity while drilling—Images from the string, Oilfield Review, Spring 1996, p. 4–19.

Bullard, E.C., 1954, The flow of heat through the floor of the Atlantic Ocean: Proceedings of the Royal Society A, v. 222, p. 408–429.

Collett, T.S., 1993, Natural gas hydrates of the Prudhoe Bay–Kuparuk River area, North Slope, Alaska: American Association of Petroleum Geologists Bulletin, v. 77, p. 793–812.

Collett, T.S., 1998a, Well log characterization of sediment porosities in gas-hydrate-bearing reservoirs, Paper SPE 49298 *in* Annual Technical Conference Exhibition Society of Petroleum Engineers, New Orleans, September 1998, Proceedings: Richardson, Tex., Society of Petroleum Engineers.

Collett, T.S., 1998b, Well log evaluation of gas hydrate saturations: Transactions of the Society of Petrophysicists and Well Log Analysts 39th Annual Logging Symposium, Houston, p. MM.

Collett, T.S., 2000, A review of well-log analysis techniques used to assess gas-hydrate-bearing reservoirs, *in* Paull, C.K., and Dillon, W.P., eds., Natural gas hydrates—Occurrence, distribution, and detection: Geophysical Monograms, American Geophysical Union, p. 189–210.

Davis, E.E., Hyndman, R.D., and Villinger, H., 1990, Rates of fluid expulsion across the northern Cascadia accretionary prism—Constraints from new heat flow and multichannel seismic reflection data: Journal of Geophysical Research, v. 95, p. 8869–8889.

Davis, E.E., Villinger, H., MacDonald, R.D., Meldrum, R.D., and Grigel, J., 1997, A robust rapid-response probe for measuring bottom-hole temperatures in deep ocean boreholes: Marine Geophysical Researches*.,* v. 19, p. 267–281.

Dickens, G.R., Paull, C.K., Wallace, P., and the ODP Leg 164 Scientific Party, 1997, Direct measurement of *in situ* methane quantities in a large gas-hydrate reservoir: Nature, v. 385, p. 426–428.

Dickens, G.R., Borowski, W.S., Wehner, H., Paull, C.K., and the ODP Leg 164 Scientific Party, 2000a, Data Report—Additional shipboard information for the pressure core sampler (PCS), *in* Paull, C.K., Matsumoto, R., Wallace, P.J., and Dillon, W.P., eds., Proceedings of the Ocean Drilling Program*,* Scientific Results*,* v. 164: College Station, Tex., Ocean Drilling Program, p. 439–443. [CD-ROM; available from: Ocean Drilling Program, Texas A&M University, College Station, Tex. 77845-9547, U.S.A.]

Dickens, G.R., Wallace, P.J., Paull, C.K., and Borowski, W.S., 2000b, Detection of methane gas hydrate in the pressure core sampler (PCS)—Volume-pressure-time relations during controlled degassing experiments, *in* Paull, C.K., Matsumoto, R., Wallace, P.J., and Dillon, W.P., eds., Proceedings of the Ocean Drilling Program*,* Scientific Results, v. 164: College Station, Tex., Ocean Drilling Program, p. 113–126. [CD-ROM; available from: Ocean Drilling Program, Texas A&M University, College Station, Tex. 77845-9547, U.S.A.]

Dickens, G.R., Schroeder, D., Hinrichs, K.-U., and the Leg 201 Scientific Party, 2003, The pressure core sampler (PCS) on Ocean Drilling Program Leg 201—General operations and gas release, *in* D'Hondt, S.L., Jørgensen, B.B., Miller, D.J., and the Shipboard Scientific Party, Proceedings of the Ocean Drilling Program*,* Initial Reports, v. 201: College Station, Tex., Ocean Drilling Program, p. 1–22 [CD-ROM].

Droser, M.L., and Bottjer, D.J., 1986, A semiquantitative field classification of ichnofabric: Journal of. Sedimentary Petrology, v. 56, p. 558–559.

Duan, Z., Møller, N., Greenberg, J., and Weare, J.H., 1992, The prediction of methane solubility in natural waters to high ionic strengths from 0° to 250 °C and from 0 to 1600 bar: Geochimica et Cosmochimica Acta*,* v. 56, p. 1451–1460.

Dunham, R.J., 1962, Classification of carbonate rocks according to depositional texture, *in* Ham, W.E., ed., Classification of carbonate rocks: American Association of Petroleum Geologists, p. 108–121.

Ellis, D.V., 1987, Well logging for earth scientists: New York, Elsevier, 548 p.

Embry, A.F., and Klovan, J.E., 1971, A late Devonian reef tract on northeastern Banks Island, Northwest Territories: Bulletin of Canadian Petroleum Geology, v. 19, p. 730–781.

Erickson, S.N., and Jarrard, R.D., 1998, Velocity-porosity relationships for water-saturated siliciclastic sediments: Journal of Geophysical Research, v. 103, p. 30, 385–30, 406.

Expedition 311 Scientists, 2005, Cascadia margin gas hydrates: Integrated Ocean Drilling Program Preliminary Report*,* 311, doi:10.2204/iodp.pr.311.2005.

Fofonoff, N.P., 1985, Physical properties of seawater: Journal of Geophysical Research*,* v. 90, no. C2, p. 3332–3342.

Gealy, E.L., Winterer, E.L., and Moberly, R., Jr., 1971, Methods, conventions, and general observations, *in* Winterer, E.L., Riedel, W.R., Broennimann, P., Gealy, E.L., Heath, G.R., Kroenke, L.W., Martini, E., Moberly, R., Jr., Resig, J.M., and Worsley, T.R., Initial Reports of the Deep Sea Drilling Project 7 Part 1: Washington, p. 9–26.

Gieskes, J.M., Gamo, T., and Brumsack, H., 1991, Chemical methods for interstitial water analysis aboard *JOIDES Resolution*: Ocean Drilling Program Technical Note 15.

Giosan, L., Flood, R.D., Grützner, J., and Mudie, P., 2002, Paleoceanographic significance of sediment color on western North Atlantic Drifts—I. Origin of color: Marine Geology, v. 189 p. 25–41.

Goldberg, D., 1997, The role of downhole measurements in marine geology and geophysics: Reviews of Geophysics, v. 35, p. 315–342.

Goldberg, D., Collett, T.S., and Hyndman, R.D., 2000, Ground truth—*In-situ* properties of hydrate, *in* Max, M.D., ed., Natural gas hydrate in oceanic and permafrost environments—The Netherlands: Kluwer Academic Publishers, p. 295–310.

Graber, K.K., Pollard, E., Jonasson, B., and Schulte, E., eds., 2002, Overview of Ocean Drilling Program engineering tools and hardware: Ocean Drilling Program Technical Note 31. Accessed August 4, 2006, at *http://www-odp.tamu.edu/publications/tnotes/tn31/INDEX.HTM*.

Guerin, G., and Goldberg, D., 2002, Sonic attenuation measurements in the Mallik 2L-38 gas hydrates research well, MacKenzie Delta, NWT Canada: Journal of Geophysical Research, v. 107, p. 10.1029/2001JB000556.

Guerin, G., Goldberg, D., and Meltser, A., 1999, Characterization of *in situ* elastic properties of gas-hydrate bearing sediments on the Blake Ridge: Journal of Geophysical Research, v. 104, p. 17,781–17,795.

Heeseman, M., Villinger, H., Fisher, A.T., Trehu, A.M., and Witte, S., 2006, Data report—Testing and deployment of the new APCT–3 tool to determine *in situ* temperatures while piston coring, *in* M. Riedel, Collett, T.S., Malone, M.J., and the Expedition 311 Scientists, Proceedings of the Integrated Ocean Drilling Program, v. 311: College Station, Tex., Ocean Drilling Program.

Helgerud, M.B., Dvorkin, J., and Nur, A., 2000, Rock physics characterization for gas hydrate reservoirs—Elastic properties, *in* Holder, G.D., and Bishnoi, P.R., eds., Gas hydrates—Challenges for the future: Annals of the New York Academy of Sciences, v. 912, p. 116–125.

Horai, K., and Von Herzen, R.P., 1985, Measurement of heat flow on Leg 86 of the Deep Sea Drilling Project, *in* Heath, G.R., Burckle, L.H., et al., Initial Reports of the Deep Sea Drilling Project, v. 86: Washington D.C., U.S. Government Printing Office, p. 759–777.

Hunt, J.M. 1979, Petroleum geochemistry and geology: San Francisco, W.H. Freeman, 617 p.

Kleinberg, R.L., Flaum, C., and Collett, T.S., 2005, Magnetic resonance log of Mallik 5L-38—Hydrate saturation, growth habit, and relative permeability, *in* Dallimore, S.R., and Collett, T.S., Scientific results from the Mallik 2002 Gas Hydrate Production Research Well Program, Mackenzie Delta, Northwest Territories, Canada: Geological Survey of Canada, Bulletin no. 585.

Kristiansen, J.I., 1982, The transient cylindrical probe method for determination of thermal parameters of earth materials: Aaehus University [Ph.D. dissertation].

Kvenvolden, K.A., and Lorenson, T.D., 2000, Methane and other hydrocarbon gases in sediment from the southeastern North American continental margin, *in* Paull, C.K., Matsumoto, R., Wallace, P.J., Black, N.R., Borowski,W.S.,Collett, T.S., Damuth, J.E., Dickens, G.R., Egeberg, P.K., Goodman,K., Hesse, R.F., Hiroki, Y., Holbrook, W.S., Hoskins, H., Ladd, J. ,Lodolo, E., Lorenson, T.D.,Musgrave, R.J., Naehr, T.H., Okada, H., Pierre, C., Ruppel, C.D., Satoh, M., Thiery, R., Watanabe, Y., Wehner, H., Winters, W.J., and Wood, W.T., Gas hydrate sampling on the Blake ridge and Carolina rise; covering leg 164 of the cruises of the drilling vessel *JOIDES Resolution*, Halifax, Nova Scotia, to Miami, Florida, sites 991–997, 31 October–19 December 1995: Proceedings of the Ocean Drilling Program, Scientific Results, v. 164, p. 29–36.

Lamont-Doherty Earth Observatory Borehole Research Group, 2001, ODP logging services electronic manual, Version 2.0: College Station, Tex., Ocean Drilling Program, accessed September 28, 2005, at *http://www.ldeo.columbia.edu/BRG/ODP/LOGGING/MANUAL/index.html*.

Luthi, S. M., 2001, Geological well logs—Their use in reservoir modeling: Springer-Verlag, Berlin, 373 p.

Manheim, F.T., and Sayles, F.L., 1974, Composition and origin of interstitial waters of marine sediments, based on deep sea drilled cores, *in* Goldberg, E.D., ed., The sea, volume 5—Marine chemistry—The sedimentary cycle: New York, Wiley, p. 527–568.

Mathews, M., 1986, Logging characteristics of methane hydrate: The Log Analyst, v. 27, p. 26–63.

Mazzullo, J., and Graham, A.G., eds., 1988, Handbook for shipboard sedimentologists: Ocean Drilling Program Technical Note 8.

Mikada, H., Becker, K., Moore, J.C., Klaus, A., Austin, G.L., Bangs, N.L., Bourlange, S., Broilliard, J., Brückmann, W., Corn, E.R., Davis, E.E., Flemings, P.B., Goldberg, D.S., Gulick, S.S., Hansen, M.B., Hayward, N., Hills, D.J., Hunze, S., Ienaga, M., Ishiguro, H., Kinoshita, M., Macdonald, R.D., McNeill, L., Obana, S., Hong, O.S., Peacock, S., Pettigrew, T.L., Saito, S. Sawa, T., Thaiprasert, N., Tobin, H.J., and Tsurumi, H., 2002, Proceedings of the Ocean Drilling Program, Initial Reports, v. 196: College Station, Tex., Ocean Drilling Program, accessed September 28, 2005, at *http:// www-odp.tamu.edu/publications/196_IR/196ir.htm*.

Milkov, A.V., Dickens, G.R., Claypool, G.E., Lee, Y.-J., Borowski, W.S., Torres, M.E., Xu, W., Tomaru, H., Tréhu, A.M., and Schultheiss, P., 2004, Co-existence of gas hydrate, free gas, and brine within the regional gas hydrate stability zone at Hydrate Ridge (Oregon margin)—Evidence from prolonged degassing of a pressurized core: Earth and Planetary Science Letters, v. 222, p. 829–843.

Munsell Color Company, Inc., 1975, Munsell soil color charts: Baltimore, Md.

Paull, C.K., Matsumoto, R., Wallace, P.J., et al., 1996, Proceedings of the Ocean Drilling Program, Initial Reports, v.164: College Station, Tex., Ocean Drilling Program.

Paull, C.K., and Ussler, W., III, 2000. History and significance of gas sampling during DSDP and ODP drilling associated with gas hydrates, *in* Paull, C.K., and Dillon, W.P., eds., Natural Gas Hydrates: Occurrence, Distribution, and Detection. Am. Geophys. Union, Geophys. Monogr. Ser., 124:53–66.

Pearson, C.F., Halleck, P.M., McGuire, P.L., Hermes, R., and Mathews, M., 1983, Natural gas hydrate deposits—A review of *in situ* properties: Journal of Physical Chemistry, v. 87, p. 4180–4185.

Pettigrew, T.L. 1992, The design and operation of a wireline pressure core sampler (PCS): College Station, Tex., Ocean Drilling Program, ODP Technical Note 17, accessed August 4, 2006, at *http://www-odp.tamu.edu/publications/tnotes/tn17/INDEX.HTM*.

Pimmel, A., and Claypool, G., 2001, Introduction to shipboard organic geochemistry on the JOIDES Resolution: College Station, Tex., Ocean Drilling Program, ODP Technical Note 30, accessed August 4, 2006, at *http://www-odp.tamu.edu/publications/tnotes/tn30/INDEX.HTM*.

Rider, M., 1996, The geological interpretation of well logs (2d ed.): Caithness, Scotland, Whittles Publishing, 288 p.

Schlager, W., and James, N.P., 1978, Low-magnesian calcite limestones forming at the deep-sea floor, Tongue of the Ocean, Bahamas: Sedimentology, v. 25, p. 675–702.

Schlumberger, 1989. Log Interpretation Principles/Applications—Houston*:* Schlumberger Education Services, SMP–7017.

Schlumberger, 1994. Log Interpretation Charts—Sugar Land: Schlumberger Education Services, SMP-7006.

Serra, O., 1984. Fundamentals of Well-Log Interpretation (vol. 1): The Acquisition of Logging Data: Dev. Pet. Sci*.,* 15A.

Serra, O., 1986, Fundamentals of well-log interpretation—2. The interpretation of logging data: Amsterdam, Elsevier Science, 15B, 684 p. [Developments in Petroleum Science Series]

Serra, O., 1989. Formation MicroScanner Image Interpretation: Houston (Schlumberger Educ. Services), SMP-7028.

Schultheiss, P.J., Francis, T.J.G., Holland, M., Roberts, J.A., Amann, H., Thjunjoto, Parkes, R. J., Martin, D., Rothfuss, M., Tyunder, F., and P.D. Jackson, 2006, Pressure coring, logging and sub-sampling with the HYACINTH system, *in* New ways of looking at sediment cores and core data, Rothwell R.G. ed.: Geological Society of London, Special Publications 267, p. 151–165.

Shepard, F., 1954, Nomenclature based on sand-silt-clay ratios: Journal of Sedimentary Petrology, v. 24, p. 151–158.

Shipboard Scientific Party, 1998. Introduction, *in* Becker, K., Malone, M.J., and others., Proc. ODP, Init. Repts., 174B: College Station, Tex. (Ocean Drilling Program), 3–9.

Shipboard Scientific Party, 2003, Explanatory notes, *in* Tréhu, A.M, Bohrmann, G., Rack, F.R., Torres, M.E., et al., Proceedings of the Ocean Drilling Program*,* Initial Reports*,* v. 204: College Station, Tex., Ocean Drilling Program, p. 1–102 [CD-ROM]. [Available from: Ocean Drilling Program, Texas A&M University, College Station Tex. 77845-9547, USA.]

Sloan, E.D., 1998. Clathrate Hydrates of Natural Gases (2d ed.): New York (Marcel Dekker).

Smith, D.C., Spivack, A.J., Fisk, M.R., Haveman, S.A., Staudigel, H., and ODP Leg 185 Scientific Party, 2000, Methods for quantifying potential microbial contamination during deep ocean coring: College Station, Tex., Ocean Drilling Program, ODP Technical Note 28, accessed August 4, 2006, at *http://www-odp.tamu.edu/publications/tnotes/tn28/INDEX.HTM*.

Soffientino B., Spivack A.J., Smith D.C., Roggenstein E.B., D Hondt S.J., 2006, A versatile and sensitive tritium-based radioassay for measuring hydrogenase activity in aquatic sediments: Microbiological Methods, v. 66, no. 1, p. 136–146. [Epub December 13,2005]

Terry, R.D., and Chilingarian, G.V., 1955, Summary of "Concerning some additional aids in studying sedimentary formations" by M.S. Shvetsov: Journal of Sedimentary Petrology, v. 25, no. 3, p. 229-234.

Tréhu, A.M., 2006, Subsurface temperatures beneath southern Hydrate Ridge, *in* Tréhu, A.M., Bohrmann, G., Torres, M.E., and Colwell, F.S., eds., Proc. ODP, Sci. Results, 204: College Station, Tex. (Ocean Drilling Program), 1–26. doi:10.2973/odp.proc.sr.204.114.2006.

Tréhu, A.M., Bohrmann, G., Rack, F.R., Torres, M.E., Delwiche, M.E., Dickens, G.R., Goldberg, D.S., Gracia, E., Guerin, G., Holland, M., Johnson, J.E., Lee, Y.J., Liu, C.S., Long, P.S., Milkov, A.V., Riedel, M., Schultheiss, P., Su, X., Teichert, B., Tomaru, H., Vanneste, M., Watanabe, M., and Weinberger, J.L., 2003, Proceedings of the Ocean Drilling Program, Initial Reports, v. 204: College Station, Tex., Ocean Drilling Program, 81 p. [CD-ROM; available from: Ocean Drilling Program, Texas A&M University, College Station, Tex. 77845-9547, USA.]

UNESCO, 1981, Tenth report of the joint panel on oceanographic tables and standards: Marine Science, v. 36, 25 p. [UNESCO Technical Paper]

Ussler, W., III, Paull, C.K., McGill, P., Schroeder, D., and Ferrell, D., 2006. A test of the temperature, pressure, and conductivity tool prototype at Hydrate Ridge, *in* Tréhu, A.M., Bohrmann, G., Torres, M.E., and Colwell, F.S., eds., Proc. ODP, Sci. Results, 204: College Station, Tex. (Ocean Drilling Program), 1–41. doi:10.2973/odp.proc.sr.204.112.2006

von Herzen, R.P., and Maxwell, A.E., 1959, The measurement of thermal conductivity of deep-sea sediments by a needle-probe method: Journal of Geophysical Research, v. 64, p. 1557–1563.

Wallace, P.J., Dickens, G.R., Paull, C.K., and Ussler III, W., 2000, Effects of core retrieval and degassing on the carbon isotope composition of methane in gas hydrate- and free gas-bearing sediments from the Blake Ridge, *in* Paull, C.K., Matsumoto, R., Wallace, P.J., and Dillon, W.P., eds., Proceedings of the Ocean Drilling Program*,* Scientific Results, v. 164: College Station, Tex., Ocean Drilling Program, p. 101–112 [CD-ROM; available from: Ocean Drilling Program, Texas A&M University, College Station, Tex. 77845-9547, U.S.A.]

Waxman, M.H., and Smits, L. J. M., 1968, Electrical conductivities in oil-bearing shaly sands: SPE Journal, Jun., 107–122.

Wentworth, C.K., 1922, A scale of grade and class terms of clastic sediments: Journal of Geology, v. 30, p. 377–392.

Winters, W.J., Novosel, I., Boldina, O., Waite, W.F., and Jablonski, S., 2004, Physical Properties of Sediment Obtained During the IMAGES VIII/PAGE 127 Gas Hydrate and Paleoclimate Cruise on the RV Marion Dufresne in the Gulf of Mexico, 2-18 July 2002, *in* Winters, W.J., Lorenson, T.D., Paull, C.K., eds., Initial report of the IMAGES VIII/PAGE 127 gas hydrate and paleoclimate cruise on the RV Marion Dufresne in the Gulf of Mexico, 2–18 July 2002: U.S. Geological Survey Open-File Report 2004–1358, unpaged. (Also available at *http://woodshole.er.usgs.gov/pubs/of2004-1358/*)

Westbrook, G.K., Carson, B., Musgrave, R.J., et al., 1994, Proceedings of the Ocean Drilling Program, Initial Reports, v. 146 (pt. 1): College Station, Tex., Ocean Drilling Program.

Xu, W., 2002, Phase balance and dynamic equilibrium during formation and dissociation of methane gas hydrate, *in* International Conference on Gas Hydrates, 4th, Yokohama, Japan, May 2002, Proceedings: Yokohama, Japan, International Conference on Gas Hydrates, p. 195–200.

Xu, W., 2004, Modeling dynamic marine gas hydrate systems: American Mineralogist, v. 89, p. 1271–1279.